NSF/CEE-82023 PB82-249012

Research Report R82-03 Order No. 718

DYNAMIC STIFFNESS AND SEISMIC RESPONSE OF PILE GROUPS

by

AMIR M. KAYNIA

Supervised by

E. KAUSEL

January 1982

Sponsored by the National Science Foundation
Division of Problem-Focused Research
Grant PFR 79-02989

Additional Copies May Be Obtained From:

National Technical Information Service
U.S. Department of Commerce
5285 Port Royal Road
Springfield, Virginia 22161

50272-101

REPORT DOCUMENTATION PAGE	1. REPORT NO. NSF/CEE-82023	2.	3. Recipient's Accession No.
4. Title and Subtitle: Dynamic Stiffness and Seismic Responses of Pile Groups			5. Report Date: January 1982
			6.
7. Author(s): A.M. Kaynia, E. Kausel			8. Performing Organization Rept. No. 718
9. Performing Organization Name and Address: Massachusetts Institute of Technology, Department of Civil Engineering, Cambridge, MA 02139			10. Project/Task/Work Unit No.
			11. Contract(C) or Grant(G) No. (C) (G) PFR7902989
12. Sponsoring Organization Name and Address: Directorate for Engineering (ENG), National Science Foundation, 1800 G Street, N.W., Washington, DC 20550			13. Type of Report & Period Covered
			14.

15. Supplementary Notes
Submitted by: Communications Program (OPRM)
National Science Foundation
Washington, DC 20550

16. Abstract (Limit: 200 words)

A formulation for the analysis of pile groups in layered semi-infinite media is presented. The formulation is based on the introduction of a soil flexibility matrix as well as on dynamic stiffness and flexibility matrices of the piles to relate the discretized uniform forces to the corresponding displacements at the pile-soil interface. Pile group analyses revealed that behavior is highly frequency dependent as the result of wave interferences occurring between the various piles in the group. Large values for stiffnesses as well as large magnification factors for the groups essentially follow the low frequency components of the gorund motion. The rotational component is negligible for typical dimensions of the foundation. The quasi-three-dimensional method and the superposition method for the solution of pile groups are shown to compare well with the full three-dimensional solution.

17. Document Analysis a. Descriptors

Pile structures
Earthquakes
Displacement
Vibration
Soils
Seismic waves
Soil properties
Foundations
Stiffness
Earthquake resistant structures

b. Identifiers/Open-Ended Terms

Ground motion
Seismic response

J.M. Biggs, /PI

c. COSATI Field/Group

18. Availability Statement	19. Security Class (This Report)	21. No. of Pages
NTIS	20. Security Class (This Page)	22. Price

Massachusetts Institute of Technology
Department of Civil Engineering
Constructed Facilities Division
Cambridge, Massachusetts 02139

DYNAMIC STIFFNESS AND SEISMIC RESPONSE OF PILE GROUPS

by

AMIR M. KAYNIA

Supervised by

Eduardo Kausel

January 1982

Sponsored by the National Science Foundation
Division of Problem-Focused Research
Grant PFR 79-02989

Publication No. R82-03 Order No. 718

ABSTRACT

A formulation for the analysis of pile groups in layered semi-infinite media is presented. The formulation was based on the introduction of a soil flexibility matrix as well as on dynamic stiffness and flexibility matrices of the piles, in order to relate the discretized uniform forces to the corresponding displacements at the pile-soil interface.

The result of pile group analyses showed that the pile group behavior is highly frequency-dependent as the result of wave interferences taking place between the various piles in the group. Large values for stiffnesses as well as large magnification factors for the force on certain piles is expected at some frequencies. As for the seismic response, pile groups essentially follow the low-frequency components of the ground motion, and the rotational component is negligible for typical dimensions of the foundation.

A numerical study on the accuracy of the approximate superposition method as well as the quasi-three-dimensional formulation in which the pile-soil compatibility conditions are accounted for in the formulation only in the direction of vibration, showed that these solutions compare very well with the full three-dimensional solution.

ACKNOWLEDGEMENTS

This is the fourth report issued under the research project entitled "Flexible Sub-surface Building-Foundation Interfaces for Aseismic Design." The project is supported by the National Science Foundation, Division of Problem-Focused Research Applications, under Grant PFR-79-02989. Dr. John B. Scalzi is the cognizant NSF program official, and his support is gratefully acknowledged.

The opinions, findings and conclusions or recommendations expressed in this report are those of the authors and do not necessarily reflect the views of the National Science Foundation.

Table of Contents

List of Figures

List of Symbols

a_o	nondimensional frequency
A_p	area of the pile cross section
c_{xx}, c_{zz}, $c_{\phi\phi}$, $c_{\psi\psi}$	dampings of the foundation (pile group) associated with horizontal, vertical, rocking and torsional modes of vibration
C_s	shear wave velocity of the soil medium
d	diameter of the piles
E_p and E_s	moduli of elasticity of the piles and of the soil
f_r, f_θ, f_z	body forces in the soil medium in the r, θ, and z directions
f_{rn}, $f_{\theta n}$, f_{zn}	amplitudes of Fourier sine or cosine series of f_r, f_θ, and f_z
f_{1n}, f_{2n}, f_{3n}	combinations of Hankel transforms of f_{rn}, $f_{\theta n}$ and f_{zn}
F	axial force in a beam (pile)
F_p	dynamic flexibility matrix of fixed-end piles
F_s	dynamic soil flexibility matrix
h	thickness of a layer
H	constant axial force in a beam (pile)
i	$= \sqrt{-1}$
I_p	moment of inertia of the pile cross section
$I_{u_x F_x}$, $I_{u_z F_z}$, $I_{u_x M_x}$, $I_{\phi_x M_x}$	interaction factors
$J_n(kr)$	nth order Bessel function of the 1st kind
k	parameter of a Hankel transfor
k_{xx}, k_{zz}, $k_{\phi\phi}$, $k_{\psi\psi}$	stiffnesses of the foundation (pile groups) associated with horizontal, vertical, rocking and torsional modes of vibration.

List of Symbols (Continued)

K	dynamic stiffness of the foundation (pile group)
K_p	dynamic stiffness matrix of the piles
ℓ	no. of segments along the pile length
L	length of the piles
m	mass per unit length of the piles
M	moment at a pile section
N	total no. of piles in a group
p_x, p_y, p_z	forces developed at the pile-soil interface in the x, y, and z directions
P	vector of forces developed at pile-soil interface
P_e	vector of forces at pile ends
P^*	vector of free-field forces
r	distance in the radial direction
R	radius of the piles
R_x, R_y, R_z	forces (reactions) at the pile ends in the x, y and z directions
s	distance (spacing) between adjacent piles
t	time
u_g	free-field ground-surface displacement
u_x, u_y, u_z	displacements of the pile-soil interface in the x, y and z directions
u_r, u_θ, u_z	displacements in the soil medium in the r, θ and z directions
u_{rn}, $u_{\theta n}$, u_{zn}	amplitudes of Fourier sine or cosine series of u_r, u_θ and u_z
u_{1n}, u_{2n}, u_{3n}	combinations of Hankel transforms of u_{rn}, $u_{\theta n}$ and u_{zn}
U_e	vector of displacements of the pile-soil interface
U	vector of displacements of the pile ends

List of Symbols (Continued)

U^*	vector of free-field displacements
V	shear at a pile section
α	a parameter defined for the soil medium (eq. (2.46))
β_p, β_s	material dampings in the piles and in the soil
γ	a parameter defined for the soil medium (eq. (2.47))
Δ	dilatation (eq. (2.23))
ζ	a parameter defined for the piles (eq. (2.143))
η	a parameter defined for the piles (eq. (2.132))
θ	angle between a vertical plane and the x-z plane
λ, μ	Lame's constants
ν_p and ν_s	Poisson ratios of the piles and the soil
ξ	a parameter defined for the piles (eq. (2.132))
ρ_p and ρ_s	mass densities of the piles and the soil
σ_{rz}, $\sigma_{\theta z}$, σ_{zz}	stresses on a horizontal plane
σ_{rzn}, $\sigma_{\theta zn}$, σ_{zzn}	amplitudes of Fourier sine or cosine series of σ_{rz}, $\sigma_{\theta z}$ and σ_{zz}
σ_{21n}, σ_{22n}, σ_{23n}	combinations of Hankel transforms of σ_{rzn}, $\sigma_{\theta zn}$ and σ_{zzn}
ϕ	rotation of the pile cap
ϕ_x, ϕ_y	rotations of the pile cross section
Ψ	dynamic flexibility matrix of the piles for end displacements
ω	frequency of steady-state vibration.

Also the superscripts "G" and "s" were used to refer to the quantities in the pile group and in the single pile, respectively.

CHAPTER 1 - INTRODUCTION

A pile is a structural element installed in the ground which is connected to the structural frame, either directly or through a foundation block, in order to transfer the loads from the superstructure to the ground. Piles are seldom used singly; more often, they are used in groups or clusters, in which case they are connected to a common foundation block (pile cap).

Pile foundations, under certain circumstances, are preferred over shallow foundations; for instance, in sites where near-surface soil strata are so weak that either soil properties do not have the required strength, or the settlement and/or movements of a shallow footing on such ground would be intolerable.

Behavior of pile foundations, sometimes referred to as deep foundations, has been a subject of considerable research. Most studies have focussed primarily on short- and long-term static pile behavior, pile-installation effects, estimation of ultimate load capacity and settlement, prediction of ultimate lateral resistance, and estimation of lateral deflection. Extensive field testings and experimental investigations on different aspects of pile behavior have resulted in a number of empirical and approximate analytical methods for the pile-foundation design. In addition, other studies have resulted in more rigorous schemes for pile analysis. Among these studies the works of Poulos (1968), Poulos and Mattes (1971), Poulos (1971), Butterfield and Banerjee (1971) and Banerjee (1978) are related to the present study. These researchers discretized the piles into several segments and related the displacements of the segments to the corresponding forces in both the soil medium, using

Mindlin's fundamental solution (1936) and in the piles, using pile differential equations (in discretized form). Introduction of the condition of displacement compatibility between the soil and the piles and imposition of appropriate boundary conditions lead to the desired pile solution. The results of these studies, especially by Poulos and his colleagues, have highlighted the important aspects of static pile-group behavior, including distribution of loads among the piles in a group, stiffnesses of pile groups, and the variation of these quantities with geometric parameters (spacing, length, and number of piles) as well as material properties. For a comprehensive review of these results and other analytical and empirical techniques of static pile-foundation analysis see Poulos (1980).

The fact that static pile behavior studies were unable to provide any qualitative information on dynamic aspects of the problem, along with an increasing demand for the construction of nuclear power plants and offshore structures, have stimulated extensive research on dynamic pile behavior. For these studies, which have dealt primarily with the behavior of single piles, a variety of different models and solution schemes have been used. Tajimi (1969), Nogami and Novak (1976), Novak and Nogami (1977), Kobori, Minai and Baba (1977, 1981). Kagawa and Kraft (1981) have obtained analytical solutions for the response of dynamically-excited single piles. Finite-element techniques, on the other hand, have been used by Blaney, Kausel and Roesset (1976) and Kuhlemeyer (1979a, 1979b). In addition, less involved models based on the theory of beams on elastic foundations, commonly referred to as the subgrade-reaction approach, were used by Novak (1974), Matlock (1970), Reese, Cox and Koop (1974) and Reese and Welch (1975). The advantage of this technique is that the results

of field testing can be directly incorporated in the model ("p-y" and "t-w" techniques).

In spite of considerable achievements in characterizing the dynamic response of single piles, the dynamic behavior of pile groups is not yet well understood. In fact, only a few attempts have been made to study this problem. The earlier contributions are due to Wolf and Von Arx (1978), and to Nogami (1979). Wolf and Von Arx used an axisymmetric finite-element scheme to obtain Green functions for ring loads which were used to form the soil flexibility matrix. The dynamic stiffness matrix of the pile-soil system was then obtained by simply assembling those of the soil and piles. Using this formulation, Wolf and Von Arx studied some characteristics of horizontal as well as vertical dynamic stiffnesses of pile groups in a layered soil stratum resting on a rigid bedrock. Later this methodology was employed by Waas and Hartmann (1981), who implemented an efficient and rigorous technique for the computation of the Green's functions (Waas, 1980), to study the behavior of pile groups in lateral vibration.

On the other hand, the vertical vibration characteristics of pile groups in a uniform soil stratum underlain by a rigid bedrock has been studied analytically by Nogami (1979). To incorporate in his model the interaction of piles through the soil medium, Nogami used an analytical solution to the axisymmetric vibration of the stratum obtained earlier by Nogami and Novak (1976). Later he extended his studies to the case of layered strata (Nogami, 1980). For this case, however, the interaction effects were obtained using an analytical expression for the displacement field due to the axial vibration of an infinitely long rigid cylinder in an infinite medium (Novak, Nogami and Aboul-Ella, 1978).

The results of these studies indicate that: 1) behavior of pile groups is strongly frequency-dependent; 2) spacing and number of piles have a considerable effect on dynamic stiffnesses, but only a minor effect on the lateral seismic response; and 3) interaction effects are stronger for more flexible soil media.

The objective of the present work is to study the three-dimensional dynamic behavior of pile groups in layered semi-infinite media and to investigate the accuracy of certain approximate approaches. Chapter 2 of this report is devoted to the formulation and the associated analytical derivations. In Chapter 3 the results of the three-dimensional analyses are presented. These results include dynamic stiffnesses and seismic response of pile groups as well as the distribution of loads among the piles in the group. Special attention is paid to the effect of frequency, spacing, and number of piles on these quantities. In Chapter 4 the accuracy of a "quasi three-dimensional" solution is investigated (a quasi three-dimensional solution here refers to the solution obtained for symmetric rectangular arrangement of piles by assuming that the dynamic effects in the vertical and in the two horizontal directions of symmetry are uncoupled from one another).

The applicability of the superposition scheme to dynamic pile-group analysis is examined in Chapter 5. In addition, the characteristics of dynamic interaction curves (the influence of vibration of one pile on another for a group of two piles) and their connection to pile-group behavior are studied.

Finally, Chapter 6 includes a summary of the important aspects of the pile-group behavior as well as conclusions on the applicability of approximate solution schemes.

CHAPTER 2 - FORMULATION AND ANALYTICAL DERIVATIONS

In the present study it is assumed that 1) the soil medium is a viscoelastic layered halfspace, 2) the piles are made of linear elastic materials, and 3) there is no loss of bondage between the piles and the soil; however, the frictional effects due to torsion and bending of piles are neglected. (The overall pile group behavior is controlled primarily by the frictional and lateral forces caused by axial motion and bending of the piles, respectively.)

In what follows, the formulation of the problem, along with the associated analytical derivations and their numerical implementation, are presented. Any time-dependent variable such as $u(t)$ used in this formulation is of the form $u(t) = u \exp(i\omega t)$, in which u is a complex quantity, ω is the frequency of steady-state harmonic vibration, and $i = \sqrt{-1}$. However, the factor $\exp(i\omega t)$ is deleted in the equations, since it is shared by all time-dependent variables involved in the problem.

2.1 Formulation

Consider the pile group shown in Fig. 2.1. The actual distribution of lateral as well as frictional forces developed at the pile-soil interface are shown for one of the piles in the group (pile j).

The pile is discretized into ℓ arbitrary segments, and the pile-tip is considered to be segment $(\ell+1)$. The pile head and the center of the pile segments define then $(\ell+2)$ "nodes" which are assigned numbers 0, 1, 2, ... , $(\ell+1)$, respectively. Subsequently, the actual force distributions are replaced by piecewise constant distributions which are also shown in the figure. These forces are assumed positive if they are in the positive direction of axes.

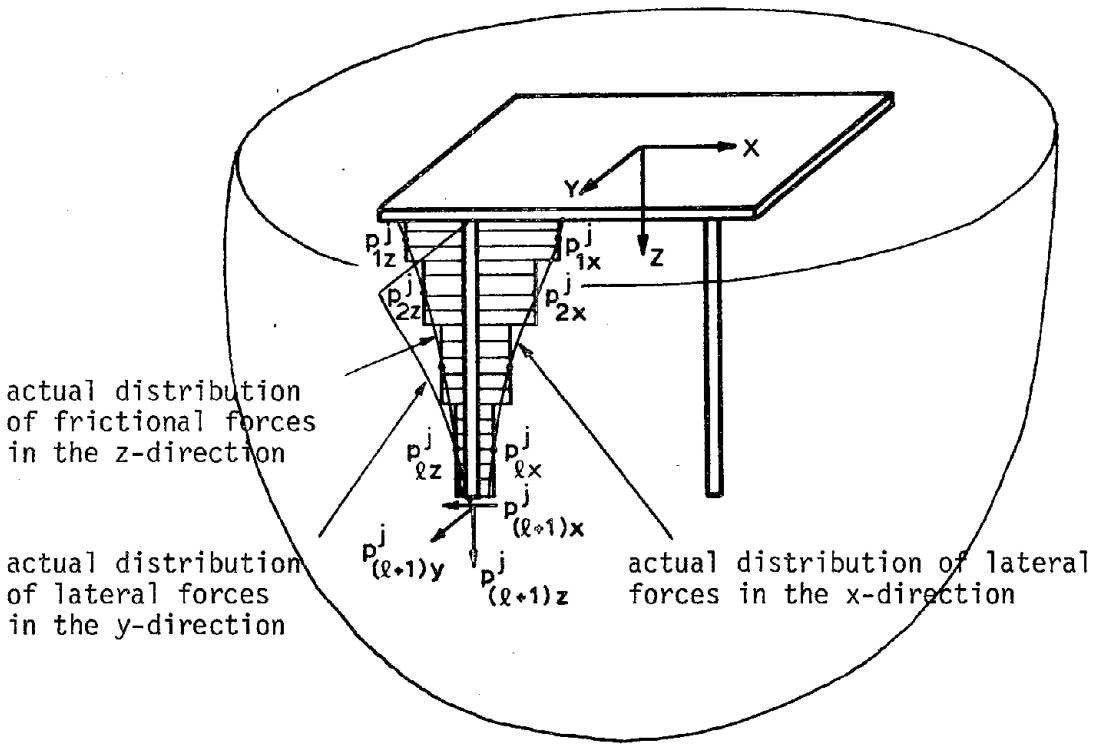

Fig. 2.1 - Distribution of Forces on the j^{th} Pile of the Group

Consider first the equilibrium of pile j under the pile-soil interface forces. If one denotes the vector of the resultant of these forces by P^j, that is:

$$P^j = [p^j_{1x}\ p^j_{1y}\ p^j_{1z}\ \cdots\cdots\ p^j_{(\ell+1)x}\ p^j_{(\ell+1)y}\ p^j_{(\ell+1)z}]^T \qquad (2.1)$$

and the vector of displacements of nodes 1 through $(\ell+1)$ by U^j, that is:

$$U^j = [u^j_{1x}\ u^j_{1y}\ u^j_{1z}\ \cdots\cdots\ u^j_{(\ell+1)x}\ u^j_{(\ell+1)y}\ u^j_{(\ell+1)z}]^T \qquad (2.2)$$

Then U^j can be expressed as the summation of the displacements caused by the translations and rotations of the two pile ends when there are no loads on the pile, and the displacements caused by forces on the piles $(-P^j)$ when the two ends of the pile are clamped. This can be expressed as:

$$U^j = \Psi^j\ U^j_e - F^j_p\ P^j \qquad (2.3)$$

in which U^j_e is the vector of end displacements for pile j, given by:

$$U^j_e = [u^j_{ox}\ \phi^j_{ox}\ u^j_{oy}\ \phi^j_{oy}\ u^j_{oz}\ u^j_{(\ell+1)x}\ \phi^j_{(\ell+1)x}\ u^j_{(\ell+1)y}\ \phi^j_{(\ell+1)y}\ u^j_{(\ell+1)z}]^T \qquad (2.4)$$

Ψ^j is a $(3(\ell+1)\ x\ 10)$ matrix defining displacements of the center of segments (nodes 1 through $(\ell+1)$ due to end displacements of the pile when P^j are not present (to be more specific, the i^{th} column of Ψ^j defines the three components of translation at the center of the segments due to a unit harmonic pile end displacement associated with the i^{th} component of U^j_e), and F^j_p is the flexibility matrix of pile j associated with nodes 1 through $(\ell+1)$, for the fixed-end condition. (Since the ends of the pile

are fixed, the entries in F_p^j corresponding to node $(\ell+1)$ are zero.)

If, in addition, one denotes the dynamic stiffness matrix of pile j by K_p^j, and the vector of external forces and moments at the two ends of this pile by P_e^j, that is

$$P_e^j = [R_{ox}^j \; M_{ox}^j \; R_{oy}^j \; M_{oy}^j \; R_{oz}^j \; R_{(\ell+1)x}^j \; M_{(\ell+1)x}^j \; R_{(\ell+1)y}^j \; M_{(\ell+1)y}^j \; R_{(\ell+1)z}^j]^T \quad (2.5)$$

Then one can write

$$P_e^j = K_p^j \, U_e^j + \psi^{j^T} P^j \quad (2.6)$$

The first term in Eq. (2.6) corresponds to pile-end forces due to pile-end displacements (U_e^j) when there are no loads on the pile, and the second term corresponds to pile-end forces due to loads on the pile ($-P^j$) when the two ends of the pile are fixed. Since the forces at the pile tips are included in P^j and matrices F_p^j and ψ^j are constructed such that they contain the effects of forces and displacements at this point, one has to set $R_{(\ell+1)x}^j$, $R_{(\ell+1)y}^j$ and $R_{(\ell+1)z}^j$ equal to zero. In addition, for floating piles $M_{(\ell+1)x}^j$ and $M_{(\ell+1)y}^j$ are taken to be zero as well.

Defining now the global load and displacement vectors for the N piles in the group:

$$P = \begin{Bmatrix} P^1 \\ P^2 \\ \vdots \\ P^N \end{Bmatrix} \; ; \quad U = \begin{Bmatrix} U^1 \\ U^2 \\ \vdots \\ U^N \end{Bmatrix} \; ; \quad P_e = \begin{Bmatrix} P_e^1 \\ P_e^2 \\ \vdots \\ P_e^N \end{Bmatrix} \; ; \quad U_e = \begin{Bmatrix} U_e^1 \\ U_e^2 \\ \vdots \\ U_e^N \end{Bmatrix} \quad (2.7)$$

as well as the matrices:

$$K_p = \begin{Bmatrix} K_p^1 & & & \\ & K_p^2 & & \\ & & \ddots & \\ & & & K_p^N \end{Bmatrix}$$

$$F_p = \begin{Bmatrix} F_p^1 & & & \\ & F_p^2 & & \\ & & \ddots & \\ & & & F_p^N \end{Bmatrix} \qquad (2.8)$$

$$\Psi = \begin{Bmatrix} \psi^1 & & & \\ & \psi^2 & & \\ & & \ddots & \\ & & & \psi^N \end{Bmatrix}$$

One can then write the following equations for the ensemble of piles in the group (compare with eqns. (2.3) and (2.6)):

$$\begin{cases} U = \Psi U_e - F_p P \\ P_e = K_p U_e + \Psi^T P \end{cases} \qquad (2.9)$$

Consider next the equilibrium of the soil mass under forces P (distributed uniformly over each segment; see Fig. 2.1). If F_s denotes the flexibility matrix of the soil medium, relating piecewise-constant segmental loads to the average displacements along the segments, then

$$U = F_s P \qquad (2.10)$$

Finally combining eqns. (2.9) and (2.10) one gets:

$$P_e = [K_p + \Psi^T (F_s + F_p)^{-1} \Psi]U_e = K_e U_e \qquad (2.11)$$

K_e is a (10N x 10N) matrix which relates only the five components of forces at each end of the piles to their corresponding displacements. In other words, the degrees of freedom along the pile length have been condensed out without forming a complete stiffness matrix. It is also important to notice that in the solution of eq. (2.11) it is not necessary to invert $(F_s + F_p)$ as indicated; instead, one only needs to perform a triangular decomposition of this matrix.

Matrix K_e relates forces and displacements at the pile ends in a group of unrestrained piles. In order to obtain dynamic stiffnesses of a rigid foundation (pile cap) to which the piles are connected, one needs to impose the appropriate geometric (kinematic) and force boundary conditions at the pile heads and pile tips. (The boundary conditions at pile tips, as discussed earlier, are zero forces at these points for floating piles.) At pile heads, on the other hand, the boundary conditions are in general a combination of geometric and force conditions, unless all the piles are rigidly connected to the foundation, in which case only geometric conditions should be considered. Once the pile head forces for the possible modes of vibration (horizontal, vertical, rocking and torsional) are computed, dynamic stiffnesses of the foundation at a prescribed point are obtained by simply calculating, in each mode, the resultant of these forces at the prescribed point.

To extend the formulation to seismic analysis, one only needs to express the displacements U as the summation of seismic displacements

in the medium when the piles are removed (i.e., soil with cavities) $\bar{U}$, and the displacements caused by pile-soil interface forces P, that is:

$$U = \bar{U} + F_s P \tag{2.12}$$

Combination of eqns. (2.8) and (2.12) results in

$$P_e = [K_p + \Psi^T (F_s + F_p)^{-1} \Psi] U_e - \Psi^T (F_s + F_p)^{-1} \bar{U} \tag{2.13}$$

or

$$P_e = K_e U_e + \bar{P}_e \tag{2.14}$$

where K_e (as in eq. (2.11)) is the dynamic stiffness for the ensemble of piles associated with the degrees of freedom at pile heads and pile tips, and $\bar{P}_e = - \Psi^T (F_s + F_p)^{-1} \bar{U}$ defines consistent fictitious forces at these points which reproduce the seismic effects.

In order to calculate the response of the rigid foundation to which the piles are connected, one has to impose the necessary geometric and force boundary conditions. (The procedure is similar to that described for the calculation of foundation stiffnesses, except that for the seismic case one has to use the fact that the resultant of pile-head forces on the foundation is zero.)

From the development of the preceding formulation it is clear that F_s is the flexibility of a soil mass which results from the removal of the piles; in other words, F_s corresponds to the soil mass with N cavities. Similarly, $\bar{U}$ refers to the seismic displacements in the medium with the cavities. Due to the fact that evaluation of the same quantities in a uniform soil mass, in which the cavities have been filled with

the soil, requires much less computational effort than the original problem, it is very desirable to modify the formulation in order to make use of this numerical efficiency. The following discussion pertains to such a modification.

Consider the semi-infinite soil medium and the pile shown in Fig. 2.2a. It is assumed that p(z) and u(z) define lateral soil pressure and lateral pile displacement, respectively. (For convenience, only one pile and one type of force at the pile-soil interface are considered. The modification procedure, however, is independent of the number of piles and the type of interaction force.) For a pile element shown in Fig. 2.2b, one can write the equilibrium equation as:

$$\frac{dV}{dz} + \rho_p A\omega^2 u = p \qquad (2.15)$$

in which A and ρ_p denote the cross-sectional area and mass density of the pile, respectively.

Next, consider the same soil medium except that the pile is removed and the resulting cavity is filled with soil such that the original uniform soil mass (before the installation of the pile) is obtained. The dashed line in Fig. 2.2c shows the periphery of the added soil column. Further, suppose that f(z) defines a force distribution along the height of the soil column which causes approximately the same displacement u(z) at the centerline of this soil column. Now consider the equilibrium of forces on a soil differential element shown in Fig. 2.2d. (The vertical sides of this element extend just beyond the dashed line); one can then write:

$$\frac{dV'}{dz} + \rho_s A\omega^2 u + f = p' \qquad (2.16)$$

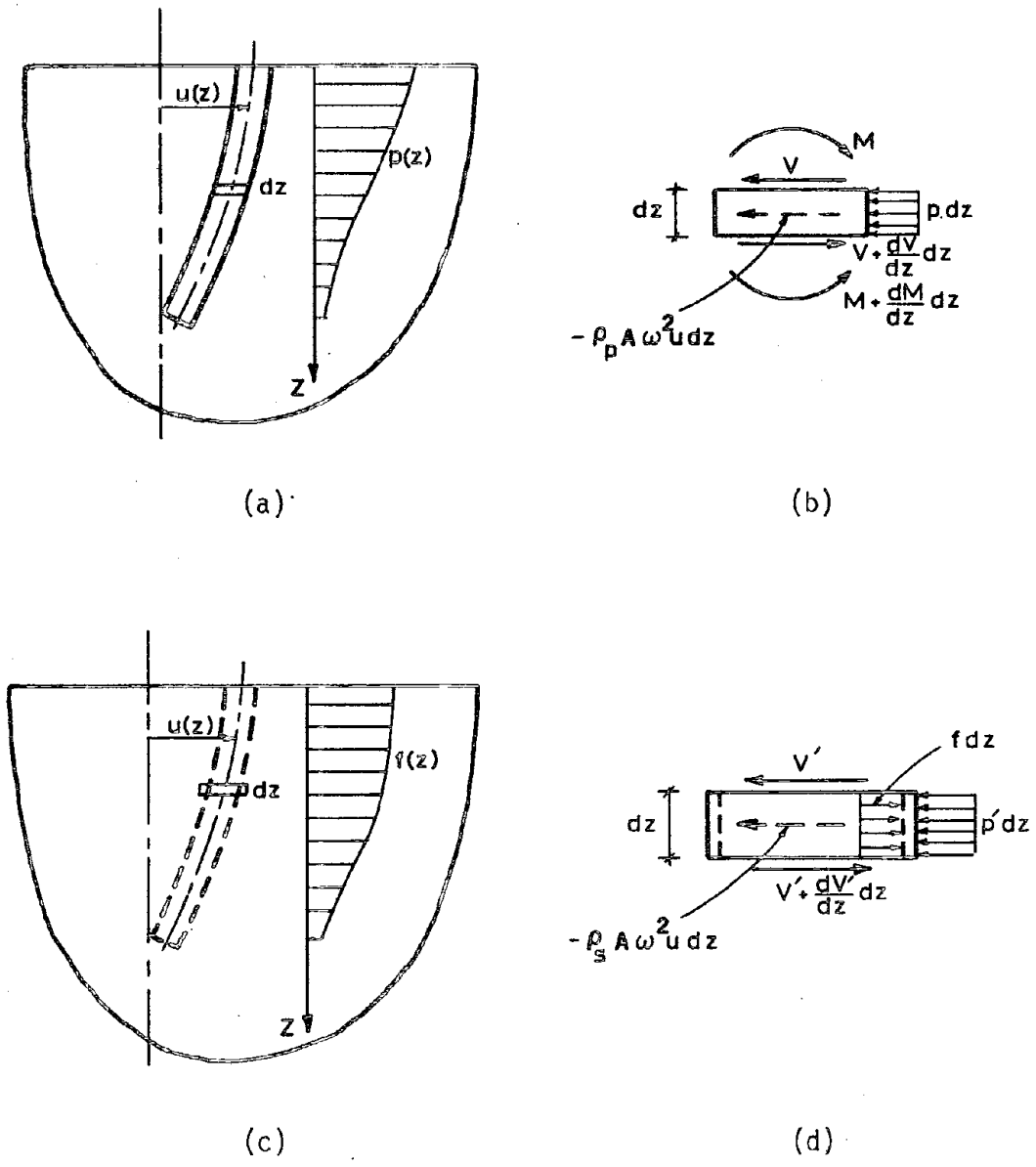

Fig. 2.2 - Forces on the Pile and in the Free Field.

where p' is the lateral force on the element. This equation implies that one can remove the soil column and apply the distributed force p' on the cavity's wall to preserve the equilibrium of the soil mass. (This is clearly an approximate scheme, since the effects of frictional forces due to the lateral displacement of the soil column are neglected.)

If one takes p' to be equal to p, eq. (2.16) can be rewritten as

$$\frac{dV'}{dz} + \rho_s A\omega^2 u + f = p \tag{2.17}$$

Thus the displacement $u(z)$ due to a distributed force $p(z)$ in the soil mass with the cavity can be reproduced by the application of the distributed force $f(z)$ to the uniform (no cavity) soil medium. $f(z)$ is given by:

$$f = p - \rho_s A\omega^2 u - \frac{dV'}{dz} \tag{2.18}$$

Similarly, the equilibrium of the differential pile element can be expressed in terms of the distributed force f; introducing eq. (2.17) into eq. (2.15), one gets:

$$\frac{d}{dz}(V - V') + (\rho_p - \rho_s)A\omega^2 u = f \tag{2.19}$$

Eq. (2.19) can be interpreted as the differential equation of a beam with a mass density $(\rho_p - \rho_s)$ and a modulus of elasticity $(E_p - E_s)$ and subjected to a distributed force $f(z)$. (E_s is the elasticity modulus of the soil.)

The approximate scheme presented here suggests that if one replaces P in eqns. (2.9) and (2.10) by the vectorial equivalent of the distributed forces f (say, F), then the soil flexibility matrix F_s should be taken

as that corresponding to a uniform (no cavity) soil mass and the matrices K_p, F_p and Ψ corresponding to piles with reduced mass density and elasticity modulus (obtained by subtracting the mass density and elasticity modulus of the soil from the corresponding quantities of the piles). The final expression relating pile-head forces with displacements is then of the same form as that given by eq. (2.11), except that F_s corresponds to a soil without cavities, and K_p, F_p, Ψ to piles with reduced properties.

A similar modification applies to the seismic analysis. In addition, the seismic displacements in the soil mass with the cavities ($\overline{U}$ in eq. 2.12)) can be related to the associated free-field (no cavity) seismic displacements. If the free-field displacements are denoted by U^* and the corresponding free-field forces are denoted by P^*, then one can write: (since $\overline{P} = 0$):

$$\overline{U} = U^* - F_s P^* \tag{2.20}$$

However, the effect of free-field forces, in most pile-soil interaction problems, can be neglected. Therefore one might approximate $\overline{U}$ by U^* in the formulation of the seismic problem.

In what follows a numerical technique to evaluate a soil flexibility matrix is presented, and expressions for the elements of K_p, F_p and Ψ are derived.

2.2 Response of Viscoelastic Layered Soil Media to Dynamic Stress Distributions

The formulation presented in Sec. 2.1 requires the evaluation of a dynamic flexibility matrix, F_s, for the soil medium. This matrix defines a relationship between piecewise-uniform loads distributed over cylindrical or circular surfaces (corresponding to pile shafts and pile tips) and the average displacement of these regions. Although there are a number of ways to obtain a value to represent the displacement of a loaded region, the weighted averaging, originally proposed by Arnold, Bycroft and Warburton (1955), is believed to provide the most meaningful displacement value. In order to understand the basis for the weighted average displacement, consider the response of a medium to a set of distributed loads q_1, q_2, ... acting on regions D_1, D_2 .... , respectively. Suppose a virtual displacement $v(x,y,z)$ is introduced in the medium. If the component of this displacement in the direction of q_i is denoted by $v_i(x,y,z)$, then the virtual work done by the total dynamic force $Q_i = \int_{D_i} q_i \, dA$ is given by:

$$Q_i \, \bar{v}_i = \int_{D_i} q_i \, v_i \, dA \tag{2.21}$$

where $\bar{v}_i$ is the weighted average virtual displacement in region D_i. Equation (2.21) shows that, on the basis of the work done by the total force, the weighted average displacement is the most appropriate quantity to represent the displacement field. For uniformly distributed loads, as eq. (2.21) indicates, the weighted average displacement is identical to the average displacement in the region.

The objective of this section is to present details of a numerical technique which enables one to compute displacements caused by loads uniformly distributed over cylindrical or circular surfaces in layered viscoelastic soil media. The types of load involved in the problem are shown in Fig. 2.3; the loads on cylindrical surfaces are associated with stresses on pile shaft and those on circular surfaces correspond to pile tip stresses.

The method used here for response calculation is similar to that presented by Apsel (1980). For the present work, however, the stiffness approach, based on assemblage of layer stiffness matrices, is used.

2.2.1 - Solution of the equations of motion

If u_r, u_θ and u_z are the displacements in the radial, tangential, and vertical directions, and f_r, f_θ and f_z are the associated external loads per unit volume, the equations of motion of an elastic body in cylindrical coordinates are:

$$\begin{cases} (\lambda+2\mu)\dfrac{\partial \Delta}{\partial r} - \dfrac{2\mu}{r}\dfrac{\partial \omega_z}{\partial \theta} + 2\mu\dfrac{\partial \omega_\theta}{\partial z} + \omega^2 \rho u_r + f_r = 0 \\ (\lambda+2\mu)\dfrac{1}{r}\dfrac{\partial \Delta}{\partial \theta} - 2\mu\dfrac{\partial \omega_r}{\partial z} + 2\mu\dfrac{\partial \omega_z}{\partial r} + \omega^2 \rho u_\theta + f_\theta = 0 \\ (\lambda+2\mu)\dfrac{\partial \Delta}{\partial z} - \dfrac{2\mu}{r}\dfrac{\partial}{\partial r}(r\omega_\theta) + \dfrac{2\mu}{r}\dfrac{\partial \omega_r}{\partial \theta} + \omega^2 \rho u_z + f_z = 0 \end{cases} \qquad (2.22)$$

where λ and μ are Lamé's constant, ρ is the mass density, and ω is the frequency of steady-state vibration; the dilatation Δ and the rotations ω_r, ω_θ and ω_z are given by:

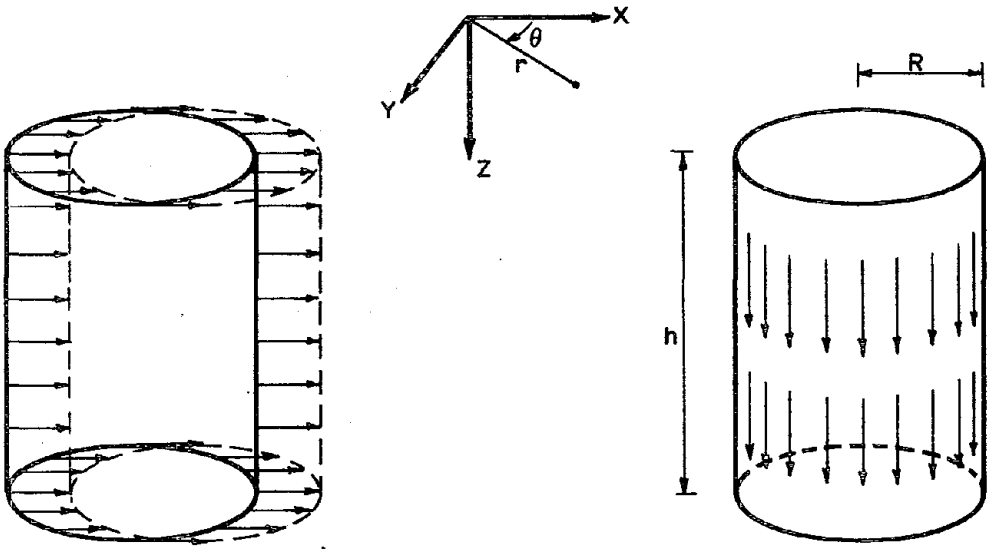

a) uniform horizontal load on cylindrical surface

b) uniform vertical load on cylindrical surface

c) uniform horizontal load on circular surface

d) uniform vertical load on circular surface

Fig. 2.3 - The Type of Loads in the Soil Medium.

$$\Delta = \frac{1}{r}\frac{\partial}{\partial r}(ru_r) + \frac{1}{r}\frac{\partial u_\theta}{\partial \theta} + \frac{\partial u_z}{\partial z} \tag{2.23}$$

$$\begin{cases} \omega_r = \frac{1}{2}\left[\frac{1}{r}\frac{\partial u_z}{\partial \theta} - \frac{\partial u_\theta}{\partial z}\right] \\ \omega_\theta = \frac{1}{2}\left[\frac{\partial u_r}{\partial z} - \frac{\partial u_z}{\partial r}\right] \\ \omega_z = \frac{1}{2r}\left[\frac{\partial}{\partial r}(ru_\theta) - \frac{\partial u_r}{\partial \theta}\right] \end{cases} \tag{2.24}$$

For a viscoelastic medium with an internal energy dissipative behavior of the hysteretic type, one only needs to replace λ and μ in Eqns. (2.22) by the complex Lamé moduli given by:

$$\begin{cases} \lambda^c = \lambda(1 + 2\beta i) \\ \mu^c = \mu(1 + 2\beta i) \end{cases} \tag{2.25}$$

where β is commonly referred to as the fraction of critical damping.

The first step in the solution of Eqns. (2.22) is to separate variables. This can be achieved by expanding displacements and body forces in a Fourier series in tangential direction, that is

$$\begin{cases} u_r(r,\theta,z) = \sum_{n=0}^{\infty} u_{rn}(r,z)\cos n\theta \\ u_\theta(r,\theta,z) = \sum_{n=0}^{\infty} u_{\theta n}(r,z)\sin n\theta \\ u_z(r,\theta,z) = \sum_{n=0}^{\infty} u_{zn}(r,z)\cos n\theta \\ f_r(r,\theta,z) = \sum_{n=0}^{\infty} f_{rn}(r,z)\cos n\theta \\ f_\theta(r,\theta,z) = \sum_{n=0}^{\infty} f_{\theta n}(r,z)\sin n\theta \\ f_z(r,\theta,z) = \sum_{n=0}^{\infty} f_{zn}(r,z)\cos n\theta \end{cases} \tag{2.26}$$

Introduction of these expansions, along with Eqns. (2.23) and (2.24), into Eqns. (2.22) leads to

$$\sum_{n=0}^{\infty} \left\{\mu\left[\frac{\partial^2 u_{rn}}{\partial r^2} + \frac{1}{r}\frac{\partial u_{rn}}{\partial r} - \frac{n^2+1}{r^2} u_{rn} + \frac{\partial^2 u_{rn}}{\partial z^2}\right] + (\lambda+\mu)\frac{\partial \Delta_n}{\partial r}\right.$$

$$\left. - 2\mu \frac{n}{r^2} u_{\theta n} + \omega^2 \rho u_{rn} + f_{rn}\right\} \cos n\theta = 0 \qquad (2.27)$$

$$\sum_{n=0}^{\infty} \left\{\mu\left[\frac{\partial^2 u_{\theta n}}{\partial r^2} + \frac{1}{r}\frac{\partial u_{\theta n}}{\partial r} - \frac{n^2+1}{r^2} u_{\theta n} + \frac{\partial^2 u_{\theta n}}{\partial z^2}\right] - (\lambda+\mu)\frac{n}{r}\Delta_n\right.$$

$$\left. -2\mu \frac{n}{r^2} u_{rn} + \omega^2 \rho u_{\theta n} + f_{\theta n}\right\} \sin n\theta = 0 \qquad (2.28)$$

$$\sum_{n=0}^{\infty} \left\{\mu\left[\frac{\partial^2 u_{zn}}{\partial r^2} + \frac{1}{r}\frac{\partial u_{zn}}{\partial r} - \frac{n^2}{r^2} u_{zn} + \frac{\partial^2 u_{zn}}{\partial z^2}\right] + (\lambda+\mu)\frac{\partial \Delta_n}{\partial z}\right.$$

$$\left. + \omega^2 \rho u_{zn} + f_{zn}\right\} \cos n\theta = 0 \qquad (2.29)$$

where

$$\Delta_n = \frac{1}{r}\frac{\partial}{\partial r}(r u_{rn}) + \frac{n}{r} u_{\theta n} + \frac{\partial u_{zn}}{\partial z} \qquad (2.30)$$

In order that Eqns. (2.27), (2.28) and (2.29) be satisfied, it is necessary that the terms in accolades be identically zero. If, in addition, one combines the two equations resulting from (2.27) and (2.28), then the following three conditions, to be satified for any value of n, are obtained:

$$\mu\left[\frac{\partial^2}{\partial r^2}(u_{rn}+u_{\theta n}) + \frac{1}{r}\frac{\partial}{\partial r}(u_{rn}+u_{\theta n}) - \frac{(n+1)^2}{r^2}(u_{rn}+u_{\theta n}) + \frac{\partial^2}{\partial z^2}(u_{rn}+u_{\theta n})\right]$$

$$+ (\lambda+\mu)\left(\frac{\partial \Delta_n}{\partial r} - \frac{n}{r}\Delta_n\right) + \omega^2 \rho (u_{rn}+u_{\theta n}) + (f_{rn}+f_{\theta n}) = 0 \qquad (2.31)$$

$$\mu\left[\frac{\partial^2}{\partial r^2}(u_{rn}-u_{\theta n})+\frac{1}{r}\frac{\partial}{\partial r}(u_{rn}-u_{\theta n})-\frac{(n-1)^2}{r^2}(u_{rn}-u_{\theta n})+\frac{\partial^2}{\partial z^2}(u_{rn}-u_{\theta n})\right]$$

$$+(\lambda+\mu)\left[\frac{\partial \Delta_n}{\partial r}+\frac{n}{r}\Delta_n\right]+\omega^2\rho(u_{rn}-u_{\theta n})+(f_{rn}-f_{\theta n})=0 \qquad (2.32)$$

$$\mu\left[\frac{\partial^2 u_{zn}}{\partial r^2}+\frac{1}{r}\frac{\partial u_{zn}}{\partial r}-\frac{n^2}{r^2}u_{zn}+\frac{\partial^2 u_{zn}}{\partial z^2}\right]+(\lambda+\mu)\frac{\partial \Delta_n}{\partial z}+\omega^2\rho u_{zn}+f_{zn}=0 \qquad (2.33)$$

If now the following Hankel Transforms are defined

$$\begin{cases} u_{1n}(k,z)+u_{3n}(k,z)=\int_0^\infty (u_{rn}+u_{\theta n})J_{n+1}(kr)\,rdr \\ -u_{1n}(k,z)+u_{3n}(k,z)=\int_0^\infty (u_{rn}-u_{\theta n})J_{n-1}(kr)\,rdr \\ u_{2n}(k,z)=\int_0^\infty u_{zn}J_n(kr)\,rdr \\ f_{1n}(k,z)+f_{3n}(k,z)=\int_0^\infty (f_{rn}+f_{\theta n})J_{n+1}(kr)\,rdr \\ -f_{1n}(k,z)+f_{3n}(k,z)=\int_0^\infty (f_{rn}-f_{\theta n})J_{n-1}(kr)\,rdr \\ f_{2n}(k,z)=\int_0^\infty f_{zn}J_n(kr)\,rdr \end{cases} \qquad (2.34)$$

where $J_n(kr)$ is the n^{th} order Bessel function of the 1^{st} kind, and if the following identities are used,

$$\int_0^\infty\left[\frac{\partial^2}{\partial r^2}+\frac{1}{r}\frac{\partial}{\partial r}-\frac{m^2}{r^2}+\frac{\partial^2}{\partial z^2}\right]\phi J_m(kr)\,rdr=\left(\frac{d^2}{dz^2}-k^2\right)\int_0^\infty \phi J_m(kr)\,rdr \qquad (2.35)$$

$$\int_0^\infty \left(\frac{d}{dr} - \frac{m}{r}\right) \phi \, J_{m+1} (kr) \, rdr = -k \int_0^\infty \phi \, J_m (kr) \, rdr \tag{2.36}$$

$$\int_0^\infty \left(\frac{d}{dr} + \frac{m}{r}\right) \phi \, J_{m-1} (kr) \, rdr = k \int_0^\infty \phi \, J_m (kr) \, rdr \tag{2.37}$$

Then one can show that application of Hankel Transforms to Eqns. (2.31), (2.32) and (2.33) leads to:

$$\begin{cases} \mu \left[\frac{d^2}{dz^2} - k^2 + \omega^2 \frac{\rho}{\mu}\right](u_{1n} + u_{3n}) + (\lambda+\mu)(-k \, \Delta_n') + f_{1n} + f_{3n} = 0 & (2.38) \\ \mu \left[\frac{d^2}{dz^2} - k^2 + \omega^2 \frac{\rho}{\mu}\right](-u_{1n} + u_{3n}) + (\lambda+\mu)(k \, \Delta_n') - f_{1n} + f_{3n} = 0 & (2.39) \\ \mu \left[\frac{d^2}{dz^2} - k^2 + \omega^2 \frac{\rho}{\mu}\right] u_{2n} + (\lambda+\mu) \frac{d}{dz} \Delta_n' + f_{2n} = 0 & (2.40) \end{cases}$$

where $\Delta_n' = \int_0^\infty \Delta_n \, J_n (kr) \, rdr$ is the n^{th} order Hankel Transform of Δ_n. Using Eqns. (2.36) and (2.37) and the following property of Bessel functions,

$$\frac{n}{r} J_n (kr) = \pm \frac{d}{dr} J_n (kr) + k \, J_{n\pm1} (kr) \tag{2.41}$$

one can show that

$$\Delta_n' = k u_{1n} + \frac{d}{dz} u_{2n} \tag{2.42}$$

Finally, if one introduces Eq. (2.42) into Eqns. (2.38) - (2.40), and Eqns. (2.38) and (2.39) are combined (by adding and subtracting them), the following ordinary differential equations are obtained:

$$\left\{ \left[\mu \frac{d^2}{dz^2} - k^2 (\lambda+2\mu) + \rho\omega^2\right] u_{1n} - (\lambda+\mu)\, k \frac{d}{dz} u_{2n} + f_{1n} = 0 \right. \tag{2.43}$$

$$\left. (\lambda+\mu)\, k \frac{d}{dz} u_{1n} + \left[(\lambda+2\mu) \frac{d^2}{dz^2} - \mu k^2 + \rho\omega^2\right] u_{2n} + f_{2n} = 0 \right\} \tag{2.44}$$

$$\left(\mu \frac{d^2}{dz^2} - \mu k^2 + \rho\omega^2\right) u_{3n} + f_{3n} = 0 \tag{2.45}$$

Equations (2.43) and (2.44) define a system of two ordinary linear differential equations for u_{1n} and u_{2n}. u_{3n}, on the other hand, is uncoupled from u_{1n} and u_{2n} and can be obtained by solving Eq. (2.45).

It is convenient at this point to introduce the following two parameters:

$$\alpha = \sqrt{k^2 - \frac{\rho\omega^2}{\lambda+2\mu}} = \sqrt{k^2 - \frac{\omega^2}{C_p^2}} \tag{2.46}$$

$$\gamma = \sqrt{k^2 - \frac{\rho\omega^2}{\mu}} = \sqrt{k^2 - \frac{\omega^2}{C_s^2}} \tag{2.47}$$

where C_s and C_p are the velocities of shear waves and pressure waves, respectively. (For viscoelastic materials C_s and C_p are complex quantities). Introduction of these parameters into Eqns. (2.43), (2.44) and (2.45) leads to:

$$\left\{ (\lambda+2\mu)\left[\frac{\mu}{\lambda+2\mu} \frac{d^2}{dz^2} - \alpha^2\right] u_{1n} - (\lambda+\mu)\, k \frac{d}{dz} u_{2n} + f_{1n} = 0 \right. \tag{2.48a}$$

$$\left. (\lambda+\mu)\, k \frac{d}{dz} u_{1n} + \mu\left[\frac{\lambda+2\mu}{\mu} \frac{d^2}{dz^2} - \gamma^2\right] u_{2n} + f_{2n} = 0 \right\} \tag{2.48b}$$

$$\mu\left(\frac{d^2}{dz^2} - \gamma^2\right) u_{3n} + f_{3n} = 0 \tag{2.49}$$

In order to obtain the homogenous solution of Eqns. (2.48), one can take $u_{1n} = Ae^{\eta z}$ and $u_{2n} = Be^{\eta z}$ and substitute in Eqns. (2.48). The

resulting system of algebraic equations for η and A/B yields four sets of solutions, which can be used to define the general homogeneous solutions for u_{1n} and u_{2n}. Following this procedure, one obtains:

$$\begin{cases} u_{1n}^{H}(k,z) = -k\,C_{1n}\,e^{-\alpha z} + \gamma\,C_{2n}\,e^{-\gamma z} - k\,C_{3n}\,e^{\alpha z} + \gamma\,C_{4n}\,e^{\gamma z} \\ u_{2n}^{H}(k,z) = -\alpha\,C_{1n}\,e^{-\alpha z} + k\,C_{2n}\,e^{-\gamma z} + \alpha\,C_{3n}\,e^{\alpha z} - k\,C_{4n}\,e^{\gamma z} \end{cases} \tag{2.50}$$

where $C_{1n}(k)$, $C_{2n}(k)$, $C_{3n}(k)$ and $C_{4n}(k)$ are unknown constants. To obtain a particular solution one can use the method of variation of parameters; however, for the loadings involved in the present problem, f_{1n} and f_{2n}, as will be shown in section 2.2.4, are independent of z; therefore particular solutions can be obtained by inspection. One such set of solutions for u_{1n} and u_{2n} are:

$$\begin{cases} u_{1n}^{P} = \dfrac{1}{\alpha^2(\lambda+2\mu)}\, f_{1n} \\ u_{2n}^{P} = \dfrac{1}{\gamma^2\mu}\, f_{2n} \end{cases} \tag{2.51}$$

Finally, the solutions of Eqns. (2.48) are given by:

$$\begin{Bmatrix} u_{1n}(k,z) \\ u_{2n}(k,z) \end{Bmatrix} = \begin{bmatrix} -k & \gamma & -k & \gamma \\ -\alpha & k & \alpha & -k \end{bmatrix} \begin{Bmatrix} C_{1n}\,e^{-\alpha z} \\ C_{2n}\,e^{-\gamma z} \\ C_{3n}\,e^{\alpha z} \\ C_{4n}\,e^{\gamma z} \end{Bmatrix} + \begin{Bmatrix} f_{1n}/\alpha^2(\lambda+2\mu) \\ f_{2n}/\gamma^2\mu \end{Bmatrix} \tag{2.52}$$

A similar procedure applied to Eq. (2.49) leads to the solution of this equation:

$$u_{3n}(k,z) = \begin{bmatrix} 1 & 1 \end{bmatrix} \begin{Bmatrix} C_{5n}\, e^{-\gamma z} \\ C_{6n}\, e^{\gamma z} \end{Bmatrix} + \frac{1}{\gamma^2 \mu} f_{3n} \tag{2.53}$$

2.2.2 - Layer and halfspace stiffness matrices

In order to determine the unknown constants in Eqns. (2.52) and (2.53) it is necessary to use the appropriate kinematic and force boundary conditions of the problem. Since Eqns. (2.52) and (2.53) express displacements in the transformed space, it is necessary to derive expressions for the associated transformed stresses.

The three components of stress on a plane perpendicular to the z-axis in cylindrical coordinates are given by:

$$\begin{cases} \sigma_{rz} = \mu\left(\dfrac{\partial u_z}{\partial r} + \dfrac{\partial u_r}{\partial z}\right) \\ \sigma_{\theta z} = \mu\left(\dfrac{\partial u_\theta}{\partial z} + \dfrac{1}{r}\dfrac{\partial u_z}{\partial \theta}\right) \\ \sigma_{zz} = 2\mu\dfrac{\partial u_z}{\partial z} + \lambda\Delta \end{cases} \tag{2.54}$$

If the Fourier expansion of u_r, u_θ and u_z, given by Eq. (2.26), are used in the above equations, one gets

$$\begin{cases} \sigma_{rz} = \sum_{n=0}^{\infty} \sigma_{rzn} \cos n\theta \\ \sigma_{\theta z} = \sum_{n=0}^{\infty} \sigma_{\theta zn} \sin n\theta \\ \sigma_{zz} = \sum_{n=0}^{\infty} \sigma_{zzn} \cos n\theta \end{cases} \tag{2.55}$$

where σ_{rzn}, $\sigma_{\theta zn}$ and σ_{zzn} are given by

$$\begin{cases} \sigma_{rzn} = \mu\left(\dfrac{\partial u_{zn}}{\partial r} + \dfrac{\partial u_{rn}}{\partial z}\right) & (2.56) \\ \sigma_{\theta zn} = \mu\left(\dfrac{\partial u_{\theta n}}{\partial z} - \dfrac{n}{r} u_{zn}\right) & (2.57) \\ \sigma_{zzn} = 2\mu \dfrac{\partial u_{zn}}{\partial z} + \lambda \Delta_n & (2.58) \end{cases}$$

and Δ_n is given by Eq. (2.30).

By combining Eqns. (2.56) and (2.57) and reordering Eq. (2.58), one can write:

$$\begin{cases} \sigma_{rzn} + \sigma_{\theta zn} = \mu\left[\dfrac{\partial u_{zn}}{\partial r} - \dfrac{n}{r} u_{zn} + \dfrac{\partial}{\partial z}(u_{rn} + u_{\theta n})\right] \\ \sigma_{rzn} - \sigma_{\theta zn} = \mu\left[\dfrac{\partial u_{zn}}{\partial r} + \dfrac{n}{r} u_{zn} + \dfrac{\partial}{\partial z}(u_{rn} - u_{\theta n})\right] & (2.59) \\ \sigma_{zzn} = (\lambda+2\mu) \dfrac{\partial u_{zn}}{\partial z} + \lambda\left(\dfrac{\partial u_{rn}}{\partial r} + \dfrac{u_{rn}}{r} + \dfrac{n}{r} u_{\theta n}\right) \end{cases}$$

If the following Hankel Transforms are defined,

$$\begin{cases} \sigma_{21n}(k,z) + \sigma_{23n}(k,z) = \displaystyle\int_0^\infty (\sigma_{rzn} + \sigma_{\theta zn})\, J_{n+1}(kr)\, r\,dr \\ -\sigma_{21n}(k,z) + \sigma_{23n}(k,z) = \displaystyle\int_0^\infty (\sigma_{rzn} - \sigma_{\theta zn})\, J_{n-1}(kr)\, r\,dr & (2.60) \\ \sigma_{22n}(k,z) = \displaystyle\int_0^\infty \sigma_{zzn}\, J_n(kr)\, r\,dr \end{cases}$$

Then Hankel transforms of Eqns. (2.59) leads to:

$$\begin{cases} \sigma_{21n} + \sigma_{23n} = \mu\left[-\, ku_{2n} + \dfrac{d}{dz}\,(u_{1n} + u_{3n})\right] \\ -\sigma_{21n} + \sigma_{23n} = \mu\left[ku_{2n} + \dfrac{d}{dz}\,(-\, u_{1n} + u_{3n})\right] \\ \sigma_{22n} = (\lambda+2\mu)\,\dfrac{du_{2n}}{dz} + \lambda(ku_{1n}) \end{cases} \tag{2.61}$$

Finally by using the expressions obtained for u_{1n}, u_{2n}, and u_{3n} (Eqns. (2.52) and (2.53)), one can express the transformed stresses σ_{21n}, σ_{23n}, and σ_{22n} as:

$$\begin{Bmatrix} \sigma_{21n}(k,z) \\ \sigma_{22n}(k,z) \end{Bmatrix} = \mu \begin{bmatrix} 2\alpha k & -(k^2+\gamma^2) & -2\alpha k & (k^2+\gamma^2) \\ (k^2+\gamma^2) & -2\gamma k & (k^2+\gamma^2) & -2\gamma k \end{bmatrix} \begin{Bmatrix} C_{1n}\, e^{-\alpha z} \\ C_{2n}\, e^{-\gamma z} \\ C_{3n}\, e^{\alpha z} \\ C_{4n}\, e^{\gamma z} \end{Bmatrix} + \begin{Bmatrix} -kf_{2n}/\gamma^2 \\ \lambda k f_{1n}/\alpha^2(\lambda+2\mu) \end{Bmatrix} \tag{2.62}$$

$$\sigma_{23n}(k,z) = \mu\,[-\gamma \quad \gamma] \begin{Bmatrix} C_{5n}\, e^{-\gamma z} \\ C_{6n}\, e^{\gamma z} \end{Bmatrix} \tag{2.63}$$

At this point it is convenient to distinguish between the solutions corresponding to u_{1n} and u_{2n} and those corresponding to u_{3n}. Since the solution of u_{3n} involves only γ, all quantities associated with u_{3n} will be identified as "SH-wave" quantities. In a similar manner, "SV-P waves" will be used to refer to quantities associated with u_{1n} and u_{2n}.

Consider the layered soil medium shown in Fig. 2.4a. The medium consists of M layers resting on a halfspace. Fig. 2.4b shows the j^{th}

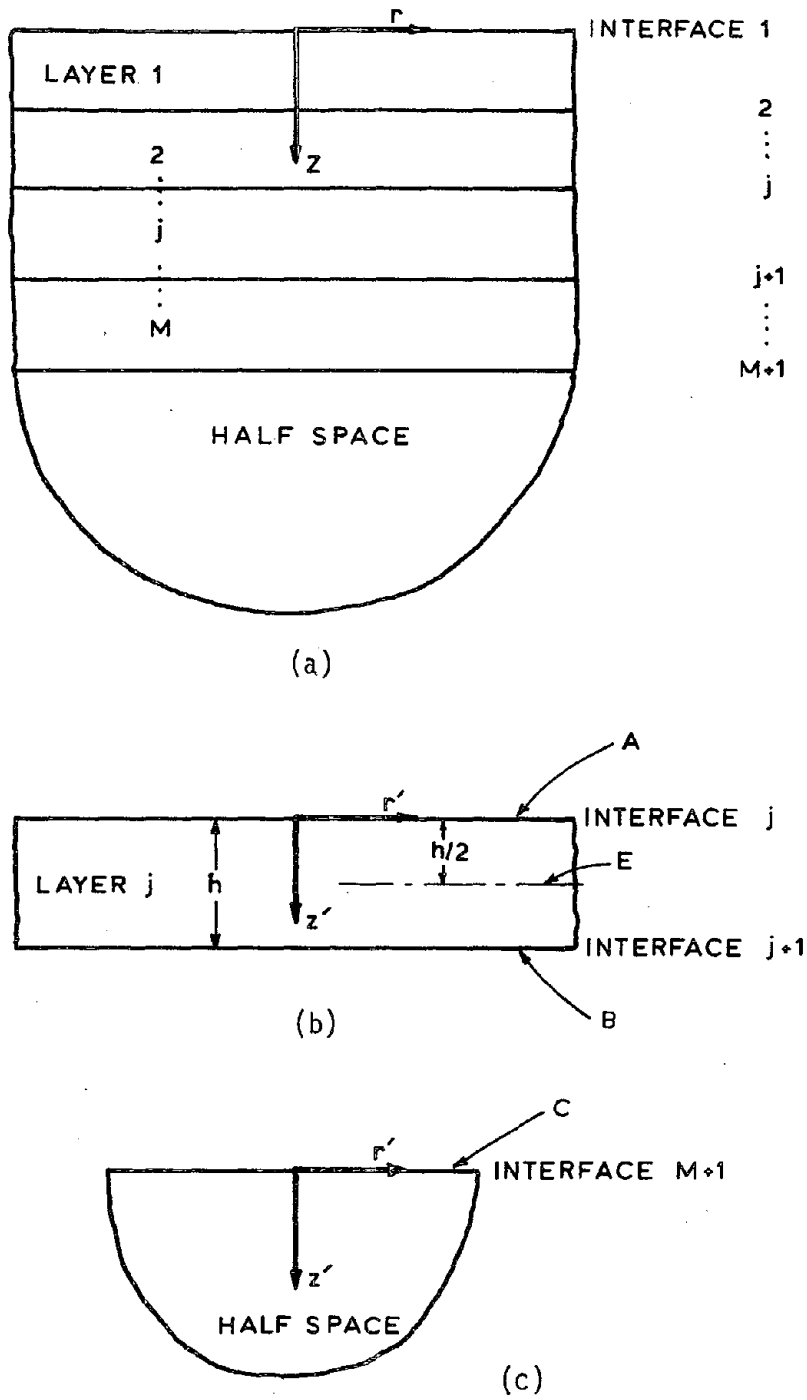

Fig. 2.4 - A Layered Soil Medium.

layer confined between the two planes denoted by A and B, and Fig. 2.4c shows the halfspace bounded by the plane C. The objective is now to obtain a relationship between the transformed stresses on the two planes A and B in Fig. 2.4b and the transformed displacements of these planes. Such a relationship can be used to define layer "stiffness matrices" as well as layer "fixed-end stresses." In a similar manner, a relationship between stresses and displacements for plane C in Fig. 2.4c results in halfspace stiffness matrices. For a given value of k, the stiffness matrices of the layers and the halfspace and the associated force vectors can be used to assemble the stiffness matrix and the load vector for the layered medium; the resulting system of equations then yields the transformed displacements u_{1n}, u_{2n} and u_{3n} at layer interfaces.

Layer stiffness matrix and load vector for SV-P waves

For the layer shown in Fig. 2.4b, one can use Eq. (2.52) to obtain the expressions for the transformed displacements u_{1n} and u_{2n} of the two planes A and B associated with local coordinates $z' = 0$, and $z' = h$; the result can be written in matrix form as

$$\begin{Bmatrix} u_{1n}^{A} - \bar{u}_{1n} \\ u_{2n}^{A} - \bar{u}_{2n} \\ u_{1n}^{B} - \bar{u}_{1n} \\ u_{2n}^{B} - \bar{u}_{2n} \end{Bmatrix} = \begin{bmatrix} -k & \gamma & -k & \gamma \\ -\alpha & k & \alpha & -k \\ -ke^{-\alpha h} & \gamma e^{-\gamma h} & -ke^{\alpha h} & \gamma e^{\gamma h} \\ -\alpha e^{-\alpha h} & ke^{-\gamma h} & \alpha e^{\alpha h} & -ke^{\gamma h} \end{bmatrix} \begin{Bmatrix} C_{1n} \\ C_{2n} \\ C_{3n} \\ C_{4n} \end{Bmatrix} \qquad (2.64)$$

where $\bar{u}_{1n}$ and $\bar{u}_{2n}$ are given by:

$$\begin{cases} \bar{u}_{1n} = f_{1n}/\alpha^2(\lambda+2\mu) & (2.65) \\ \bar{u}_{2n} = f_{2n}/\gamma^2\mu & (2.66) \end{cases}$$

Similarly, Eq. (2.62) can be used to express the transformed stresses σ_{21n} and σ_{22n} on the exterior side of planes A and B as:

$$\begin{Bmatrix} \sigma^A_{21n} + \bar{\sigma}_{21n} \\ \sigma^A_{22n} + \bar{\sigma}_{22n} \\ \sigma^B_{21n} - \bar{\sigma}_{21n} \\ \sigma^B_{22n} - \bar{\sigma}_{22n} \end{Bmatrix} = \mu \begin{bmatrix} -2\alpha k & (k^2+\gamma^2) & 2\alpha k & -(k^2+\gamma^2) \\ -(k^2+\gamma^2) & 2\gamma k & -(k^2+\gamma^2) & 2\gamma k \\ 2\alpha k e^{-\alpha h} & -(k^2+\gamma^2)e^{-\gamma h} & -2\alpha k e^{\alpha h} & (k^2+\gamma^2)e^{\gamma h} \\ (k^2+\gamma^2)e^{-\alpha h} & -2\gamma k e^{-\gamma h} & (k^2+\gamma^2)e^{\alpha h} & -2\gamma k e^{\gamma h} \end{bmatrix} \begin{Bmatrix} C_{1n} \\ C_{2n} \\ C_{3n} \\ C_{4n} \end{Bmatrix} \quad (2.67)$$

where $\bar{\sigma}_{21n}$ and $\bar{\sigma}_{22n}$ are given by:

$$\begin{cases} \bar{\sigma}_{21n} = -kf_{2n}/\gamma^2 & (2.68) \\ \bar{\sigma}_{22n} = \lambda k f_{1n}/\alpha^2(\lambda+2\mu) & (2.69) \end{cases}$$

Finally a relationship between the transformed stresses (σ_{21n} and σ_{22n}) on planes A and B and the transformed displacements (u_{1n} and u_{2n}) of these planes can be obtained by deleting the unknown constants C_{1n}, C_{2n}, C_{3n} and C_{4n} between Eqns. (2.64) and (2.67). The result can be written in the form

$$\left\{\sigma^{AB}_{SV-P}\right\} = [K^{AB}_{SV-P}] \left\{u^{AB}_{SV-P}\right\} + \left\{\bar{\sigma}^{AB}_{SV-P}\right\} \quad (2.70)$$

where $\left\{\sigma^{AB}_{SV-P}\right\}$ and $\left\{u^{AB}_{SV-P}\right\}$ denote the transformed stress and displacement vectors, that is

$$\left\{\sigma^{AB}_{SV-P}\right\} = \begin{Bmatrix} \sigma^{A}_{21n} \\ \sigma^{A}_{22n} \\ \sigma^{B}_{21n} \\ \sigma^{B}_{22n} \end{Bmatrix} \quad ; \quad \left\{u^{AB}_{SV-P}\right\} = \begin{Bmatrix} u^{A}_{1n} \\ u^{A}_{2n} \\ u^{B}_{1n} \\ u^{B}_{2n} \end{Bmatrix} \tag{2.71}$$

$\left\{\bar{\sigma}^{AB}_{SV-P}\right\}$ is the vector of "fixed-end stresses" given by

$$\left\{\bar{\sigma}^{AB}_{SV-P}\right\} = -[K^{AB}_{SV-P}] \begin{Bmatrix} \bar{u}_{1n} \\ \bar{u}_{2n} \\ \bar{u}_{1n} \\ \bar{u}_{2n} \end{Bmatrix} + \begin{Bmatrix} -\bar{\sigma}_{21n} \\ -\bar{\sigma}_{22n} \\ \bar{\sigma}_{21n} \\ \bar{\sigma}_{22n} \end{Bmatrix} \tag{2.72}$$

and the elements of the symmetric 4 x 4 layer stiffness matrix $[K^{AB}_{SV-P}]$ are given by the following expressions: (AB and SV-P are omitted.)

$$K_{11} = \frac{1}{D}\,\mu\alpha(k^2 - \gamma^2)\,[\alpha\gamma S^{\alpha}C^{\gamma} - k^2 S^{\gamma}C^{\alpha}]$$

$$K_{21} = \frac{1}{D}\,\mu k\,[\alpha\gamma(3k^2+\gamma^2)(C^{\alpha}C^{\gamma} - 1) - (k^4 + k^2\gamma^2 + 2\alpha^2\gamma^2)\,S^{\alpha}S^{\gamma}]$$

$$K_{31} = \frac{1}{D}\,\mu\alpha(k^2 - \gamma^2)\,[k^2 S^{\gamma} - \alpha\gamma S^{\alpha}]$$

$$K_{41} = \frac{1}{D}\,\mu k\alpha\gamma(k^2 - \gamma^2)\,[C^{\gamma} - C^{\alpha}]$$

$$K_{22} = \frac{1}{D}\mu\gamma(k^2 - \gamma^2)\,[\alpha\gamma S^{\gamma}C^{\alpha} - k^2 S^{\alpha}C^{\gamma}]$$

$$K_{32} = -K_{41}$$

$$K_{42} = \frac{1}{D}\mu\gamma(k^2 - \gamma^2)\,[k^2 S^\alpha - \alpha\gamma S^\gamma]$$

$$K_{33} = K_{11}$$

$$K_{43} = -\,K_{21}$$

$$K_{44} = K_{22} \tag{2.73}$$

In these expressions

$$D = \alpha\gamma[-2k^2 + 2k^2 C^\alpha C^\gamma - \frac{\alpha^2\gamma^2 + k^4}{\alpha\gamma} S^\alpha S^\gamma] \tag{2.74}$$

and C^α, C^γ, S^α and S^γ are used to denote the following quantities:

$$\begin{aligned} C^\alpha &\equiv \cosh(\alpha h) \quad ; \quad S^\alpha \equiv \sinh(\alpha h) \\ C^\gamma &\equiv \cosh(\gamma h) \quad ; \quad S^\gamma \equiv \sinh(\gamma h) \end{aligned} \tag{2.75}$$

For the case in which $\frac{\omega}{kC_s} \ll 1$, one might use the asymptotic values of these expressions to avoid loss of significant digits in the operations (in fact for $\omega=0$ the above stiffness terms become indefinite; i.e., zero divided by zero). For this case, one can show that

$$K_{11} \sim \frac{2}{D'}\mu k[kh(1-\varepsilon^2) - (1+\varepsilon^2)\,S^k C^k]$$

$$K_{21} \sim \frac{2}{D'}\mu k[k^2h^2(1-\varepsilon^2)^2 - \varepsilon^2(1+\varepsilon^2)(S^k)^2]$$

$$K_{31} \sim \frac{2}{D'}\mu k[(1+\varepsilon^2)S^k - kh(1-\varepsilon^2)C^k]$$

$$K_{41} \sim -\frac{2}{D'}\mu k[kh(1-\varepsilon^2)S^k]$$

$$K_{22} \sim -\frac{2}{D'}\mu k[kh(1-\varepsilon^2) + (1+\varepsilon^2)\,S^k C^k]$$

$$K_{42} \sim \frac{2}{D'} \mu k[(1+\varepsilon^2)S^k + kh(1-\varepsilon^2)C^k] \tag{2.76}$$

where

$$D' = k^2h^2(1-\varepsilon^2)^2 - (1+\varepsilon^2)^2(S^k)^2 \ . \tag{2.77}$$

$\varepsilon = C_s/C_p$ and C^k and S^k denote the following quantities

$$C^k \equiv \cosh(kh) \quad ; \quad S^k \equiv \sinh(kh) \tag{2.78}$$

Halfspace stiffness matrix for SV-P waves

To evaluate transformed displacements and stresses in a halfspace, one can use Eqns. (2.52) and (2.62) provided that, for the forced-vibration problems, the radiation conditions are satisfied. That is, as z approaches infinity, the value of stresses and displacements should tend to zero. This requires that the unknown constants C_{3n} and C_{4n} in Eqns. (2.52) and (2.62) be set equal to zero. (The real part of α and γ is positive). Thus, for the halfspace shown in Fig. 2.4c, one can write the following expressions for the transformed displacements and stresses at plane C (surface of the halfspace) associated with the local coordinate $z' = 0$; $(f_{1n} = f_{2n} = 0)$

$$\begin{Bmatrix} u^C_{1n} \\ u^C_{2n} \end{Bmatrix} = \begin{bmatrix} -k & \gamma \\ -\alpha & k \end{bmatrix} \begin{Bmatrix} C_{1n} \\ C_{2n} \end{Bmatrix} \tag{2.79}$$

$$\begin{Bmatrix} \sigma^C_{21n} \\ \sigma^C_{22n} \end{Bmatrix} = \mu \begin{bmatrix} -2\alpha k & k^2+\gamma^2 \\ -(k^2+\gamma^2) & 2\gamma k \end{bmatrix} \begin{Bmatrix} C_{1n} \\ C_{2n} \end{Bmatrix} \tag{2.80}$$

Combining Eqns. (2.79) and (2.80), one gets:

$$\begin{Bmatrix} \sigma^C_{21n} \\ \sigma^C_{22n} \end{Bmatrix} = \left[K^C_{SV-P}\right] \begin{Bmatrix} u^C_{1n} \\ u^C_{2n} \end{Bmatrix} \tag{2.81}$$

where the symmetric 2 x 2 halfspace stiffness matrix is given by:

$$[K^C_{SV-P}] = \frac{\mu}{k^2 - \alpha\gamma} \begin{bmatrix} \alpha(k^2 - \gamma^2) & k(k^2 + \gamma^2 - 2\alpha\gamma) \\ k(k^2 + \gamma^2 - 2\alpha\gamma) & \gamma(k^2 - \gamma^2) \end{bmatrix} \tag{2.82}$$

and for the case in which $\frac{\omega}{kC_s} << 1$ by

$$[K^C_{SV-P}] \sim \frac{2\mu k}{1+\varepsilon^2} \begin{bmatrix} 1 & \varepsilon^2 \\ \varepsilon^2 & 1 \end{bmatrix} \tag{2.83}$$

and $\varepsilon = C_S/C_p$.

Layer stiffness matrix and load vector for SH waves

Following the procedure described for SV-P waves, one can use Eqns. (2.53) and (2.63) to express transformed displacements and external stresses associated with planes A and B in Fig. 2.4b as

$$\begin{Bmatrix} u^A_{3n} - \bar{u}_{3n} \\ u^B_{3n} - \bar{u}_{3n} \end{Bmatrix} = \begin{bmatrix} 1 & 1 \\ e^{-\gamma h} & e^{\gamma h} \end{bmatrix} \begin{Bmatrix} C_{5n} \\ C_{6n} \end{Bmatrix} \tag{2.84}$$

$$\begin{Bmatrix} \sigma^A_{23n} \\ \sigma^B_{23n} \end{Bmatrix} = \mu \begin{bmatrix} \gamma & -\gamma \\ -\gamma e^{-\gamma h} & \gamma e^{\gamma h} \end{bmatrix} \begin{Bmatrix} C_{5n} \\ C_{6n} \end{Bmatrix} \tag{2.85}$$

where $\bar{u}_{3n} = f_{3n}/\gamma^2\mu$. (2.86)

Combining Eqns. (2.84) and (2.85), one gets

$$\left\{\sigma_{SH}^{AB}\right\} = \left[K_{SH}^{AB}\right] \left\{u_{SH}^{AB}\right\} + \left\{\bar{\sigma}_{SH}^{AB}\right\} \tag{2.87}$$

where $\left\{\sigma_{SH}^{AB}\right\}$ and $\left\{u_{SH}^{AB}\right\}$ denote the stress and displacement vectors, that is

$$\left\{\sigma_{SH}^{AB}\right\} = \begin{Bmatrix} \sigma_{23n}^{A} \\ \sigma_{23n}^{B} \end{Bmatrix} \quad ; \quad \left\{u_{SH}^{AB}\right\} = \begin{Bmatrix} u_{3n}^{A} \\ u_{3n}^{B} \end{Bmatrix} \tag{2.88}$$

$\left\{\bar{\sigma}_{SH}^{AB}\right\}$ is the vector of "fixed-end stresses" expressed as

$$\left\{\bar{\sigma}_{SH}^{AB}\right\} = - \left[K_{SH}^{AB}\right] \begin{Bmatrix} \bar{u}_{3n} \\ \bar{u}_{3n} \end{Bmatrix} \tag{2.89}$$

and the 2 x 2 layer stiffness matrix is given by:

$$\left[K_{SH}^{AB}\right] = \frac{\gamma\mu}{\sinh(\gamma h)} \begin{bmatrix} \cosh \gamma h & -1 \\ -1 & \cosh \gamma h \end{bmatrix} \tag{2.90}$$

Halfspace stiffness constant for SH waves

The use of Eqns. (2. 53) and (2.63) with the imposition of the radiation condition leads to the following expressions for the transformed stress and displacement of plane C (Fig. 2.4c).

$$u_{3n}^{C} = C_{5n} \tag{2.91}$$

$$\sigma_{23n}^{C} = \gamma\mu C_{5n} \tag{2.92}$$

Therefore, transformed stresses and displacements at the surface of the

halfspace for SH waves are related by the following expression

$$\sigma^{C}_{23n} = \gamma\mu u^{C}_{3n} \tag{2.93}$$

2.2.3 - Displacements within a Layer

In order to obtain the average displacement in the layer one needs to compute the displacements at a number of points within the layer; these displacement values along with those at the two planes confining the layer can be used to define a displacement pattern across the layer.

Consider again the layer shown in Fig. 2.4b. Having computed the transformed displacements of planes A and B, one can use Eqns. (2.64) and (2.84) to evaluate the unknown constants C_{1n}, ... , C_{6n}. Then the transformed displacements at a point within the layer can be evaluated by using Eqns. (2.52) and (2.53).

For the present study, in addition to layer interfaces, the displacements of the middle of layers are computed. These displacement values for each layer are used to define a 2^{nd} degree polynomial to approximate the variation of displacements across that layer. The average value obtained by using this interpolation function corresponds to the well-known Simpson's Rule.

Explicit expressions for the mid-layer transformed displacements are given next.

Mid-layer displacements for SV-P Waves

The transformed displacements of the mid-plane of the layer shown in Fig. 2.4b (Plane E) are related to those of planes A and B by the following expression:

$$\begin{Bmatrix} u^E_{1n} \\ u^E_{2n} \end{Bmatrix} = [T^E_{SV\text{-}P}] \begin{Bmatrix} u^A_{1n} - \bar{u}_{1n} \\ u^A_{2n} - \bar{u}_{2n} \\ u^B_{1n} - \bar{u}_{1n} \\ u^B_{2n} - \bar{u}_{2n} \end{Bmatrix} + \begin{Bmatrix} \bar{u}_{1n} \\ \\ \bar{u}_{2n} \end{Bmatrix} \tag{2.94}$$

where the elements of the $[T^E_{SV\text{-}P}]$ are given by (E and SV-P are omitted):

$$T_{11} = \frac{1}{D}\left[\alpha\gamma k^2(C^\alpha C^{\gamma/2} + C^{\alpha/2}C^\gamma) - \alpha^2\gamma^2 S^\alpha S^{\gamma/2} - k^4 S^{\alpha/2}S^\gamma - \alpha\gamma k^2(C^{\alpha/2} + C^{\gamma/2})\right]$$

$$T_{21} = \frac{1}{D}\,\alpha k\left[\alpha\gamma(C^\gamma S^{\alpha/2} - C^{\gamma/2}S^\alpha) + k^2(S^{\gamma/2}C^\alpha - S^\gamma C^{\alpha/2}) + k^2 S^{\gamma/2} + \alpha\gamma S^{\alpha/2}\right]$$

$$T_{12} = \frac{1}{D}\,\gamma k\left[\alpha\gamma(C^\alpha S^{\gamma/2} - C^{\alpha/2}S^\gamma) + k^2(S^{\alpha/2}C^\gamma - S^\alpha C^{\gamma/2}) + k^2 S^{\alpha/2} + \alpha\gamma S^{\gamma/2}\right]$$

$$T_{22} = \frac{1}{D}\left[\alpha\gamma k^2(C^\gamma C^{\alpha/2} + C^{\gamma/2}C^\alpha) - \alpha^2\gamma^2 S^\gamma S^{\alpha/2} - k^4 S^{\gamma/2}S^\alpha - \alpha\gamma k^2(C^{\gamma/2} + C^{\alpha/2})\right]$$

$$T_{13} = T_{11}$$

$$T_{23} = -\,T_{21}$$

$$T_{14} = -\,T_{12}$$

$$T_{24} = T_{22} \tag{2.95}$$

In these expressions, in addition to the previously-defined symbols, D, C^α, C^γ, S^α and S^γ (Eqns. (2.74) and (2.75)), $C^{\alpha/2}$, $C^{\gamma/2}$, $S^{\alpha/2}$ and $S^{\gamma/2}$ are used to denote the following quantities:

$$\begin{cases} C^{\alpha/2} \equiv \cosh(\alpha h/2) & S^{\alpha/2} \equiv \sinh(\alpha h/2) \\ C^{\gamma/2} \equiv \cosh(\gamma h/2) & S^{\gamma/2} \equiv \sinh(\gamma h/2) \end{cases} \tag{2.96}$$

Also $\bar{u}_{1n}$ and $\bar{u}_{2n}$ are given by Eqns. (2.65) and (2.66), respectively.

For $\frac{\omega}{kC_s} \ll 1$, one can show that the following expressions define the asymptotic value of the elements of $[T^E_{SV-P}]$.

$$T_{11} \sim \frac{1}{2D'}[khC^{k/2}(\varepsilon^2-1) + 2S^{k/2}(1+\varepsilon^2)][kh(\varepsilon^2-1) - 2C^{k/2}S^{k/2}(1+\varepsilon^2)]$$

$$T_{21} \sim \frac{1}{2D'} kh(1-\varepsilon^2)S^{k/2}[2(1+\varepsilon^2)S^{k/2}C^{k/2} - kh(1-\varepsilon^2)]$$

$$T_{12} \sim -\frac{1}{2D'} kh(1-\varepsilon^2)S^{k/2}[2(1+\varepsilon^2)S^{k/2}C^{k/2} + kh(1-\varepsilon^2)]$$

$$T_{22} \sim \frac{1}{2D'}[khC^{k/2}(1-\varepsilon^2) + 2S^{k/2}(1+\varepsilon^2)][kh(1-\varepsilon^2) - 2C^{k/2}S^{k/2}(1+\varepsilon^2)] \tag{2.97}$$

where D', C^k, and S^k and ε are defined by Eqns. (2.77) and (2.78), and $C^{k/2}$ and $S^{k/2}$ denote the following quantities:

$$C^{k/2} \equiv \cosh\,(kh/2) \quad ; \quad S^{k/2} \equiv \sinh\,(kh/2) \tag{2.98}$$

Mid-layer transformed displacement for SH waves

The following expression defines the transformed displacement of plane E in terms of the transformed displacement of planes A and B (see Fig. 2.4b).

$$u^E_{3n} = \frac{1}{2\cosh\,(\frac{\gamma h}{2})}\,(u^A_{3n} + u^B_{3n} - 2\bar{u}_{3n}) + \bar{u}_{3n} \tag{2.99}$$

where $\bar{u}_{3n}$ is given by Eq. (2.86).

2.2.4 Integral Representation and Numerical Evaluation of Displacements

The preceding analytical solution scheme can be used to evaluate the displacements in layered soil media caused by uniform load distributions over cylindrical or circular surfaces (see Fig. 2.3). For this purpose, it is necessary to divide the soil medium into a number of layers such that each layer contains only one of the cylindrical load distributions. In this way, the loads on the cylindrical surfaces can be treated as body forces for which the "fixed-end stresses," (see sec. 2.2.3) can be evaluated, whereas the loads on circular surfaces can be considered as external forces at the interface of two layers.

Consider the uniform horizontal and vertical loads on cylindrical and circular surfaces shown in Fig. 2.3. The loads on cylindrical surfaces are associated with forces developed along the pile shafts, whereas the loads on circular surfaces correspond to pile-tip forces. In the following analysis, the radii of the cylinders and circular areas will be denoted by R, and the height of the cylinders by h. (R is the radius of the piles, and h is the thickness of a layer). The load distribution in Fig. 2.3a (lateral load on a cylindrical surface) can be expressed in cylindrical coordinates as

$$\begin{cases} f_r(r,\theta,z) = \dfrac{1}{2\pi Rh}\,\delta(r-R)\cos\theta \\ f_\theta(r,\theta,z) = \dfrac{-1}{2\pi Rh}\,\delta(r-R)\sin\theta \\ f_z(r,\theta,z) = 0 \end{cases} \tag{2.100}$$

where δ is the Kronecker delta function.

Comparing Eqns. (2.100) with the expansion of loads in Eqns. (2.26), one can write

$$\begin{cases} f_{r1} = \dfrac{1}{2\pi Rh}\,\delta(r-R) \\ f_{\theta 1} = \dfrac{-1}{2\pi Rh}\,\delta(r-R) \\ f_{z1} = 0 \end{cases} \tag{2.101}$$

and

$$f_{rn} = f_{\theta n} = f_{zn} = 0 \quad ; \qquad \text{for } n \neq 1 \tag{2.102}$$

Since the amplitudes of the Fourier expansion of this load for values of n other than one are zero, the corresponding displacements are similarly contributed only by the terms associated with n=1; therefore the displacement expansions reduce to the following expressions:

$$\begin{cases} u_r(r,\theta,z) = u_{r1}(r,z)\cos\theta \\ u_\theta(r,\theta,z) = u_{\theta 1}(r,z)\sin\theta \\ u_z(r,\theta,z) = u_{z1}(r,z)\cos\theta \end{cases} \tag{2.103}$$

On the other hand, application of Hankel transforms, according to Eqns. (2.34), to f_{r1}, $f_{\theta 1}$ and f_{z1} given by Eqns. (2.101) leads to

$$\begin{cases} f_{11} = -\dfrac{J_0(kR)}{2\pi h} \\ f_{21} = 0 \\ f_{31} = \dfrac{J_0(kR)}{2\pi h} \end{cases} \tag{2.104}$$

The transformed displacements associated with these transformed forces can be obtained by the techniques described in secs. 2.2.2 and 2.2.3. If u_{11}, u_{21} and u_{31} are the transformed displacements corresponding to $f_{11} = f_{31} = \frac{1}{2\pi h}$ and $f_{21} = 0$, then actual transformed displace-

ment associated with f_{11}, f_{21} and f_{31} in Eqns. (2.104) are given by $-J_o(kR)\ u_{11}$, $-J_o(kR)\ u_{21}$ and $J_o(kR)\ u_{31}$; thus the Hankel transform of displacements in Eqns. (2.34) can be written as (n=1)

$$\begin{cases} -J_o(kR)\ u_{11} + J_o(kR)\ u_{31} = \int_o^\infty (u_{r1} + u_{\theta 1})\ J_2(kr)\ rdr \\ J_o(kR)\ u_{11} + J_o(kR)\ u_{31} = \int_o^\infty (u_{r1} - u_{\theta 1})\ J_o(kr)\ rdr \\ -J_o(kR)\ u_{21} = \int_o^\infty u_{z1} J_1(kr)\ rdr \end{cases} \tag{2.105}$$

The application of inverse Hankel transform to these equations leads to:

$$\begin{cases} u_{r1} + u_{\theta 1} = \int_o^\infty (-u_{11} + u_{31})\ J_o(kR)\ J_2(kr)\ kdk \\ u_{r1} - u_{\theta 1} = \int_o^\infty (u_{11} + u_{31})\ J_o(kR)\ J_o(kr)\ kdk \\ u_{z1} = \int_o^\infty (-u_{21})\ J_o(kR)\ J_1(kr)\ kdk \end{cases} \tag{2.106}$$

Finally, by using the recurrence relations for the Bessel functions, one can obtain the following integral representation for u_{r1}, $u_{\theta 1}$ and u_{z1}:

$$\begin{cases} u_{r1} = \int_o^\infty [u_{11}\ J_o(kr)\ J_o(kR) + (u_{31} - u_{11})\ \frac{J_1(kr)}{kr}\ J_o(kR)]\ kdk \\ u_{\theta 1} = -\int_o^\infty [u_{31}\ J_o(kr)\ J_o(kR) + (U_{11} - u_{31})\ \frac{J_1(kr)}{kr}\ J_o(kR)]kdk \\ u_{z1} = -\int_o^\infty u_{21}\ J_1(kr)\ J_o(kR)\ kdk \end{cases} \tag{2.107}$$

A similar procedure can be followed to obtain the integral representation of displacements for the load distribution shown in Fig. 2.3b (frictional force on a cylindrical surface). For this case, the load distribution can be expressed as

$$\begin{cases} f_r(r,\theta,z) = 0 \\ f_\theta(r,\theta,z) = 0 \\ f_z(r,\theta,z) = \frac{1}{2\pi Rh}\,\delta(r-R) \end{cases} \tag{2.108}$$

Comparison of these equations with the expansion for the loads in Eqns. (2.26) leads to

$$\begin{cases} f_{ro} = 0 \\ f_{\theta o} = 0 \\ f_{zo} = \frac{1}{2\pi Rh}\,\delta(r-R) \end{cases} \tag{2.109}$$

and

$$f_{rn} = f_{\theta n} = f_{zn} = 0 \quad ; \quad n \neq 0 \tag{2.110}$$

Since the only nonzero term in the load expansion corresponds to n=0, likewise, in the displacement expansion, only the n=0 term will have non-zero value, and all other terms will vanish; that is,

$$\begin{cases} u_r(r,\theta,z) = u_{ro}(r,z) \\ u_\theta(r,\theta,z) = 0 \\ u_z(r,\theta,z) = u_{zo}(r,z) \end{cases} \tag{2.111}$$

Following a procedure similar to the one described for horizontal loading, one can show that if u_{10} and u_{20} are transformed displacements due to transformed loads $f_{10} = 0$ and $f_{20} = \frac{1}{2\pi h}$; then u_{ro} and u_{zo} are given by

$$\begin{cases} u_{ro} = \int_0^\infty u_{10}\, J_1(kr)\, J_0(kR)\, kdk \\ \\ u_{zo} = \int_0^\infty u_{20}\, J_0(kr)\, J_0(kR)\, kdk \end{cases} \tag{2.112}$$

For the loads distributed over circular surfaces (Fig. 2.3c and 2.3d) it is necessary to evaluate the corresponding transformed forces directly. Consider first the load distribution shown in Fig. 2.3c (frictional force on a circular surface). One can represent this loading by the following expressions:

$$\begin{cases} \bar{\sigma}_{rz} = \frac{1}{\pi R^2} \cos\theta \\ \bar{\sigma}_{\theta z} = \frac{-1}{\pi R^2} \sin\theta \qquad r \leq R \\ \bar{\sigma}_{zz} = 0 \end{cases} \tag{2.113}$$

$$\bar{\sigma}_{rz} = \bar{\sigma}_{\theta z} = \bar{\sigma}_{zz} = 0; \qquad r > R$$

If a Fourier expansion of these loads, similar to the expansion of stresses in Eqns. (2.55), is compared with Eqns. (2.113), it can be concluded that

$$\begin{cases} \bar{\sigma}_{rz1} = \frac{1}{\pi R^2} \\ \\ \bar{\sigma}_{\theta z1} = \frac{-1}{\pi R^2} \\ \\ \bar{\sigma}_{zz1} = 0 \end{cases} \tag{2.114}$$

and

$$\bar{\sigma}_{rzn} = \bar{\sigma}_{\theta zn} = \bar{\sigma}_{zzn} = 0 \; ; \quad \text{for } n \neq 1 \tag{2.115}$$

Therefore one only needs to consider the terms associated with n=1 in the expansion of displacements; that is, u_r, u_θ and u_z can be expressed by eqns. (2.103). The transformed loads associated with $\bar{\sigma}_{rz1}$, $\bar{\sigma}_{\theta z1}$ and $\bar{\sigma}_{zz1}$ in Eqns. (2.114) can be obtained by the application of Hankel transforms according to Eqns. (2.60), the result is:

$$\begin{cases} \bar{\sigma}_{211} = -\dfrac{1}{\pi} \dfrac{J_1(kR)}{kR} \\ \bar{\sigma}_{221} = 0 \\ \bar{\sigma}_{231} = \dfrac{1}{\pi} \dfrac{J_1(kR)}{kR} \end{cases} \tag{2.116}$$

A procedure similar to the one described for the loads on cylindrical surfaces leads to the integral representation of u_{r1}, $u_{\theta 1}$ and u_{z1} similar to those presented by Eqns. (2.107) except that the term $J_0(kR)$ should be replaced by $\dfrac{J_1(kR)}{kR}$. The transformed displacements u_{11}, u_{21} and u_{31} in these equations then correspond to transformed applied stresses $\bar{\sigma}_{211} = \dfrac{1}{\pi}$, $\bar{\sigma}_{221} = 0$ and $\bar{\sigma}_{231} = \dfrac{1}{\pi}$.

Finally for the load distribution shown in Fig. 2.3d (vertical force on a circular surface) one can show that forces and displacements are contributed only by the terms associated with n=0 in the Fourier expansions and that expressions for displacements are given by Eqns. (2.112) except that in these equations the term $J_0(kR)$ should be replaced by $J_1(kR)/kR$; transformed displaements u_{10} and u_{20} in these equations then correspond to transformed applied stresses $\bar{\sigma}_{210} = 0$ and $\bar{\sigma}_{220} = \dfrac{1}{\pi}$.

The expressions for displacements obtained in this section involve, in general, integrals of the form

$$I = \int_0^\infty f\, J_n(kr)\, J_m(kR)\, dk \qquad (2.117)$$

in which the kernel, f, represents a function of k and is associated with transformed displacements, and n and m are integers that can take on values of zero and one.

The first step in the numerical evaluation of the above expression is to approximate the semi-infinite integral by a finite integral, that is:

$$I \approx \int_0^{k_u} f\, J_n(kr)\, J_m(kR)\, dk \qquad (2.118)$$

in which k_u is an upper limit of integration which can be defined on the basis of the integrand's rate of decay. The next step is to divide the integration domain $(0, k_u)$, into a number of discrete intervals and to use, in each interval, the value of the integrand at a number of points in order to define an interpolation function. These functions, which approximate the actual variation of the integrand, are used to perform the integration in each interval analytically. The final step is then to sum the results of the numerical integration over the intervals.

Before describing the quadrature implemented in the present work, it may be instructive to examine certain characteristics of the kernel f (Eq. 2.118). This function represents a transformed displacement associated with a load distribution in the medium. Fig. 2.5a shows the plot of the real part of u_{20} at the surface of a layered halfspace caused by a uniform frictional load on a cylindrical surface in the top layer. The

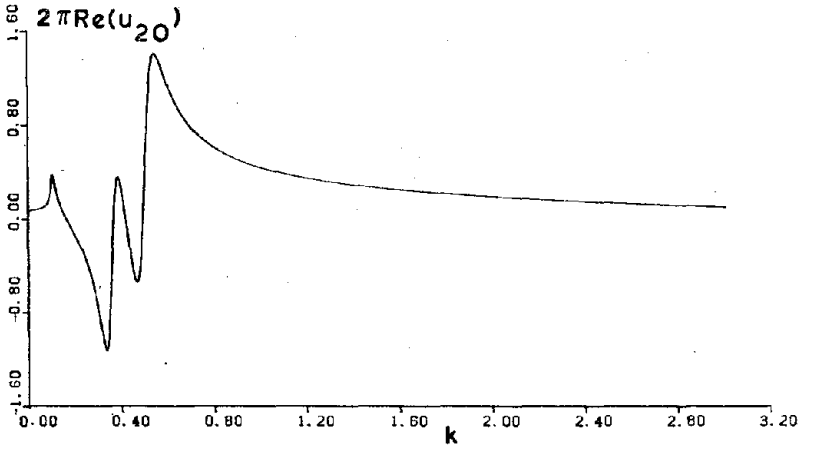

(a)

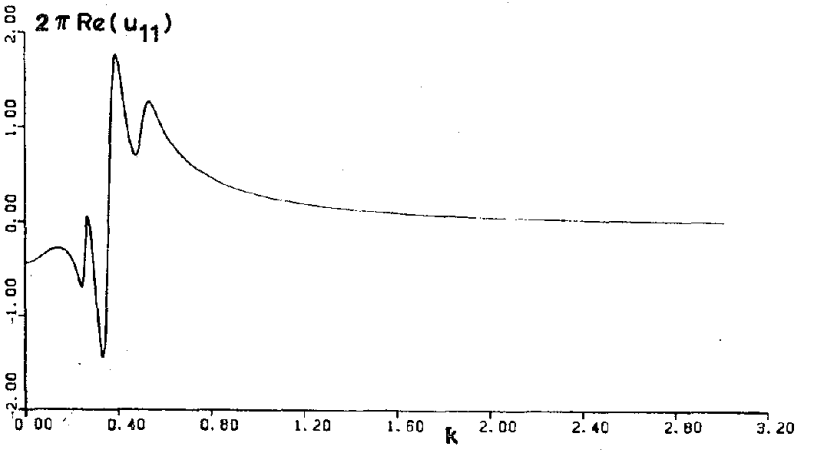

(b)

Fig. 2.5 - Transformed Displacements of the Surface of a Layered Medium.

medium consists of 5 layers resting on a viscoelastic halfspace; the following table gives the properties of this medium.

Layer	Thickness	Shear wave velocity	Mass density	Damping	Poisson ratio
Top	1.0	1.0	1.0	0.05	0.40
2nd	1.5	1.5	1.0	0.05	0.40
3rd	2.0	2.0	1.0	0.05	0.40
4th	3.0	2.5	1.0	0.05	0.40
5th	4.0	3.0	1.0	0.05	0.40
Half-space	—	4.0	1.0	0.05	0.40

In addition, the frequency of vibration, ω, is 1 rad/sec. Fig. 2.5b shows the plot of the real part of u_{11} at the surface of this medium caused by a uniform lateral load on a cylindrical surface in the top layer. In the ensuing paragraphs, the region which contains the peaks of the kernel f will be referred to as "region I," and the remaining domain will be referred to as "region II." (Region I extends to values of k which are of the order of $\frac{\omega}{C_s}$, where C_s is the shear wave velocity of the layer in which the load is applied.)

The plots in Fig. 2.5 show that the kernel f in region I is characterized by pronounced peaks. These peaks, which are associated with surface wave modes, become sharper as the material damping in the medium decreases. In addition, more peaks appear in the variation of the kernel as the number of layers increases. These plots suggest that for the purpose of numerical integration in region I, one has to select, in general,

small intervals, so that the erratic nature of the integrand can be captured by the interpolation functions.

On the other hand, the variation of the kernel in region II, which contains the decaying branch of the kernel, is very smooth (see Figs. 2.5a and 2.5b). The kernel, in this region, approaches zero ever faster as the relative distance between the layer at which f is evaluated and the layer in which the load is applied increases. This can be verified by examining Figs. 2.6a and 2.6b, which show the variation of u_{20} and u_{11} at the surface of the halfspace for the same medium and load condition associated with Figs. 2.5a and 2.5b, respectively. These observations suggest that, as far as the variation of the kernel is concerned, for numerical integration one may select larger intervals in region II than in region I.

As for the Bessel functions in the integrand, one has to make sure that, for small arguments (kR and kr smaller than, say 4.0), the size of the interval is small enough to allow a sufficiently accurate representation of these functions at the integration points. (Since the wavelength of a Bessel function is approximately 2π, in order to have, say, 10 intervals in a cycle, it is necessary that the size of the interval, Δk, be selected such that $(\Delta k)r \leq \frac{2\pi}{10}$ and $(\Delta k)R \leq \frac{2\pi}{10}$). On the other hand, for large arguments, one may use Hankel's asymptotic expansion to approximate the Bessel functions. Hankel's asymptotic expansion for $J_\nu(y)$ for large argument is given by:

$$J_\nu(y) = \sqrt{\frac{2}{\pi y}} [P(\nu,y) \cos \chi - Q(\nu,y) \sin \chi] \qquad (2.119)$$

where

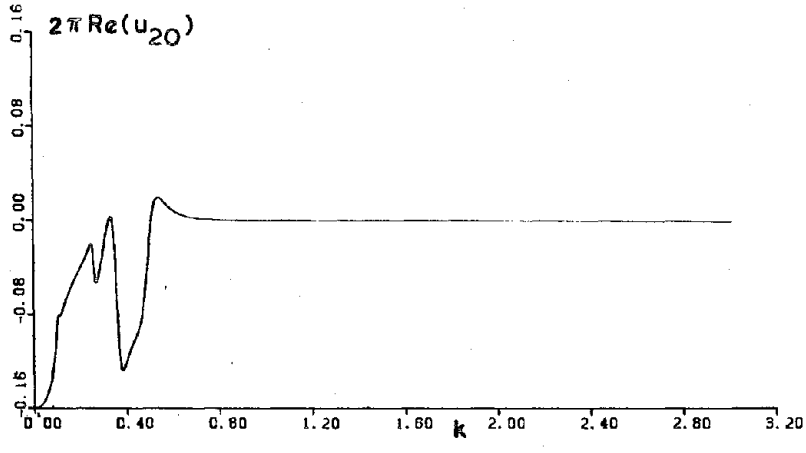

(a)

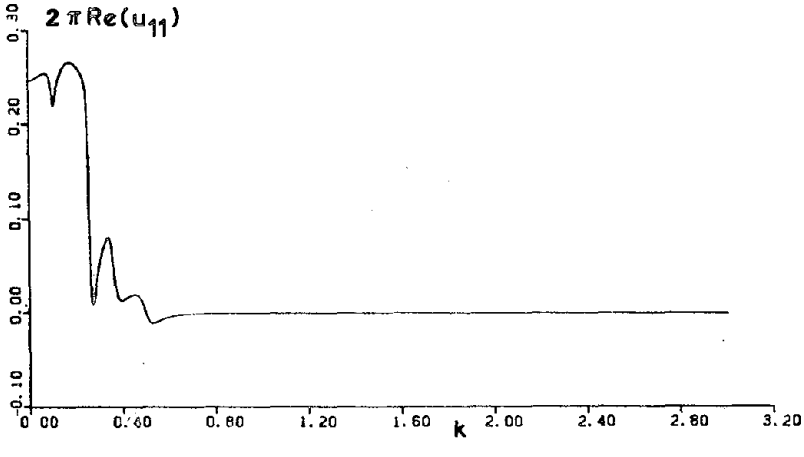

(b)

Fig. 2.6 - Transformed Displacements of a Plane in a Layered Medium.

$$\chi = y - (\frac{1}{2}\nu + \frac{1}{4})\pi, \tag{2.120}$$

$$P(\nu,y) \sim \sum_{\ell=0}^{\infty} (-1)^{\ell} \frac{(\nu,2\ell)}{(2y)^{2\ell}} = 1 - \frac{(\mu-1)(\mu-9)}{2!(8y)^2} + \frac{(\mu-1)(\mu-9)(\mu-25)(\mu-49)}{4!(8y)^4} - \ldots \tag{2.121}$$

$$Q(\nu,y) \sim \sum_{\ell=0}^{\infty} (-1)^{\ell} \frac{(\nu,2\ell+1)}{(2y)^{2\ell+1}} = \frac{\mu-1}{8y} - \frac{(\mu-1)(\mu-9)(\mu-25)}{3!(8y)^3} + \ldots. \tag{2.122}$$

In these expressions $\mu = 4\nu^2$.

Eq. (2.119) can be rewritten as:

$$J_\nu(y) = A_\nu(y) \cos y + B_\nu(y) \sin y \tag{2.123}$$

in which $A_\nu(y)$ and $B_\nu(y)$ are given by

$$\begin{cases} A_\nu(y) = \sqrt{\frac{2}{\pi y}} \left[P(\nu,y) \cos (\frac{1}{2}\nu + \frac{1}{4})\pi + Q(\nu,y) \sin (\frac{1}{2}\nu + \frac{1}{4})\pi\right] \\ B_\nu(y) = \sqrt{\frac{2}{\pi y}} \left[P(\nu,y) \sin (\frac{1}{2}\nu + \frac{1}{4})\pi - Q(\nu,y) \cos (\frac{1}{2}\nu + \frac{1}{4})\pi\right] \end{cases} \tag{2.124}$$

Now consider an interval of integration between k_1 and k_3 on the k-axis. In addition, for the present study, an integration point with $k=k_2$ is used at the center of the interval so that a quadratic polynomial can be defined to interpolate the integrand between these three values of k. Depending on the value of k_1R and k_1r, one of the following four integration procedures is then applicable: (In the following, δ is used as reference value to distinguish between small and large values of the argument for Bessel functions.)

1) $k_1R \le \delta$ and $k_1r \le \delta$: If F_1, F_2 and F_3 denote the value of the integrand, $f\, J_n(kr)\, J_m(kR)$, at k_1, k_2 and k_3, respectively, then one can

obtain the quadratic polynomial which is defined by these values. It can be shown that this polynomial is given by

$$F(k) = Pk^2 + Qk + S \quad ; \quad k_1 \leq k \leq k_3 \tag{2.125}$$

in which

$$\begin{cases} P = \dfrac{2}{(\Delta k)^2}\,[F_1 - 2F_2 + F_3] \\ Q = \dfrac{1}{(\Delta k)^2}\,[k_1(4F_2 - F_1 - 3F_3) + k_3(4F_2 - 3F_1 - F_3)] \\ S = \dfrac{1}{(\Delta k)^2}\,[k_1^2 F_3 + k_3^2 F_1 - k_1 k_3(4F_2 - F_1 - F_3)] \end{cases} \tag{2.126}$$

and $\Delta k = k_3 - k_1$. The integration of the polynomial $F(k)$ over the interval $[k_1, k_3]$ then results in Simpson's rule $(\Delta k \times \dfrac{F_1 + 4F_2 + F_3}{6})$.

2) $\underline{k_1 R \leq \delta \text{ and } k_1 r > \delta}$: For this case one can replace $J_n(kr)$ by Hankel's asymptotic expansion given by Eq. (2.123); thus one can write:

$$\begin{aligned} I_1 &= \int_{k_1}^{k_3} f(k)\, J_n(kr)\, J_m(kR)\, dk \\ &= \int_{k_1}^{k_3} f(k)\, J_m(kR)[A_n(kr)\cos(kr) + B_n(kr)\sin(kr)]\, dk \\ &= \int_{k_1}^{k_3} f(k)\, J_m(kR)\, A_n(kr)\cos(kr)\, dk \\ &\quad + \int_{k_1}^{k_3} f(k)\, J_m(kR)\, B_n(kr)\sin(kr)\, dk \end{aligned} \tag{2.127}$$

Consider the first integral in Eq. (2.127): One can approximate the coefficient of cos(kr) in this integral by a quadratic polynomial, as described in the previous case. (In this case, however, F_1, F_2 and F_3 are the value of $f(k)\, J_m(kR)\, A_n(kr)$ at k_1, k_2 and k_3, respectively). Therefore this integral is approximated by an integral of the form $\int_{k_1}^{k_3} (Pk^2 + Qk + S\,) \cos(kr)\, dk$, which can be evaluated explicitly.

Since the oscillatory nature of the Bessel function is accounted for by the trigonometric functions, the size of the interval is controlled only by the degree of smoothness of the other functions in the integrand.

3) $k_1R > \delta$ and $k_1r \leq \delta$: The procedure for this case is similar to that of the previous one, except that now one has to use the asymptotic expansion for $J_m(kR)$.

4) $k_1R > \delta$ and $k_1r > \delta$: In this case one can use the asymptotic expansion for both Bessel functions in the integrand. Then, in the final results, one gets integrals of the form:

$$\int_{k_1}^{k_3} (Pk^2 + Qk + S\,) \begin{Bmatrix} \cos(kR) \\ \sin(kR) \end{Bmatrix} \begin{Bmatrix} \cos(kr) \\ \sin(kr) \end{Bmatrix} dk,$$ in which the polynomial $(Pk^2 + Qk + S\,)$ has replaced the actual functions appearing with the trigonometric functions in the integrand. These integrals also can be evaluated explicitly.

2.3 Lateral and Axial Vibration of Prismatic Members

In Sec. 2.1 certain response quantities of a dynamically excited prismatic member (pile) were used to formulate the pile group problems. More specifically, the formulation was based on the evaluation of the dynamic stiffness matrix of the piles K_p, the dynamic flexibility matrix of clamped-end piles, F_p, and the dynamic flexibility matrix of clamped-end piles for harmonic end displacements, Ψ_p. The objective of this section is to derive the expressions for the response quantities that are needed to construct these matrices.

2.3.1 - Lateral vibration

The equilibrium equations for a differential element of a beam in lateral vibration, including the effect of axial force, are given by (see Fig. 2.7b):

$$\begin{cases} \dfrac{dV}{dz} + m\omega^2 u = 0 & (2.128) \\ V + \dfrac{dM}{dz} + H\dfrac{du}{dz} = 0 & (2.129) \end{cases}$$

in which m denotes mass per unit length of the beam and H is the constant axial force in the beam. Using Eqns. (2.128) and (2.129) along with the moment-curvature relationship, $M = EI\dfrac{d^2u}{dz^2}$, (EI being the bending rigidity of the beam), one gets:

$$\frac{d^4u}{dz^4} + \left(\frac{H}{EI}\right)\frac{d^2u}{dz^2} - \left(\frac{m\omega^2}{EI}\right)u = 0 \qquad (2.130)$$

The solution of this differential equation can be expressed as:

$$u = C_1\cos(\eta z) + C_2\sin(\eta z) + C_3\cosh(\xi z) + C_4\sinh(\xi z) \qquad (2.131)$$

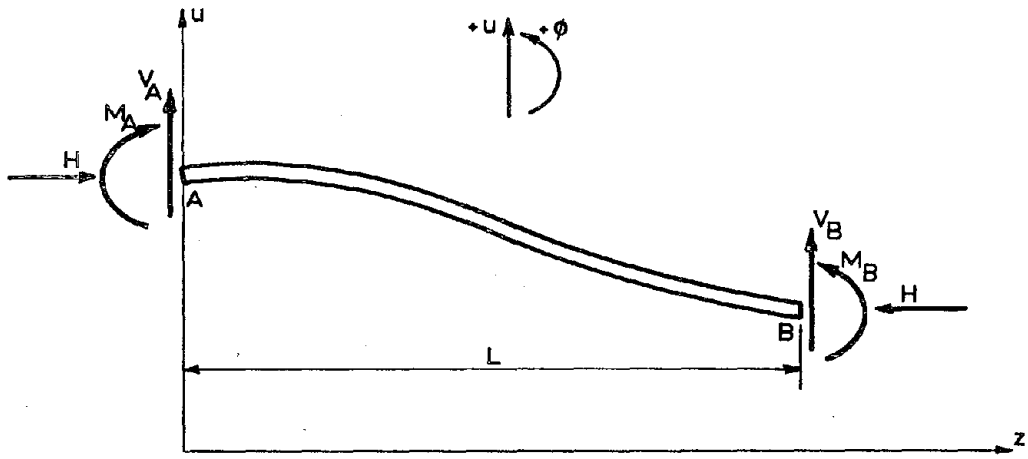

(a)

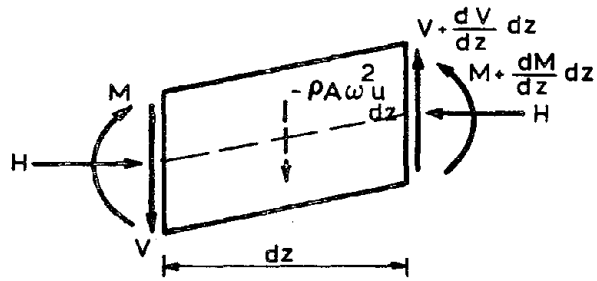

(b)

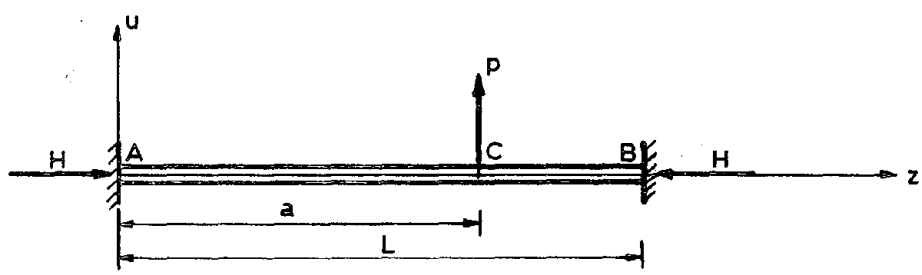

(c)

Fig. 2.7 - A Beam in the Lateral Vibration.

in which:

$$\begin{cases} \eta = \left\{ \left[\left(\frac{H}{2EI}\right)^2 + \frac{m\omega^2}{EI} \right]^{1/2} + \frac{H}{2EI} \right\}^{1/2} \\ \xi = \left\{ \left[\left(\frac{H}{2EI}\right)^2 + \frac{m\omega^2}{EI} \right]^{1/2} - \frac{H}{2EI} \right\}^{1/2} \end{cases} \tag{2.132}$$

In order to evaluate the elements of Ψ_p associated with the lateral degrees of freedom, one needs to derive the expression for the lateral displacement of the beam caused by the displacements at the two ends, u_A, ϕ_A, u_B and ϕ_B. To achieve this, one may use the equation for u (Eq. 2.131) along with its derivative to express the end displacements in terms of C_1, C_2, C_3 and C_4. If now the resulting equations are solved for these unknown constants, one gets:

$$C_1 = \frac{1}{T_o}\left[(1 + \frac{\xi}{\eta} T_4)\, u_A + \frac{1}{\eta} T_3 \phi_A + (C^\eta - C^\xi) u_B - (\frac{1}{\eta} S^\eta - \frac{1}{\xi} S^\xi)\phi_B\right]$$

$$C_2 = \frac{1}{T_o}\left[-\frac{\xi}{\eta} T_2 u_A + \frac{1}{\eta}(1 - T_1)\phi_A + (S^\eta + \frac{\xi}{\eta} S^\xi) u_B + \frac{1}{\eta}(C^\eta - C^\xi)\phi_B\right] \tag{2.133}$$

$$C_3 = \frac{1}{T_o}\left[(1 - T_1) u_A - \frac{1}{\eta} T_3 \phi_A - (C^\eta - C^\xi) u_B + (\frac{1}{\eta} S^\eta - \frac{1}{\xi} S^\xi)\phi_B\right]$$

$$C_4 = \frac{1}{T_o}\left[T_2 u_A + (\frac{1}{\eta} T_4 + \frac{1}{\xi})\phi_A - (\frac{\eta}{\xi} S^\eta + S^\xi) u_B - \frac{1}{\xi}(C^\eta - C^\xi)\phi_B\right]$$

In these expressions T_o, T_1, T_2, T_3 and T_4 are given by :

$$T_o = 2 - 2C^\eta C^\xi - (\frac{\eta}{\xi} - \frac{\xi}{\eta}) S^\eta S^\xi$$

$$T_1 = C^\eta C^\xi + \frac{\eta}{\xi} S^\eta S^\xi$$

$$T_2 = C^{\eta}S^{\xi} + \frac{\eta}{\xi} S^{\eta}C^{\xi}$$

$$T_3 = S^{\eta}C^{\xi} - \frac{\eta}{\xi} C^{\eta}S^{\xi}$$

$$T_4 = S^{\eta}S^{\xi} - \frac{\eta}{\xi} C^{\eta}C^{\xi} \qquad (2.134)$$

and C^{η}, S^{η}, C^{ξ} and S^{ξ} are used to denote the following quantities:

$$C^{\eta} \equiv \cos(\eta L) \quad ; \quad S^{\eta} \equiv \sin(\eta L)$$

$$C^{\xi} \equiv \cosh(\xi L) \quad ; \quad S^{\xi} \equiv \sinh(\xi L) \qquad (2.135)$$

and L is the length of the beam. Finally, the desired expression can be obtained by introducing Eqns. (2.133) into Eqns. (2.131). (The elements of ψ_p associated with a point C of the beam are then the coefficients of u_A, ϕ_A, u_B and ϕ_B in the expression for the displacement of point C).

The dynamic stiffness matrix of the beam is obtained by expressing the forces at the two ends of the beam in terms of the displacements of these points. This can be achieved by using Eq. (2.129) and the moment-curvature relationship along with Eqns. (2.131) and (2.133); the result can be written as:

$$\begin{Bmatrix} V_A \\ M_A \\ V_B \\ M_B \end{Bmatrix} = K \begin{Bmatrix} u_A \\ \phi_A \\ u_B \\ \phi_B \end{Bmatrix} \qquad (2.136)$$

in which the elements of the symmetric 4 x 4 dynamic stiffness matrix, K, are given by:

$$K_{11} = \frac{EI}{T_o}(\eta^2 + \xi^2)(\eta S^{\eta} C^{\xi} + \xi C^{\eta} S^{\xi})$$

$$K_{21} = \frac{EI}{T_o}[(\eta^2 - \xi^2)(1 - C^{\eta} C^{\xi}) + 2\eta\xi S^{\eta} S^{\xi}]$$

$$K_{31} = -\frac{EI}{T_o}(\eta^2 + \xi^2)(\eta S^{\eta} + \xi S^{\xi})$$

$$K_{41} = \frac{EI}{T_o}(\eta^2 + \xi^2)(C^{\xi} - C^{\eta})$$

$$K_{22} = \frac{EI}{T_o}\left(\frac{\eta}{\xi} + \frac{\xi}{\eta}\right)(\xi S^{\eta} C^{\xi} - \eta C^{\eta} S^{\xi})$$

$$K_{32} = -\frac{EI}{T_o}(\eta^2 + \xi^2)(C^{\xi} - C^{\eta})$$

$$K_{42} = \frac{EI}{T_o}\left(\frac{\eta}{\xi} + \frac{\xi}{\eta}\right)(\eta S^{\xi} - \xi S^{\eta})$$

$$K_{33} = K_{11}$$

$$K_{43} = -K_{21}$$

$$K_{44} = K_{22} \qquad (2.137)$$

In order to evaluate the elements of F_p associated with the lateral degrees of freedom, it is necessary to derive the expressions for the lateral displacement caused by a lateral point load in a fixed-end beam. Consider the beam shown in Fig. 2.7c subjected to a point force, p, at z = a. One can use Eq. (2.131) to express the displacements of the beam as:

$$\begin{cases} u = A_1\cos(\eta z) + A_2\sin(\eta z) + A_3\cosh(\xi z) + A_4\sinh(\xi z) & 0 \le z \le a \\ u = B_1\cos(\eta z) + B_2\sin(\eta z) + B_3\cosh(\xi z) + B_4\sinh(\xi z) & a \le z \le L \end{cases} \qquad (2.138)$$

where η and ξ are given by Eqns. (2.132). The unknown constants A_1, A_2, ... B_3, B_4, can be determined by imposing the kinematic boundary conditions at the two ends (zero translation and rotation) along with the displacement compatibility and equilibrium conditions at the point of application of the load. The result is:

$$A_1 = \frac{p}{EI\eta(\eta^2 + \xi^2)T_o}\left[T_3(\cosh(\xi a) - \cos(\eta a)) + (T_1 - 1)\sin(\eta a) - (T_4 + \frac{\eta}{\xi})\sinh(\xi a)\right]$$

$$A_2 = \frac{-p}{EI\eta(\eta^2 + \xi^2)T_o}\left[(T_1 - 1)\cosh(\xi a) - (1 + \frac{\xi}{\eta}T_4)\cos(\eta a) + T_2(\frac{\xi}{\eta}\sin(\eta a) - \sinh(\xi a))\right]$$

$$A_3 = -A_1$$

$$A_4 = -\frac{\eta}{\xi}A_2$$

$$B_1 = \frac{p}{EI\eta(\eta^2 + \xi^2)T_o}\left[T_3(\cosh(\xi a) - \cos(\eta a)) + (T_4 + \frac{\eta}{\xi})(\frac{\xi}{\eta}\sin(\eta a) - \sinh(\xi a))\right]$$

$$B_2 = \frac{-p}{EI\eta(\eta^2 + \xi^2)T_o}\left[(T_1 - 1)(\cosh(\xi a) - \cos(\eta a)) + T_2(\frac{\xi}{\eta}\sin(\eta a) - \sinh(\xi a))\right]$$

$$B_3 = -T_1 B_1 - T_3 B_2$$

$$B_4 = T_2 B_1 + T_4 B_2 \qquad (2.139)$$

2.3.2 Axial vibration

The equilibrium equation for a differential element of a beam in axial vibration is given by (see Fig. 2.8b):

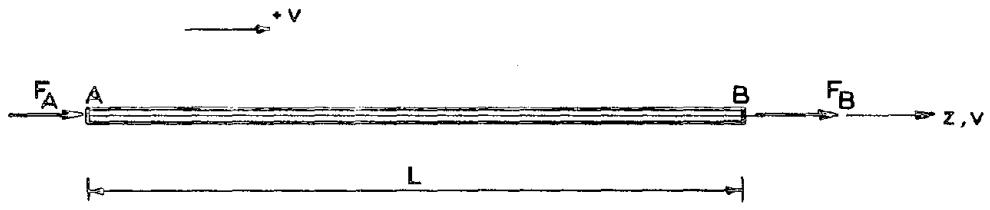

(a)

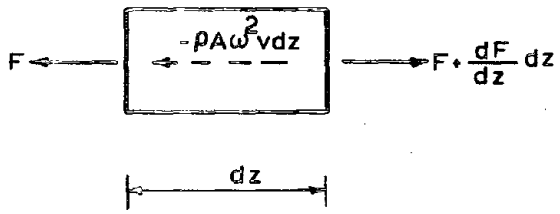

(b)

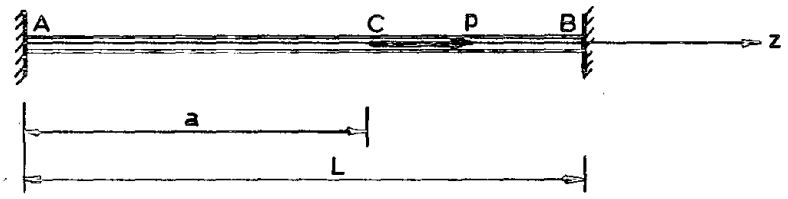

(c)

Fig. 2.8 - A Beam in the Axial Vibration

$$\frac{dF}{dz} + m\,\omega^2 v = 0 \tag{2.140}$$

Introduction of the force-displacement relationship $F = EA\,\frac{dv}{dz}$ into Eq. (2.140) leads to:

$$\frac{d^2v}{dz^2} + \frac{m}{EA}\,\omega^2\, v = 0 \tag{2.141}$$

The selection of this differential equation can be written as

$$v = C_1 \cos(\zeta z) + C_2 \sin(\zeta z) \tag{2.142}$$

in which:

$$\zeta = \left[\frac{m\omega^2}{EA}\right]^{1/2} \tag{2.143}$$

Following the procedure described for lateral vibration, one can derive the expressions for C_1 and C_2 in terms of the end displacements of the beam:

$$\begin{cases} C_1 = v_A \\ C_2 = \dfrac{1}{\sin \zeta L}\left[-\cos(\zeta L)\, v_A + v_B\right] \end{cases} \tag{2.144}$$

Therefore Eq. (2.142), with C_1 and C_2 defined by Eqns. (2.144), can be used to obtain the elements of Ψ_p associated with axial degrees of freedom.

Similarly, the axial dynamic stiffness matrix of the beam can be obtained following the procedure outlined in the previous section; one can show that:

$$\begin{Bmatrix} F_A \\ F_B \end{Bmatrix} = \frac{EA\zeta}{\sin(\zeta L)} \begin{bmatrix} \cos(\zeta L) & -1 \\ -1 & \cos(\zeta L) \end{bmatrix} \begin{Bmatrix} v_A \\ v_B \end{Bmatrix} \tag{2.145}$$

Finally, the axial displacement in a fixed-end beam caused by an axial

point load p (see Fig. 2.8c) is given by:

$$\begin{cases} v = A_1 \cos(\zeta z) + A_2 \sin(\zeta z) & 0 \leq z \leq a \\ v = B_1 \cos(\zeta z) + B_2 \sin(\zeta z) & a \leq z \leq L \end{cases} \tag{2.146}$$

The unknown constants A_1, A_2, B_1 and B_2 can be found by using the kinematic boundary conditions at the two ends of the beam together with compatibility and equilibrium conditions at the point of the application of the load; one can show that:

$$\begin{cases} A_1 = 0 \\ A_2 = \frac{p}{EA\zeta} [\cos(\zeta a) - \text{cotan}(\zeta L) \sin(\zeta a)] \\ B_1 = \frac{p}{EA\zeta} \sin(\zeta a) \\ B_2 = \frac{-p}{EA\zeta} \text{cotan}(\zeta L) \sin(\zeta a) \end{cases} \tag{2.147}$$

Eqns. (2.146) with A_1, A_2, B_1 and B_2 defined by Eqns. (2.147) can be used to obtain elements of F_p associated with axial degrees of freedom.

The expressions derived in this section apply to the dynamic excitation. The corresponding expressions for the static case are available in the literature and therefore are not repeated here.

CHAPTER 3 - DYNAMIC BEHAVIOR OF PILE GROUPS

The objective of this chapter is to present the numerical results obtained with the formulation outlined in chapter 2, and to investigate certain characteristics of the vibration of pile groups. The quantities of interest in this study are: 1) The dynamic stiffnesses of pile groups corresponding to the horizontal, vertical, rocking and torsional modes of vibration; 2) the seismic response of pile groups; and 3) the distribution of an applied load (horizontal or vertical) on the pile cap among the piles in the group. While information on the distribution of loads among the piles is necessary for the design of the piles' section, the stiffnesses, along with the transfer function of the pile cap associated with a seismic excitation, can be used, in the analysis of the superstructure, to account for the foundation-structure interaction effects. (In a conventional foundation-structure interaction analysis for seismic excitation, first the stiffnesses of the foundation are evaluated (soil springs); next the motions of the foundation in the absence of the superstructure are obtained (kinematic interaction), and finally the dynamic response of the superstructure mounted on soil springs and subjected at the base to the motion obtained from the kinematic interaction analysis is computed (inertial interaction). For details see, for example, Kausel and Roesset (1974)).

Although the results presented in this chapter cover only a limited range of parameters, it is believed that they can be used to draw general conclusions about certain aspects of the problem. In addition, these results, along with those of chapter 5, can be helpful in gaining insight into the mechanism of the dynamic behavior of pile groups.

In this chapter, as well as in chapters 4 and 5, the elasticity modulus, mass density, poisson ratio and material damping of the soil are denoted by E_s, ρ_s, ν_s and β_s, respectively; and the corresponding quantities for the piles are denoted by E_p, ρ_p, ν_p and β_p. In addition, A_p, I_p, L and d are used to denote the cross-sectional area, moment of inertia, length and diameter of the piles, respectively. Also, N refers to the total number of piles and s to the distance between adjacent piles. Finally, a_o defines the nondimensional frequency, i.e., $a_o = \frac{\omega d}{C_s}$, in which ω is the frequency of harmonic vibration and C_s is the largest shear-wave velocity of the soil profile.

In order to verify the numerical solution scheme developed in the present study, the following comparisons with the results of previous investigations are presented. Figure 3.1 shows the horizontal and vertical static stiffnesses of 3 x 3 pile groups in an elastic halfspace obtained by Poulos and Davis (1980). The same quantities evaluated by the present method are also shown in this figure (dashed line). These results correspond to $\frac{L}{d} = 25$ and $\frac{E_p I}{E_s L^4} = 10^{-3}$ for the horizontal case, and to $\frac{L}{d} = 25$ and $\frac{E_s}{E_p} = 10^{-3}$ for the vertical case. The figure shows that the results of the present method for the vertical stiffness agree very well with those of Poulos. For the horizontal case, on the other hand, the results of the two studies display some discrepancies; these results, however, do not differ by more than 20%. Therefore it can be concluded that, in general, there is a fairly good agreement between the present solution and the Poulos solution.

Figure 3.2 displays a comparison between the results of the present study and those reported by Nogami (1979) for the vertical stiffness and

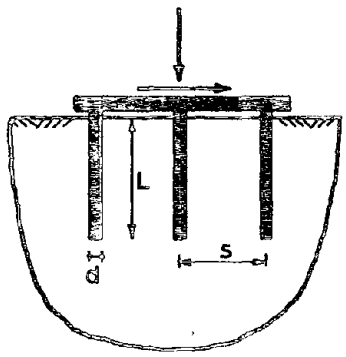

3X3 PILE GROUP

$\frac{L}{d} = 25$; $\nu_s = 0.45$; $\nu_p = 0.25$

HORIZONTAL : $\frac{E_p I}{E_s L^4} = 10^{-3}$

VERTICAL : $\frac{E_s}{E_p} = 10^{-3}$

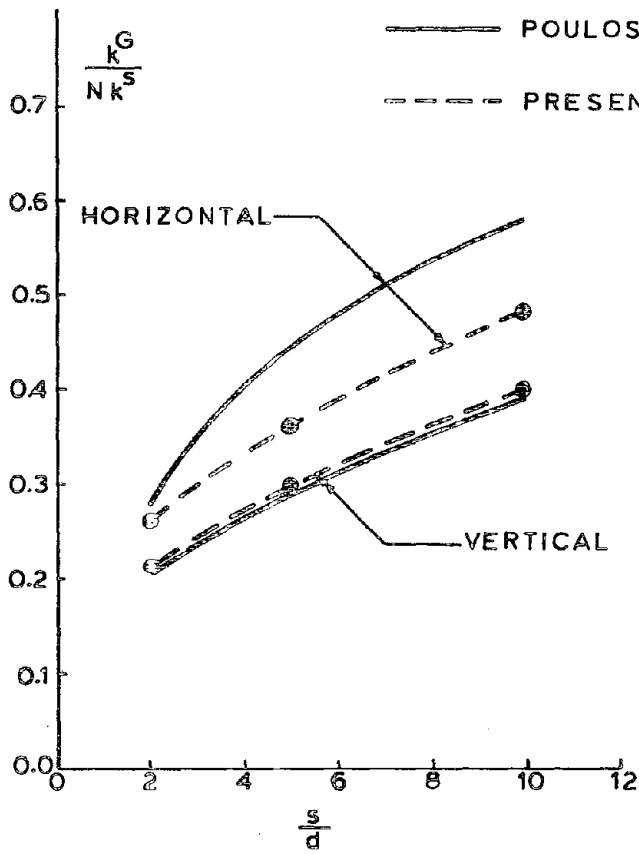

Fig. 3.1 - Comparison with Poulos's Solution (Static Case)

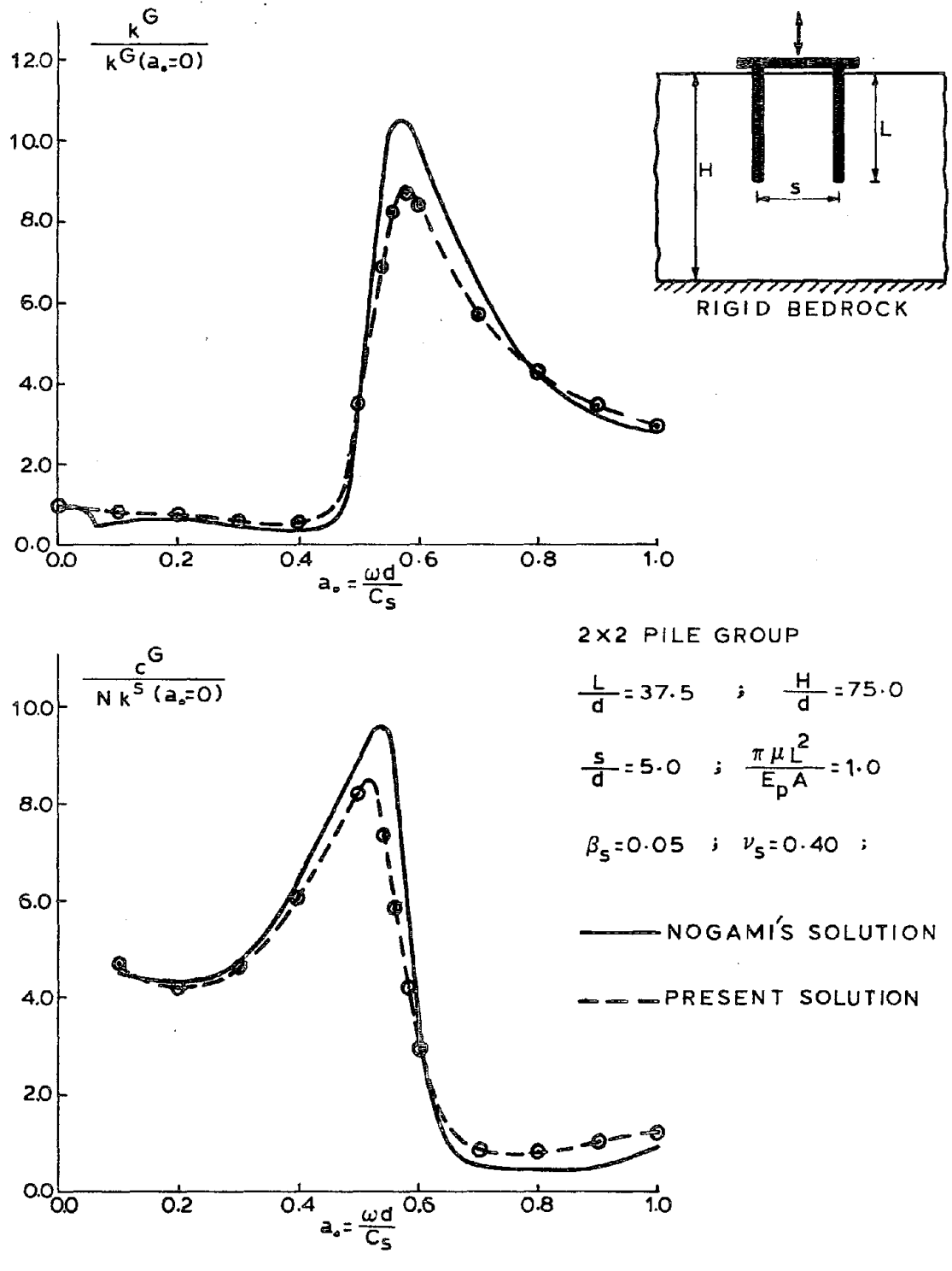

Fig. 3.2 - Comparison with Nogami's Solution (Dynamic Case).

damping of a 2 x 2 pile group. The soil medium in this case is a uniform viscoelastic stratum, with thickness H = 75 d, resting on a rigid bedrock, and the piles are characterized by $\frac{L}{d} = 37.5$ and $\frac{\pi\mu L^2}{E_p A} = 1$ (μ is the shear modulus of the soil); also $\frac{s}{d} = 5$. The figure shows that the agreement between the two solutions is fairly good. The small discrepancy observed between the two solutions is believed to be partly due to the fact that, in the analysis of friction piles, Nogami introduced a soil column beneath each pile so that he could use the formulation developed for end-bearing piles.

In the results presented in this chapter, as well as in chapters 4 and 5, it is assumed that the soil medium is a viscoelastic halfspace with $\nu_s = 0.40$ and $\beta_s = 0.05$, and the piles are made of elastic materials with $\nu_p = 0.25$ and $\beta_p = 0.00$. In addition, it is assumed that $\frac{\rho_s}{\rho_p} = 0.70$ and $\frac{L}{d} = 15$. The response quantities examined in this chapter are evaluated for a number of pile spacings ($\frac{s}{d} = 2$, 5 and 10) and group formations (2 x 2, 3 x 3 and 4 x 4 square groups), as well as two soil conditions (soft soil: $\frac{E_s}{E_p} = 10^{-3}$; stiff soil: $\frac{E_s}{E_p} = 10^{-2}$), and the two types of pile-to-cap connection (fixed or hinged).

3.1 Dynamic Stiffnesses of Pile Groups

The stiffness functions, obtained with the present formulation, are complex quantities which can be expressed as:

$$K = k + i\, a_o\, c \tag{3.1}$$

For horizontal and torsional cases, the dynamic stiffnesses are normalized with respect to the horizontal static stiffness of a single

pile in the group, $k^s_{xx}(a_o = 0)$, whereas for the vertical and rocking dynamic stiffnesses the vertical static stiffness of a single pile, $k^s_{zz}(a_o = 0)$, has been used for the normalization. More specifically, the normalization factor for the horizontal, vertical, rocking and torsional dynamic stiffnesses are: $N k^s_{xx}(a_o = 0)$, $N k^s_{zz}(a_o = 0)$, $\sum x_i^2 \, k^s_{zz}(a_o = 0)$, and $\sum r_i^2 \, k^s_{xx}(a_o = 0)$, respectively: in these factors x and r refer to the Cartesian and polar pile coordinates, respectively. (In order to distinguish between the stiffnesses of pile groups and single piles, a superscript "G" is used for the former and a superscript "s" for the latter.)

Figure 3.3 shows the horizontal and vertical stiffnesses and dampings of a 2 x 2 pile group embedded in a halfspace, for different pile spacing (s/d = 2, 5 and 10) and for $E_s/E_p = 10^{-3}$. This figure shows that the behavior of a pile group for very close spacings and up to a certain frequency, is very similar to that of a rigid footing; that is, stiffnesses decrease with frequency and even become negative, indicating a behavior dominated by inertia effects, and radiation dampings display a frequency-independent characteristic. On the other hand, interaction effects among the piles start to dominate the overall behavior of the group as frequency exceeds a certain limit. This can be verified by examining the changes in the patterns of k_{xx} and k_{zz} for different pile spacings. (For example, for s/d = 5, the figure shows that k_{xx} and k_{zz} first decrease up to a certain frequency and then start to change their pattern). The transition between the two modes of behavior occurs at smaller frequencies as the distance between the piles increases.

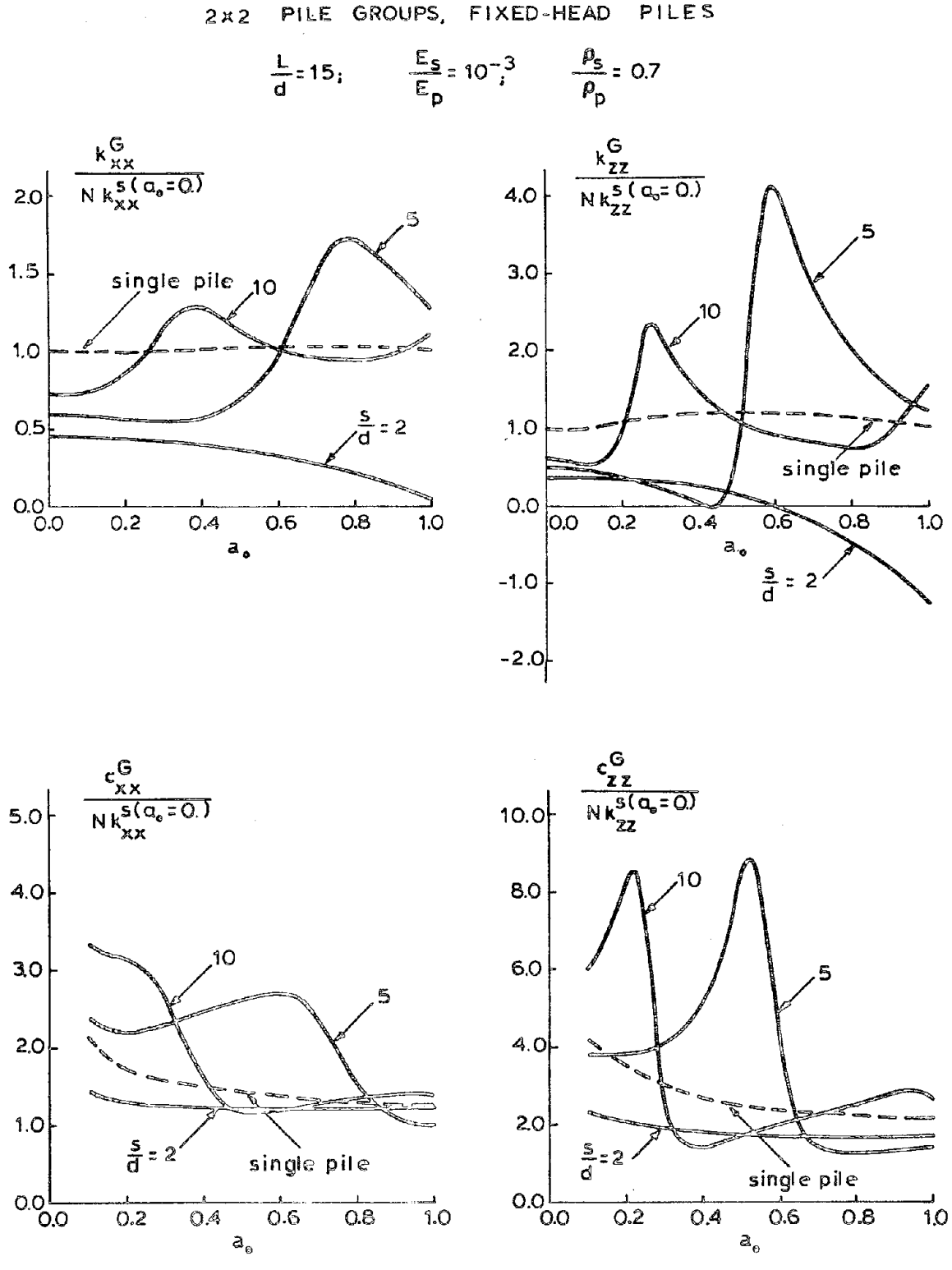

Fig. 3.3 - Horizontal and Vertical Dynamic Stiffnesses of 2 x 2 Pile Groups in a Soft Soil Medium.

Figures 3.4 and 3.5 present the results for the horizontal and vertical dynamic stiffnesses of 3 x 3 and 4 x 4 pile groups for the same soil and pile parameters used for the 2 x 2 group (Fig. 3.3). In addition to the general characteristics observed in Fig. 3.3, these figures display a more pronounced group behavior as the number of piles increases. Moreover, with an increase in the number of piles, more peaks are introduced in the variation of stiffnesses and dampings.

An interesting common feature of these results is the very large interaction effect in the group; if there had been no interaction, the curves would have coincided with those of a single pile, the real part of which deviates only slightly from unity in the frequency range considered (dashed line in Fig. 3.3). The large interaction effects, which seem to be stronger for the vertical vibration than for the horizontal, are essentially due to the out-of-phase vibration of piles. This point will be discussed again when the superposition scheme is examined in chapter 5.

Figure 3.6 shows the horizontal as well as vertical stiffnesses and dampings of 3 x 3 pile groups in which the piles are hinged to the cap. Comparing the results in this figure with those in Fig. 3.4 (corresponding to groups in which the piles are rigidly connected to the cap), one can see that there is a considerable reduction in the horizontal stiffnesses and dampings, as expected. These quantities, however, have the same features as were displayed by plots of k_{xx} and c_{xx} in Fig. 3.4.

Figure 3.7 shows the horizontal and vertical dynamic stiffnesses for a stiffer halfspace ($E_s/E_p = 10^{-2}$) and for groups with different

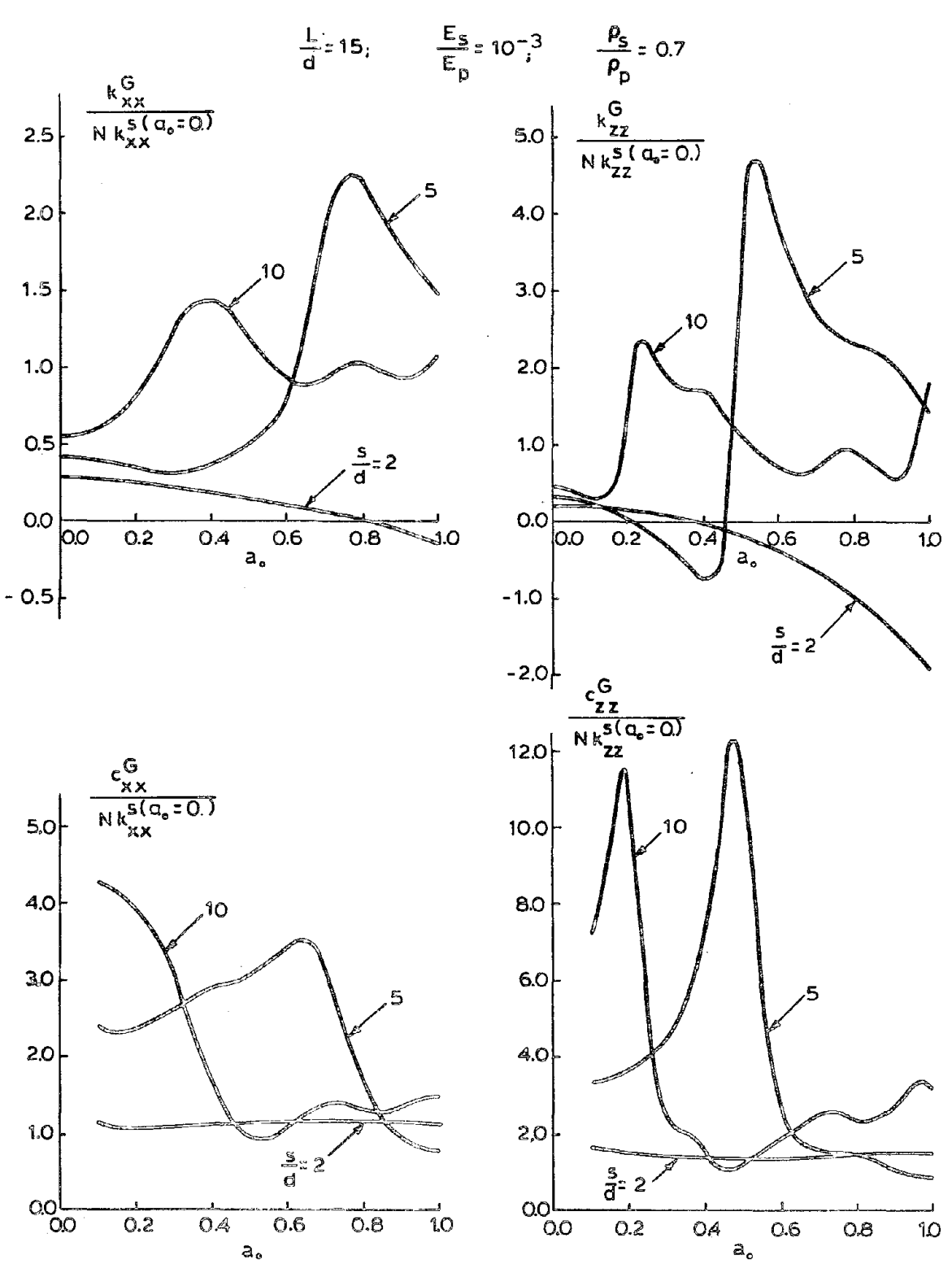

Fig. 3.4 - Horizontal and Vertical Dynamic Stiffnesses of 3 x 3 Pile Groups in a Soft Soil Medium.

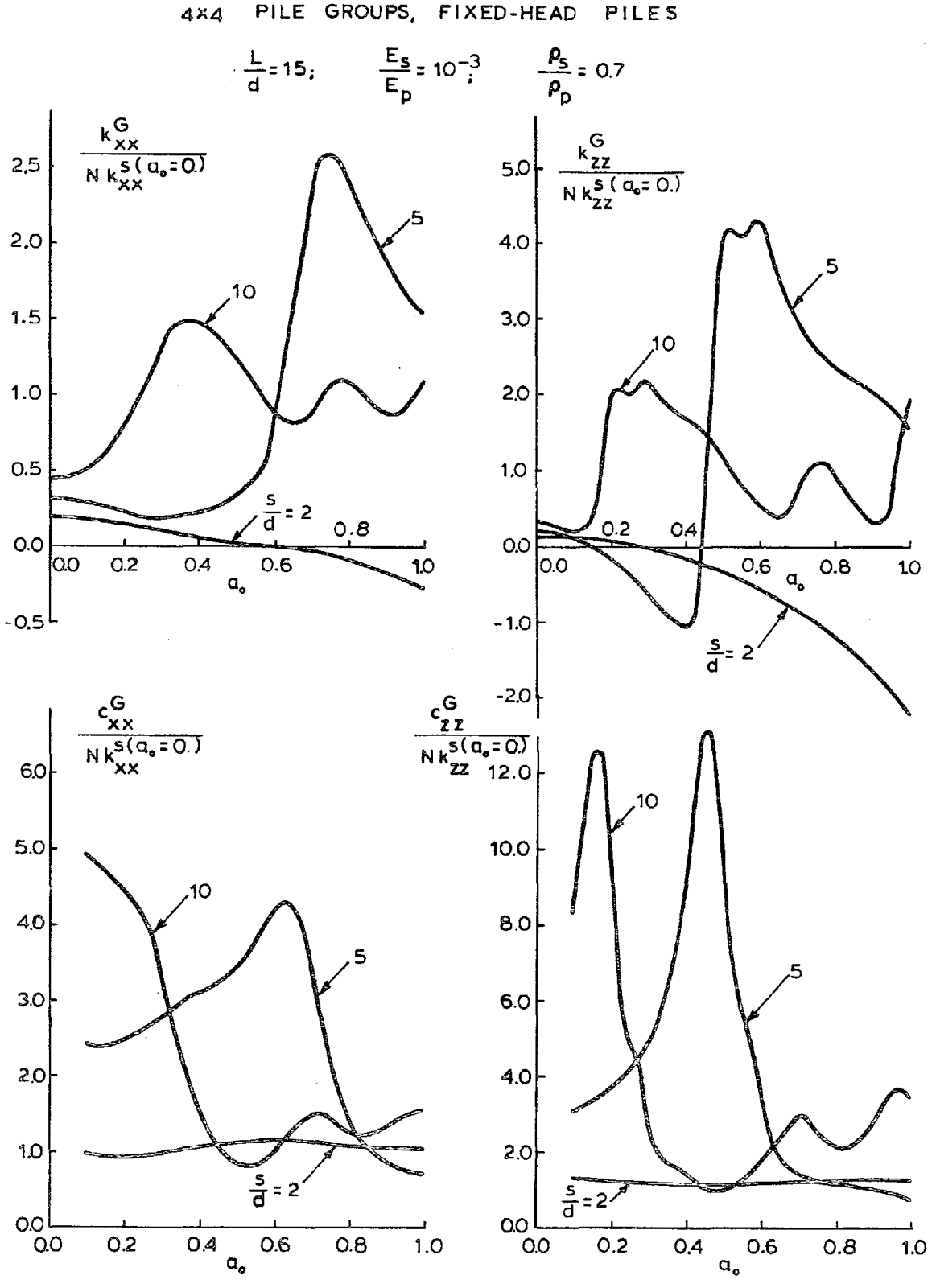

Fig. 3.5 - Horizontal and Vertical Dynamic Stiffnesses of 4 x 4 Pile Groups in a Soft Soil Medium.

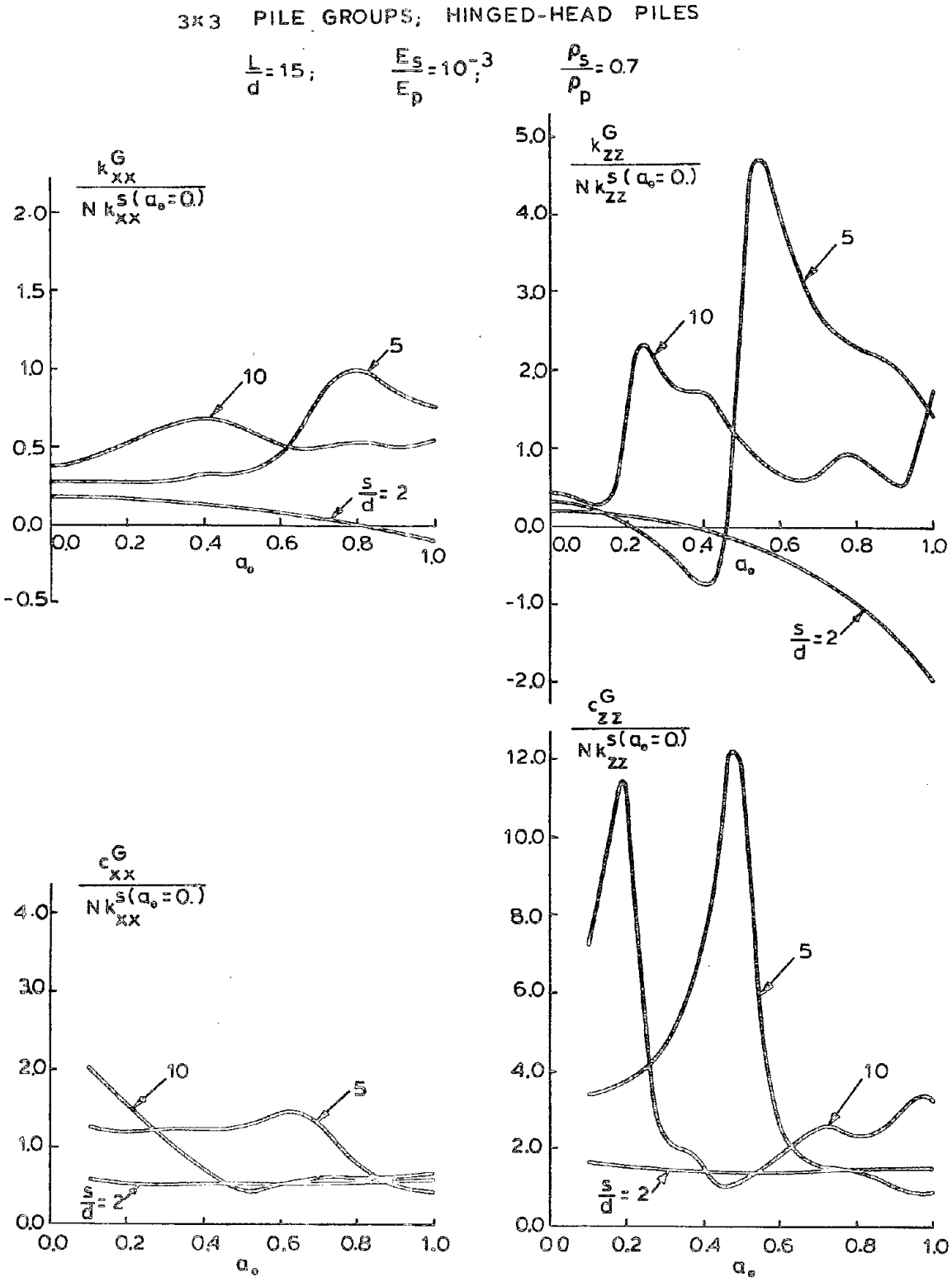

Fig. 3.6 - Horizontal and Vertical Dynamic Stiffnesses of 3 x 3 pile Groups in a Soft Soil Medium (Hinged-Head Piles).

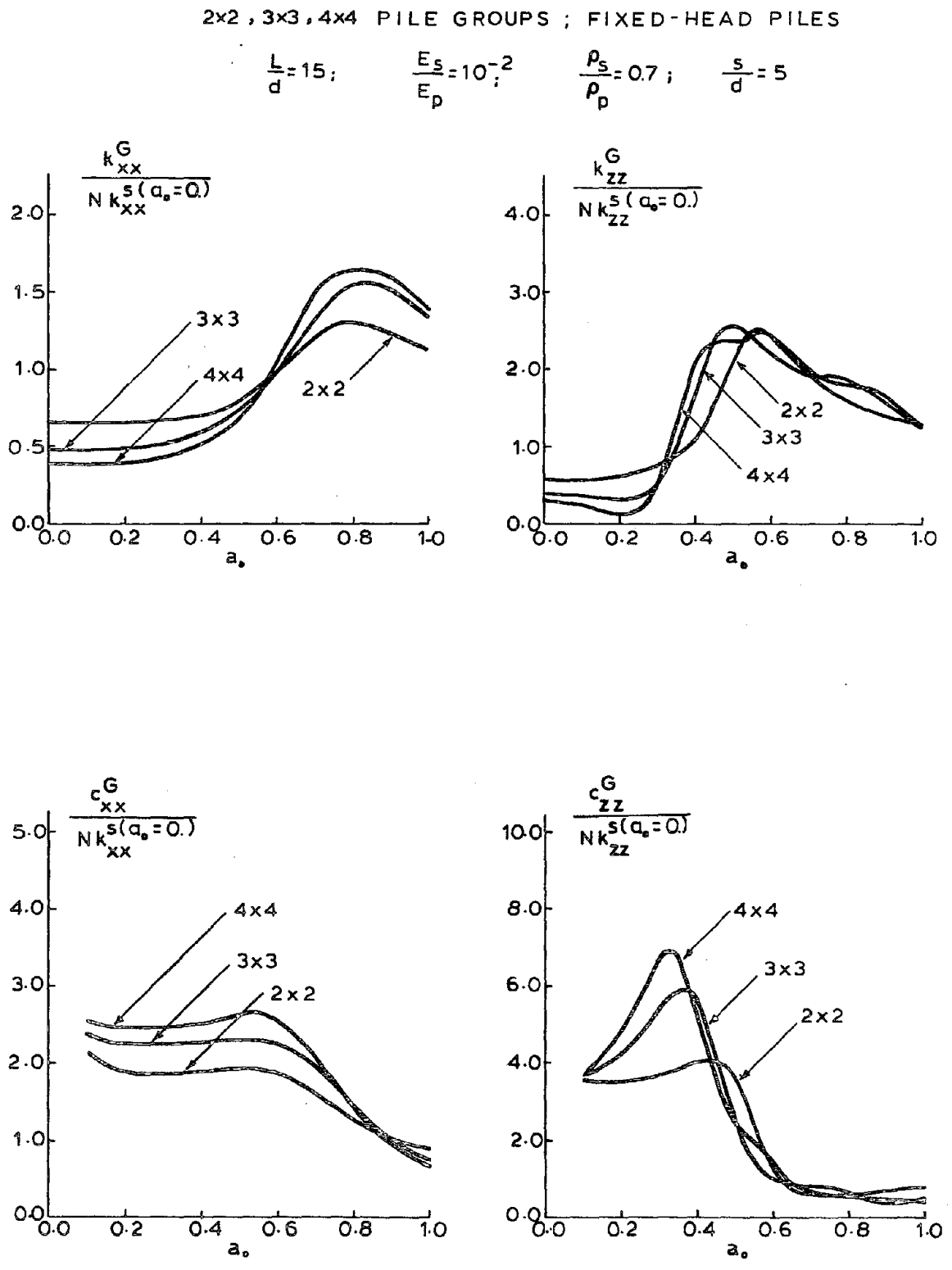

Fig. 3.7 - Horizontal and Vertical Dynamic Stiffnesses of Pile Groups with s/d = 5 in a Stiff Soil Medium.

number of piles (2 x 2, 3 x 3 and 4 x 4). For all these pile groups, s/d = 5. This figure displays basically the same features observed for the groups in the soft soil medium (Figs. 3.3, 3.4 and 3.5). However, the interaction effects seem to be less pronounced for the stiffer soil medium.

Another interesting characteristic of these results is that, for low frequencies, the radiation damping increases as the width of the foundation (pile cap) is increased.

Figures 3.8 to 3.12 show the rocking and torsional dynamic stiffnesses associated with groups for which the horizontal and vertical dynamic stiffnesses were presented in Figs. 3.3, 3.4, 3.5, 3.6 and 3.7, respectively. (The pile and soil parameters are indicated in the figures.) Most of the observations on the characteristics of the horizontal and vertical dynamic stiffnesses, such as the dependence of group stiffnesses and dampings on the pile spacing, the number of piles and the stiffness of the soil medium, apply to the torsional and rocking dynamic stiffnesses as well. Greater interaction effects for these cases are, however, associated with the in-phase vibration of piles.

An important characteristic that differentiates between the behavior of pile groups and single piles is associated with the concept of a pressure bulb. The pressure bulb is defined here as the zone in the neighborhood of the foundation where stresses (and strains) are significant. As a result, the characteristics of this zone play a major role in the behavior of the foundation. Since this zone extends to depths which are comparable to the size of the foundation, one is led to expect that the characteristics of the deeper layers influence, to a greater

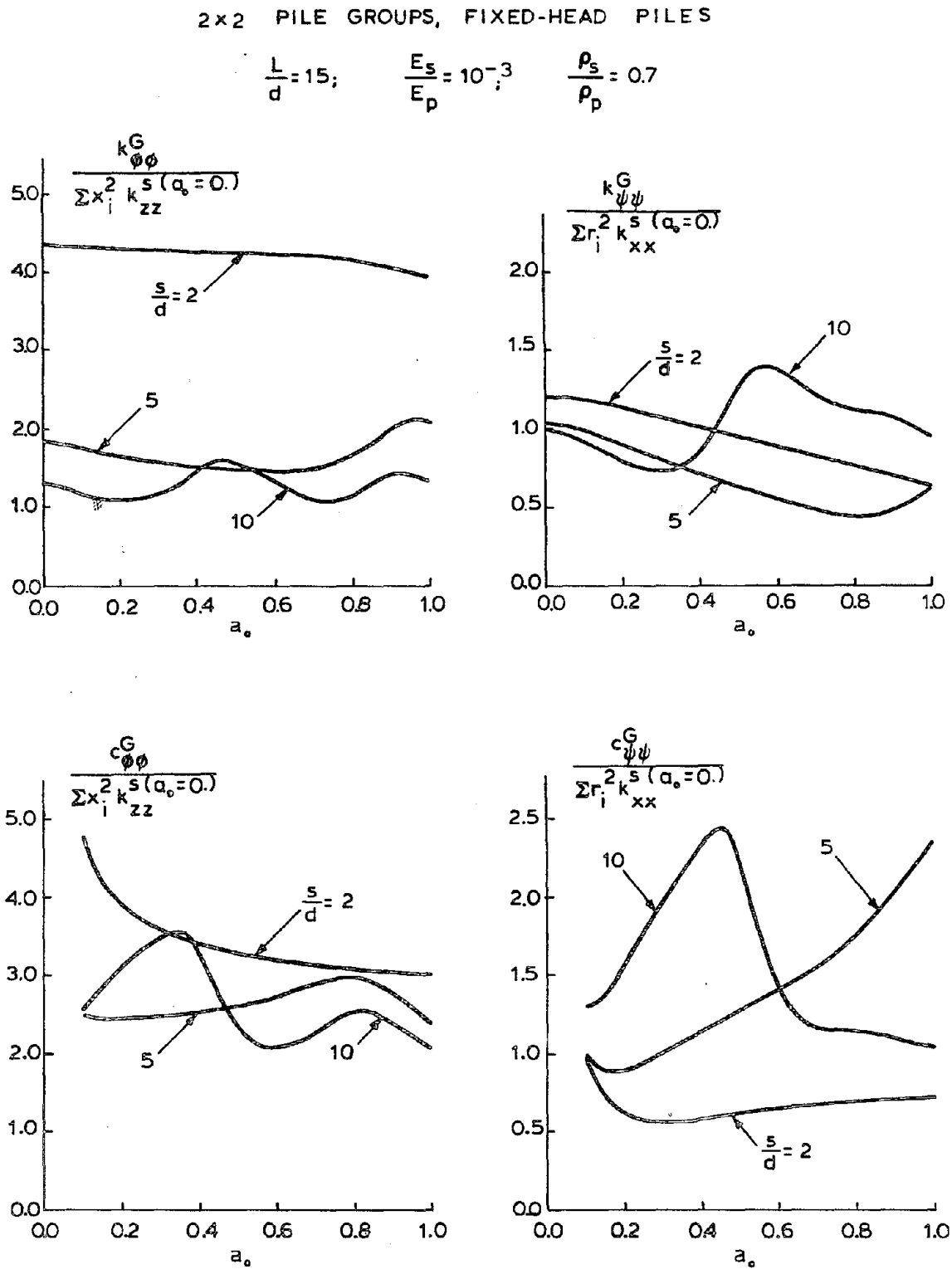

Fig. 3.8 - Rocking and Torsional Dynamic Stiffnesses of 2 x 2 Pile Groups in a Soft Soil Medium.

3x3 PILE GROUPS, FIXED-HEAD PILES

$\frac{L}{d} = 15; \quad \frac{E_s}{E_p} = 10^{-3}; \quad \frac{\rho_s}{\rho_p} = 0.7$

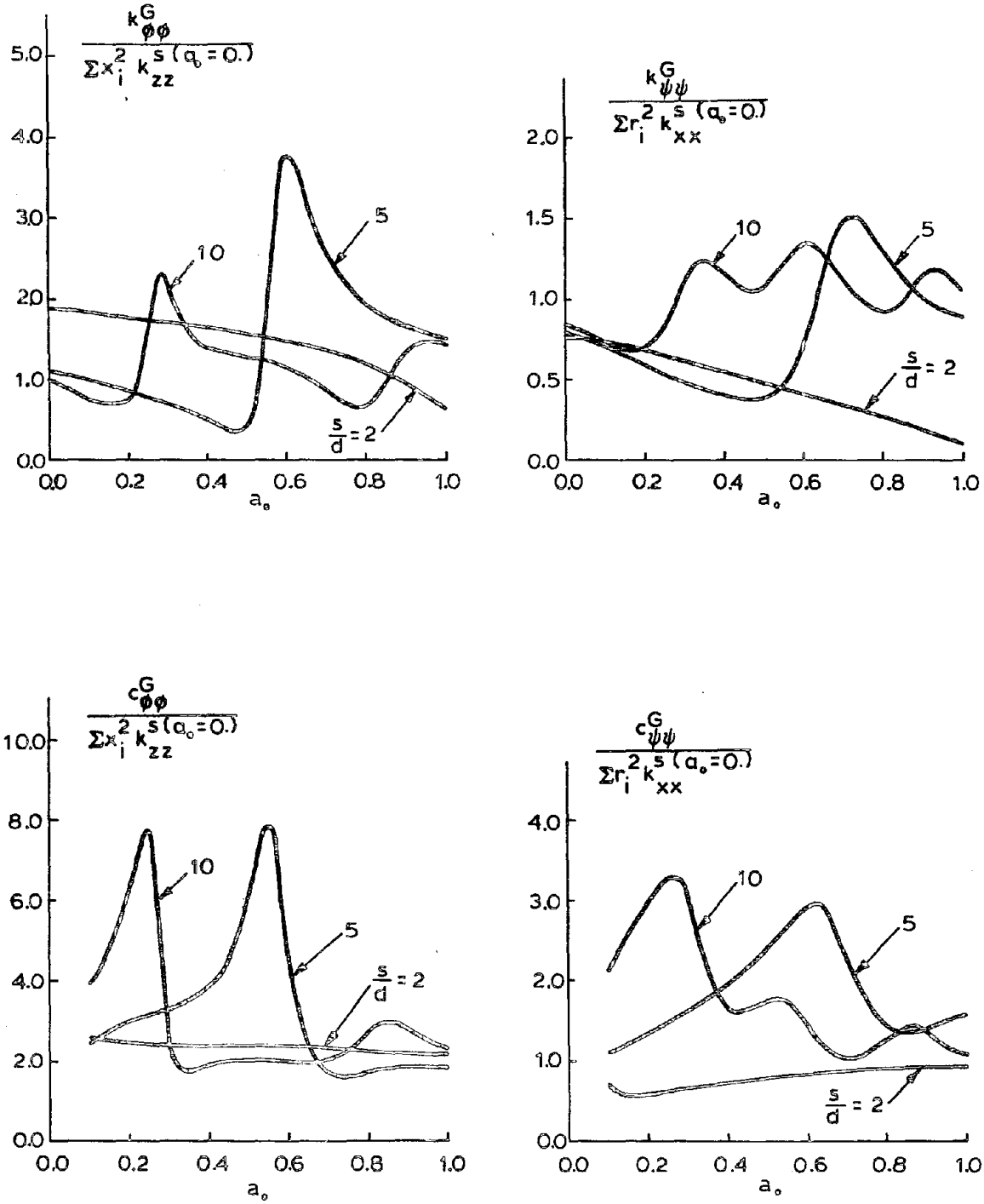

Fig. 3.9 - Rocking and Torsional Dynamic Stiffnesses of 3 x 3 Pile Groups in a Soft Soil Medium.

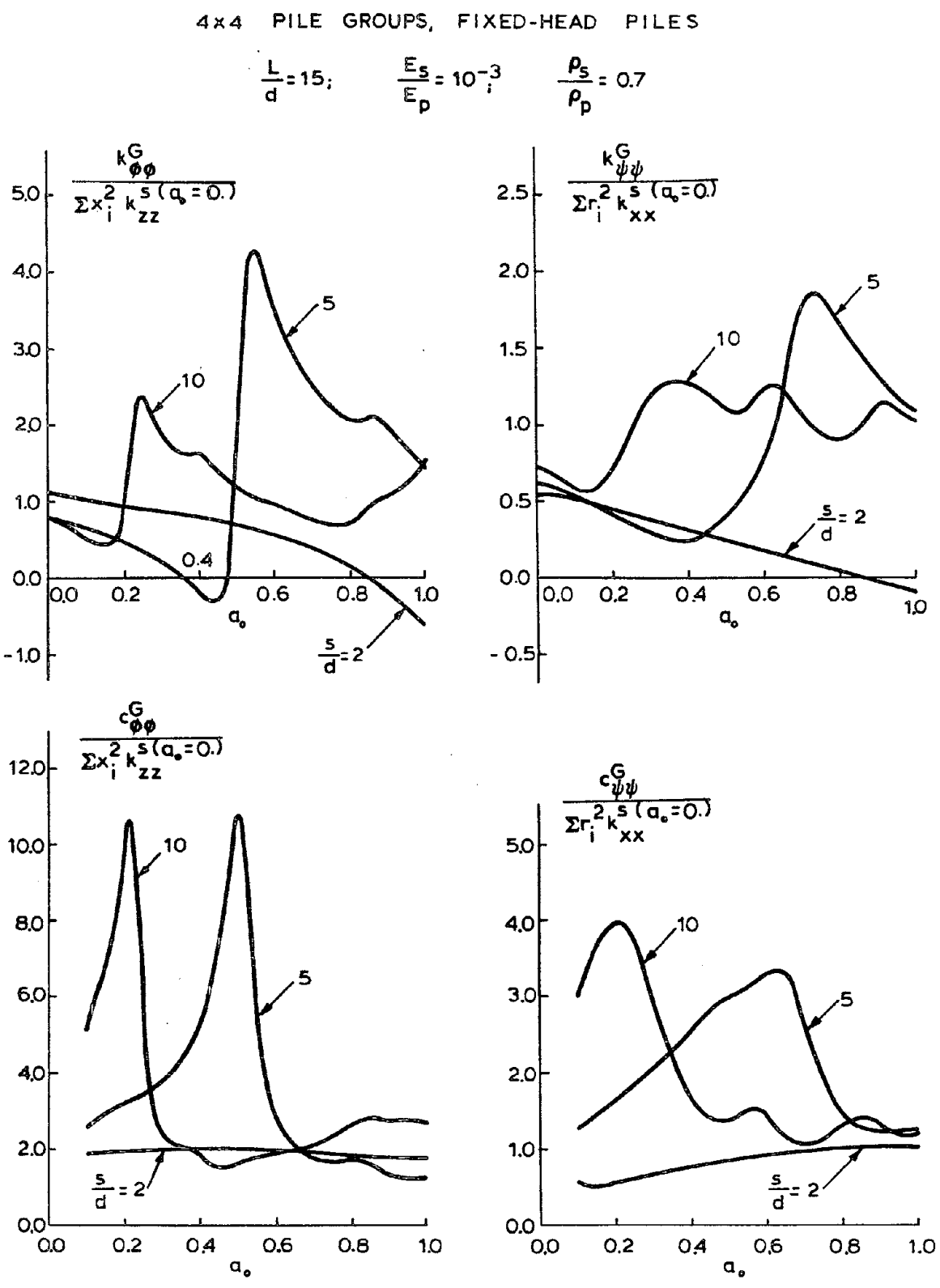

Fig. 3.10 - Rocking and Torsional Dynamic Stiffnesses of 4 x 4 Pile Groups in a Soft Soil Medium.

3x3 PILE GROUPS; HINGED-HEAD PILES

$\frac{L}{d}=15$; $\frac{E_s}{E_p}=10^{-3}$ $\frac{\rho_s}{\rho_p}=0.7$

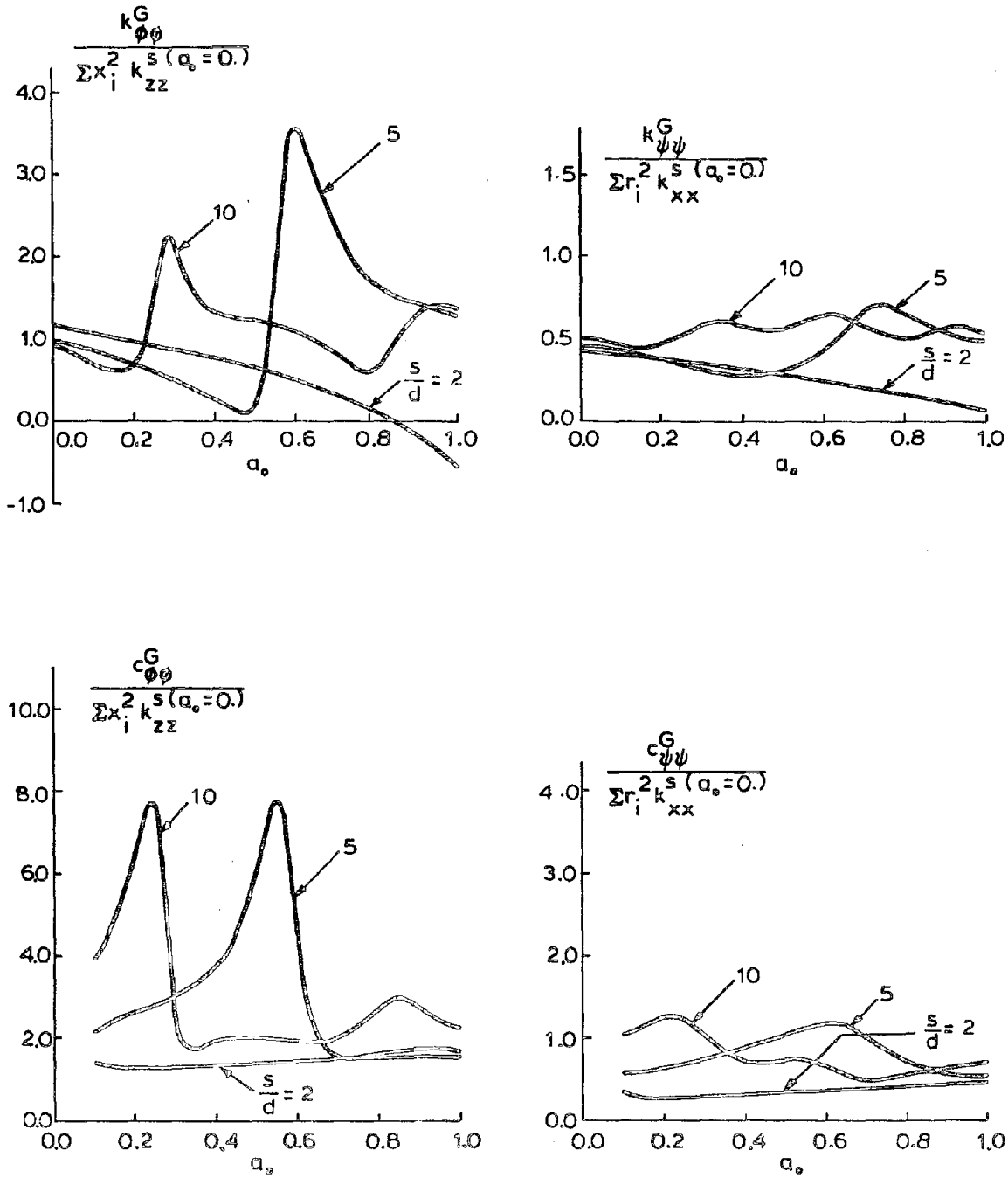

Fig. 3.11 - Rocking and Torsional Dynamic Stiffnesses of 3 x 3 Pile Groups in a Soft Soil Medium (Hinged-Head Piles).

2x2 , 3x3 , 4x4 PILE GROUPS FIXED-HEAD PILES

$\frac{L}{d} = 15$; $\frac{E_s}{E_p} = 10^{-2}$; $\frac{\rho_s}{\rho_p} = 0.7$; $\frac{s}{d} = 5$

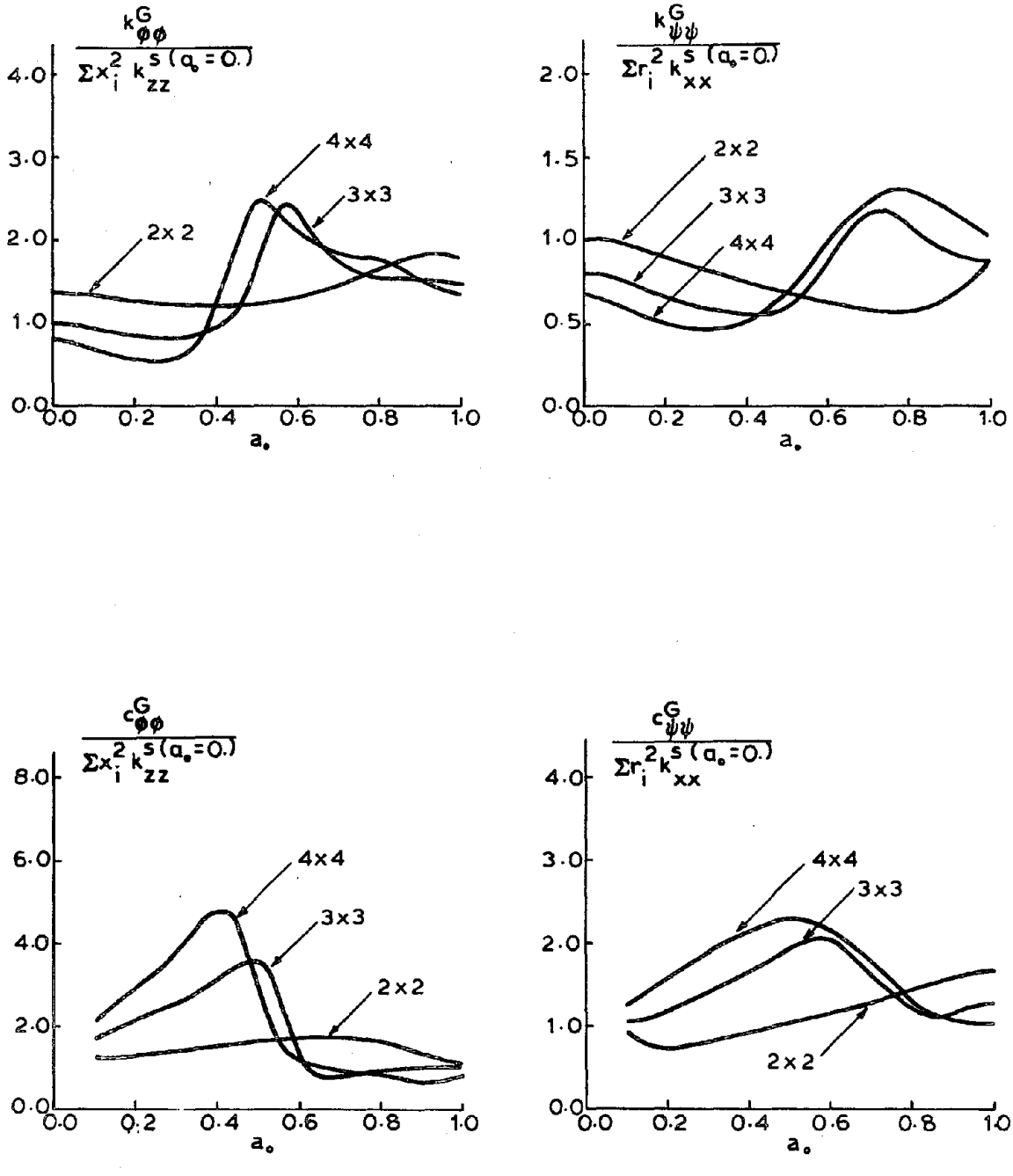

Fig. 3.12 - Rocking and Torsional Dynamic Stiffnesses of Pile Groups with s/d = 5 in a Stiff Soil Medium.

extent, the overall response of pile groups than they do the response of single piles, where behavior is controlled primarily by the near-surface soil-pile properties. This can be verified, in fact, by examining the results in Fig. 3.13. In this figure the ratio of the absolute values of the stiffnesses of a pile group, embedded in two different soil media, are compared. The first medium is a homogeneous halfspace with $E_s/E_p = 10^{-2}$, and the second, a halfspace similar to the former, but overlain by a surface layer with thickness h=d and stiffness ratio $E_s/E_p = 10^{-3}$ (i.e., 10 times softer). This second case might also be considered as a simple model to account for the nonlinear effects that may be expected in the neighborhood of the pile heads as a result of soil yielding and pile-soil separation. The results clearly show that, as the number of piles increases, the stiffness ratio at low frequencies increases, and approaches unity. Therefore, pile groups are less influenced by conditions near the surface than single piles are. This observation also bears on the accuracy of the techniques which use the result of single-pile nonlinear analyses (or field tests on single piles) along with the empirical group reduction factors to derive group stiffnesses.

3.2 Seismic Response of Pile Groups

As was stated earlier in this chapter, for a conventional foundation-structure interaction analysis for seismic excitation, one needs to evaluate the motions of the foundation (pile cap) in the absence of the superstructure. In the present study, it is assumed that the seismic motion is due to vertically propagating shear waves in the halfspace that

$\frac{L}{d}=15$; $\frac{s}{d}=5$; $\frac{\rho_s}{\rho_p}=0.70$; FIXED-HEAD PILES

1-LAYER SYSTEM : HALF SPACE; $\frac{E_s}{E_p}=10^{-2}$

2-LAYER SYSTEM : TOP LAYER: $\frac{h}{d}=1.0$; $\frac{E_s}{E_p}=10^{-3}$

BOT. LAYER: HALF SPACE; $\frac{E_s}{E_p}=10^{-2}$

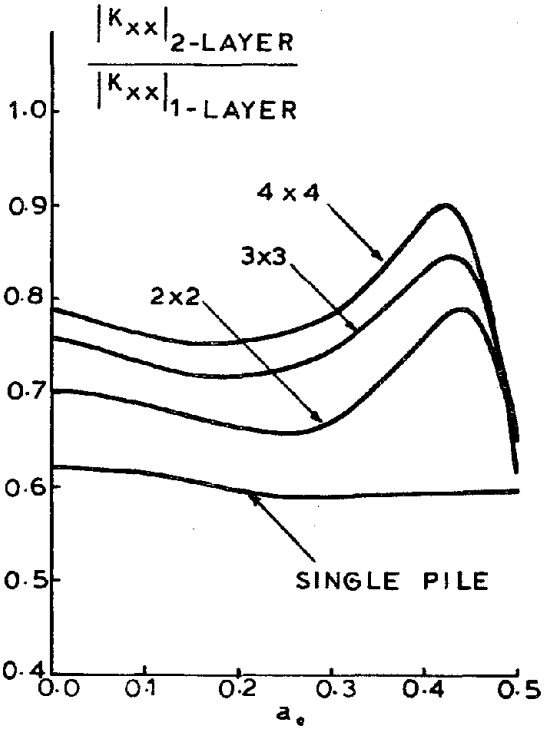

Fig. 3.13 - Effect of a Near Surface Soft Soil Layer on the Stiffness of Pile Groups and Single Piles.

produce a free-field ground-surface displacement u_g. These waves induce both a translation and a rotation in the pile cap. The transfer functions for these quantities are complex-valued functions and will be presented in terms of their absolute values.

Figure 3.14 presents the absolute value of the transfer functions for the horizontal displacement, u, and rotation, ϕ, of the pile cap for 2 x 2 pile groups with different pile spacings (s/d = 2, 5 and 10) and with $E_s/E_p = 10^{-3}$ (these are the same pile groups for which the stiffness characteristics were studied in Fig. 3.3). The transfer function for the pile-head displacement of a single pile is also shown in the figure (the dashed line). This figure shows that as the foundation width increases, the absolute value of the transfer function for the translation, $|u|/u_g$, approaches unity at low-frequency values. This implies that the pile cap essentially follows the ground motion, although it filters out to some degree its high-frequency content. For example, if C_s = 70 m/sec (soft soil), d = 1 m and s = 10 m (s/d = 10), then the fact that the values of $|u|/u_g$ up to $a_o = 0.2$ are very close to one, implies that the filter function is essentially unity up to the frequency f = 2.25. Since the seismic motion at the ground surface for the soft soil medium considered here will be characterized by low-frequency components, it can be concluded that the motion of the pile cap and the soil will be very similar.

On the other hand, the figure displays a significant dependence of $|\phi|$ on the width of the foundation. More specifically, as the foundation width increases, $|\phi|$ tends rapidly to zero. This implies that for foundations having large width, one can neglect the rotation of the foundation in seismic analyses.

2×2 PILE GROUPS, FIXED-HEAD PILES

$\frac{L}{d} = 15; \quad \frac{E_s}{E_p} = 10^{-3}; \quad \frac{\rho_s}{\rho_p} = 0.7$

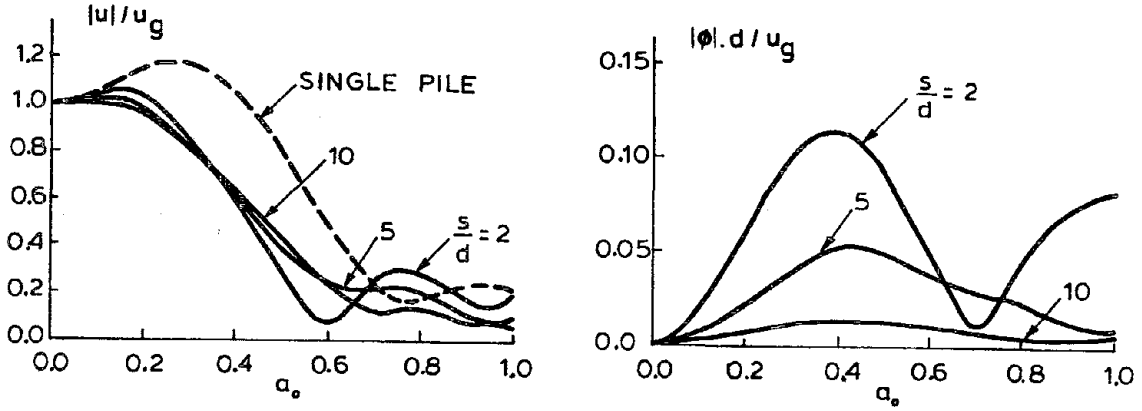

Fig. 3.14 - Absolute Value of Transfer Functions for the Horizontal Displacement and Rotation of the Pile Cap for 2 x 2 Pile Groups in a Soft Soil Medium.

3×3 PILE GROUPS, FIXED-HEAD PILES

$\frac{L}{d} = 15; \quad \frac{E_s}{E_p} = 10^{-3} \quad \frac{\rho_s}{\rho_p} = 0.7$

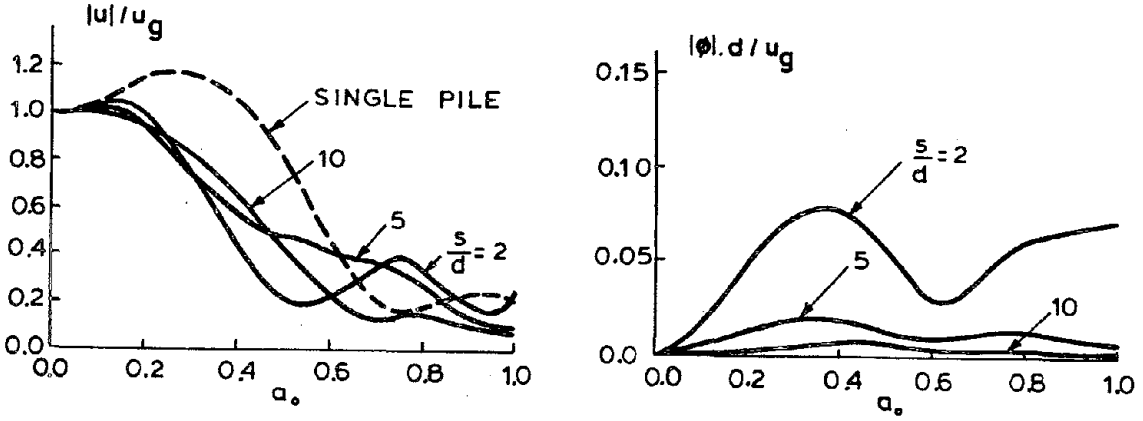

Fig. 3-15 - Absolute Value of Transfer Functions for the Horizontal Displacement and Rotation of the Pile Cap for 3 x 3 Pile Groups in a Soft Soil Medium.

Figures 3.15 and 3.16 present the absolute value of transfer functions for the translation and rotation of the pile cap for 3 x 3 and 4 x 4 pile groups for the same soil and pile parameters considered for the 2 x 2 group. These figures, in general, exhibit the same characteristics that were displayed by Fig. 3.14. It is especially interesting to note the significant reduction in $|\phi|$ for s/d = 10 in Fig. 3.16 (the 4 x 4 group).

Fig. 3.17 shows the variation of $|u|$ and $|\phi|$ for 3 x 3 pile groups in which the piles are hinged to the cap. As pile spacing increases in this case, values of $|u|$ for the group approach those of a single pile; hence the foundation tends to amplify low-frequency components of the earthquake. On the other hand, values of $|\phi|$ are considerably smaller for these groups than for groups with rigid pile-to-cap connections (compare with Fig. 3.15).

Finally, Fig. 3.18 presents the transfer functions for groups with different numbers of piles with s/d = 5, embedded in a stiff halfspace, $E_s/E_p = 10^{-2}$. (The parameters in this figure are the same as those in Fig. 3.7). Comparing these results with those for soft soil conditions (Figs. 3.14, 3.15 and 3.16), one can conclude that pile groups in stiffer media follow more closely the ground motion and that they filter out only the high-frequency content of the earthquake ($|u|/u_g$ is essentially unity up to $a_o = 0.4$ in this figure)

3.3 Distribution of Loads in Pile Groups

With the present formulation the forces (reactions) developed at the pile heads due to harmonic forces applied on the pile cap are complex

4x4 PILE GROUPS, FIXED-HEAD PILES

$\frac{L}{d}=15;\quad \frac{E_s}{E_p}=10^{-3};\quad \frac{\rho_s}{\rho_p}=0.7$

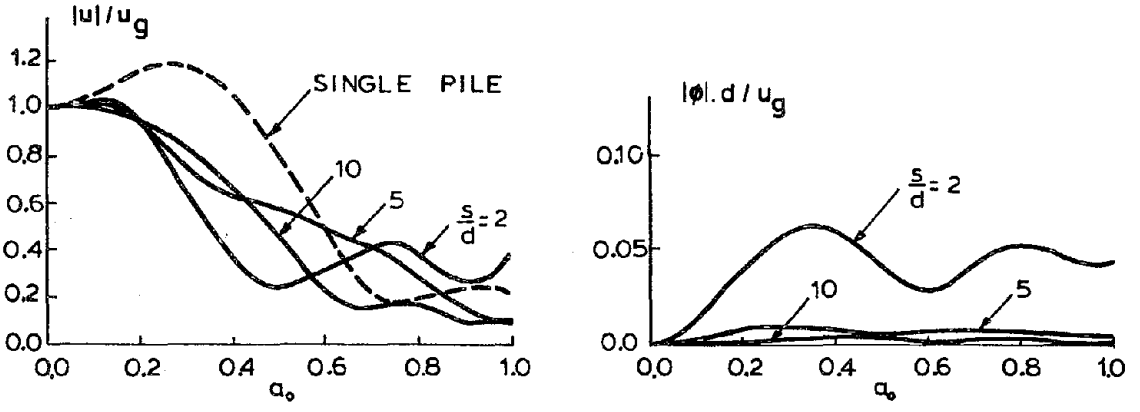

Fig. 3.16 - Absolute Value of Transfer Functions for the Horizontal Displacement and Rotation of the Pile Cap for 4 x 4 Pile Groups in a Soft Soil Medium.

3x3 PILE GROUPS; HINGED-HEAD PILES

$\frac{L}{d}=15;\quad \frac{E_s}{E_p}=10^{-3};\quad \frac{\rho_s}{\rho_p}=0.7$

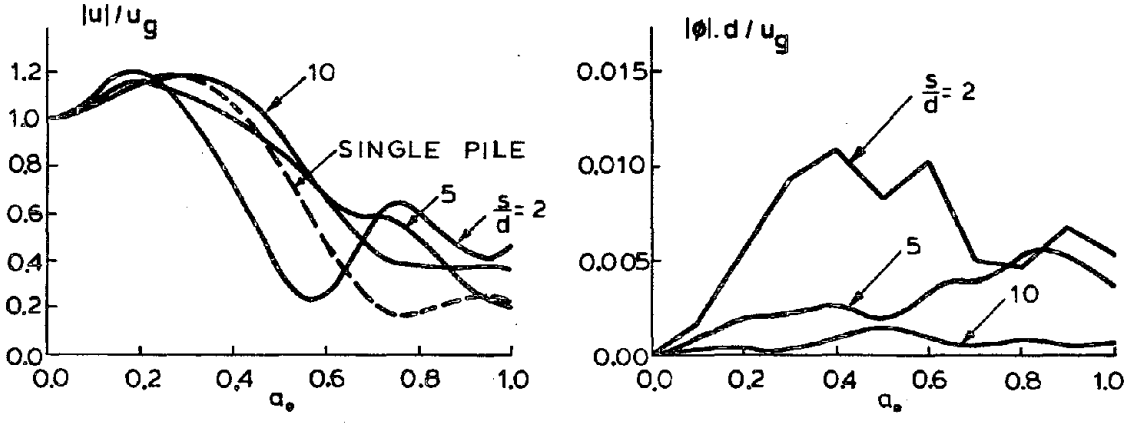

Fig. 3.17 - Absolute Value of Transfer Functions for the Horizontal Displacement and Rotation of the Pile Cap for 3 x 3 Pile Groups in a Soft Soil Medium (Hinged-Head Piles).

2x2 , 3x3 , 4x4 PILE GROUPS ; FIXED-HEAD PILES

$\frac{L}{d} = 15$; $\frac{E_s}{E_p} = 10^{-2}$; $\frac{\rho_s}{\rho_p} = 0.7$; $\frac{s}{d} = 5.0$

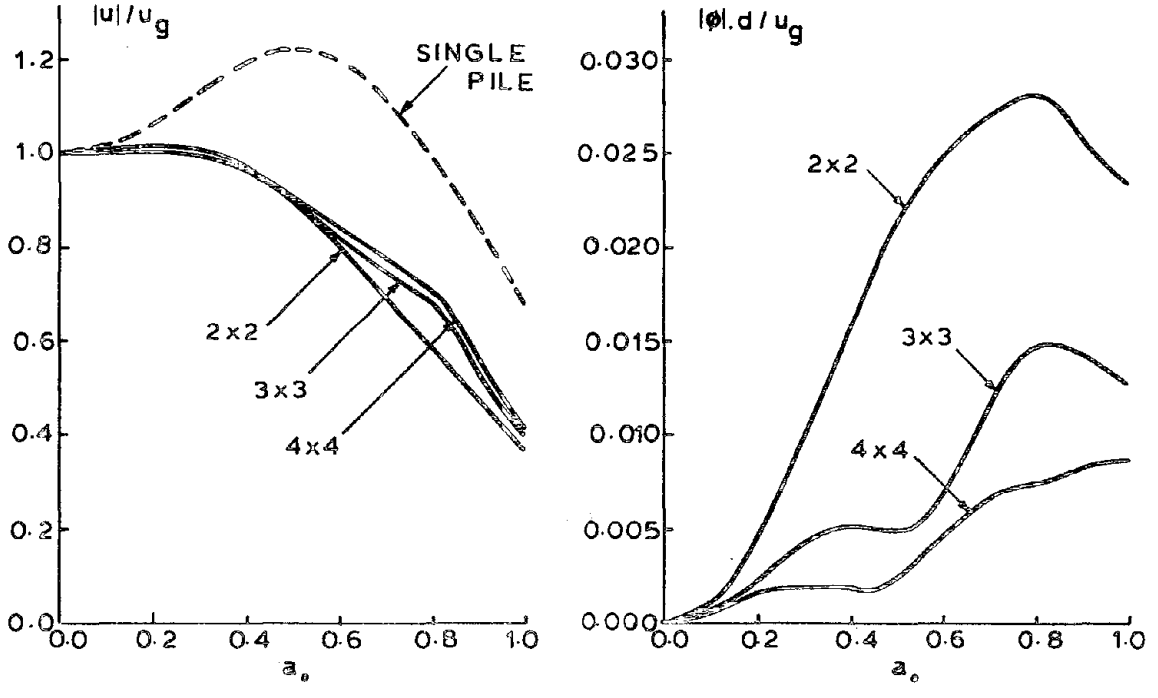

Fig. 3.18 - Absolute Value of Transfer Functions for the Horizontal Displacement and Rotation of the Pile Cap for Pile Groups with s/d = 5 in a Stiff Soil Medium.

quantities which can be expressed as:

$$R = |R|\ e^{-i\psi} \tag{3.2}$$

where $|R|$ is the maximum value of the reaction and ψ defines the phase lag between the reaction and the applied force. In this section a number of examples are investigated in order to determine the variation of $|R|$ with pile spacing, pile-to-cap fixity condition and frequency, for the different piles in a group. The fact that, at a given frequency, the value of ψ is not the same for the different piles in the group implies that the forces on the pile heads do not attain their maximum values at the same time: One might have then to consider this fact in interpreting the results to be presented.

Figure 3.19 shows the distribution of loads among the piles of the 3 x 3 group studied in Fig. 3.4 ($E_s/E_p = 10^{-3}$). The four plots in the top correspond to the shear, R_x, and the moment, M_x, at the pile heads due to a horizontal force, F_x, on the cap. The results are normalized with respect to the shear that would be observed in each pile if there were no interaction effects (i.e., F_x/N). These plots show that for the static case, the corner piles carry the largest portion of the load, while the piles closest to the center carry the smallest. However, this observation is no longer valid in the dynamic case. In fact, for some frequencies, a load distribution favorable to the corner piles may take place. This can be verified, for instance, by examining the variation with frequency of the shear force on piles I and IV for s/d = 5. The plots for these two cases show that the maximum shear in pile IV, for values of a_o between 0.6 and 0.8, is almost twice the maximum shear

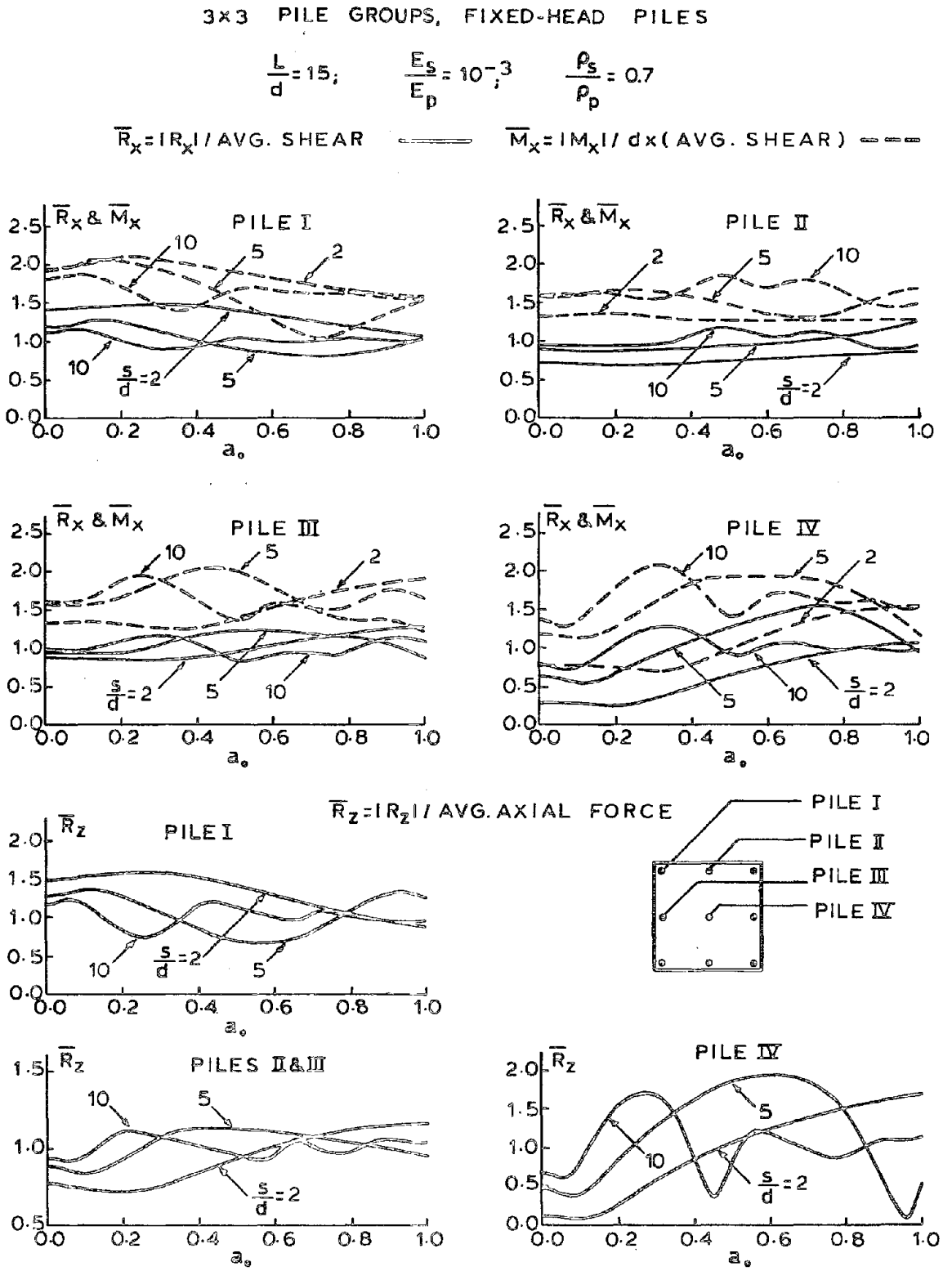

Fig. 3.19 - Distribution of Horizontal and Vertical Forces in 3 x 3 Pile Groups in a Soft Soil Medium.

in pile I. These results reveal that the magnification factor at these frequencies is considerably larger for the piles closest to the center than the corner piles. The piles on the edges of the cap, on the other hand, seem to be only slightly affected in their share of the applied load. As far as the moment at the pile heads is considered, the plots in Fig. 3.19 show that this quantity displays essentially the same characteristics as the shear does. It is very interesting to note that the plots of moment very closely follow the patterns exhibited by the plots of shear.

The remaining plots in Fig. 3.19 correspond to the axial forces, R_z, observed at pile-head level, caused by a vertical force, F_z, on the pile cap; the results are normalized with respect to the average vertical force (F_z/N). These plots show basically the same characteristics that were observed in the distribution of a horizontal force. The dynamic effects are, however, more pronounced for the vertical case (for example, observe the significant dynamic amplification of the axial force for some frequencies, which is as large as 4, on pile IV for s/d = 5).

Figure 3.20 presents the distribution of horizontal as well as vertical forces in 4 x 4 pile groups. The plots in this figure exhibit the general features of load distribution that were observed for the 3 x 3 group.

Finally, Fig. 3.21 shows the distribution of forces in 3 x 3 pile groups in which the piles are hinged to the cap. Comparing this figure with Fig. 3.19, one can see that there is only a slight change in the distribution of shear as a result of the change in the pile-head fixity condition. There is, however, no change in the distribution of axial force, as expected.

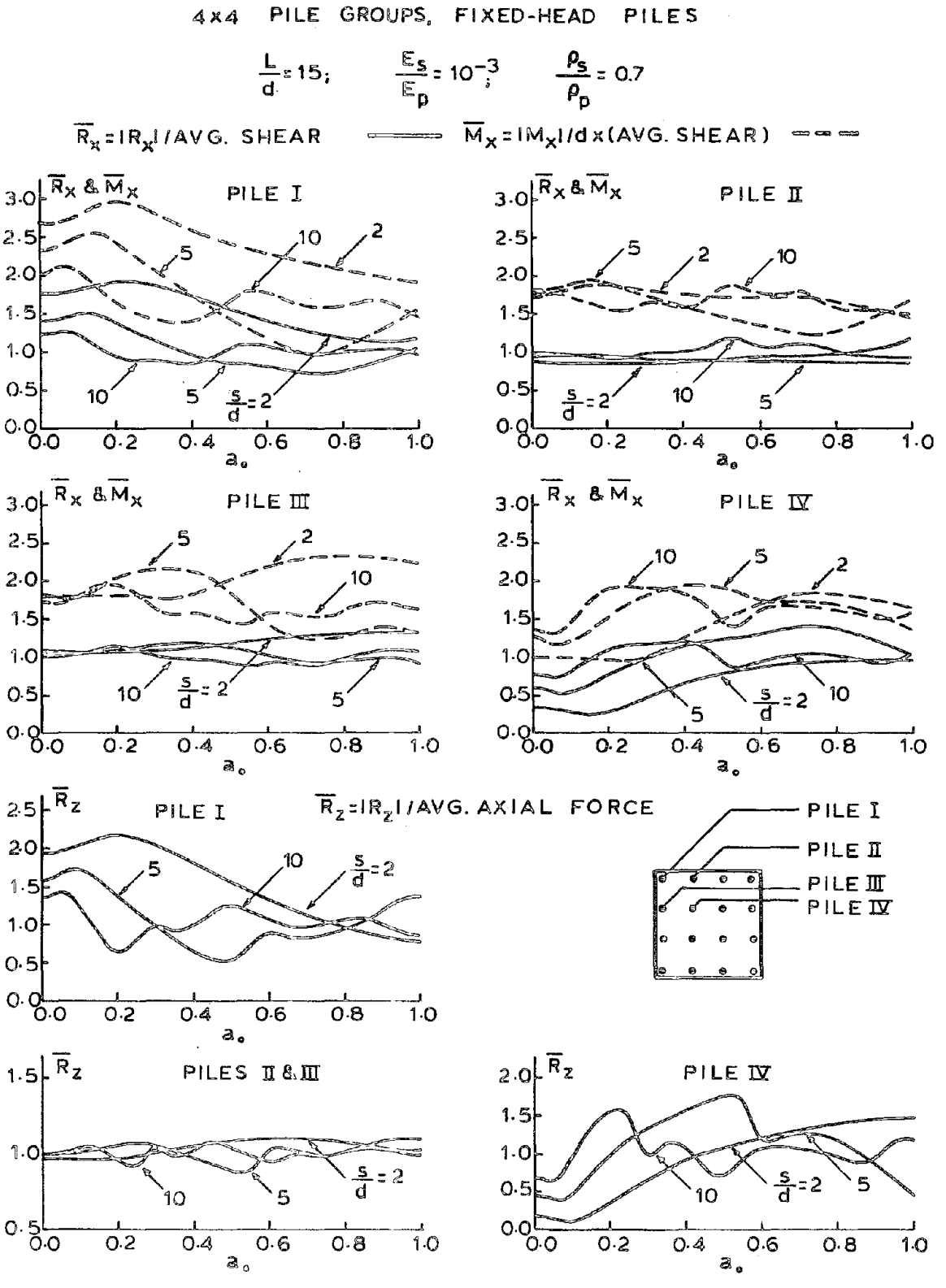

Fig. 3.20 - Distribution of Horizontal and Vertical Forces in 4 x 4 Pile Groups in a Soft Soil Medium.

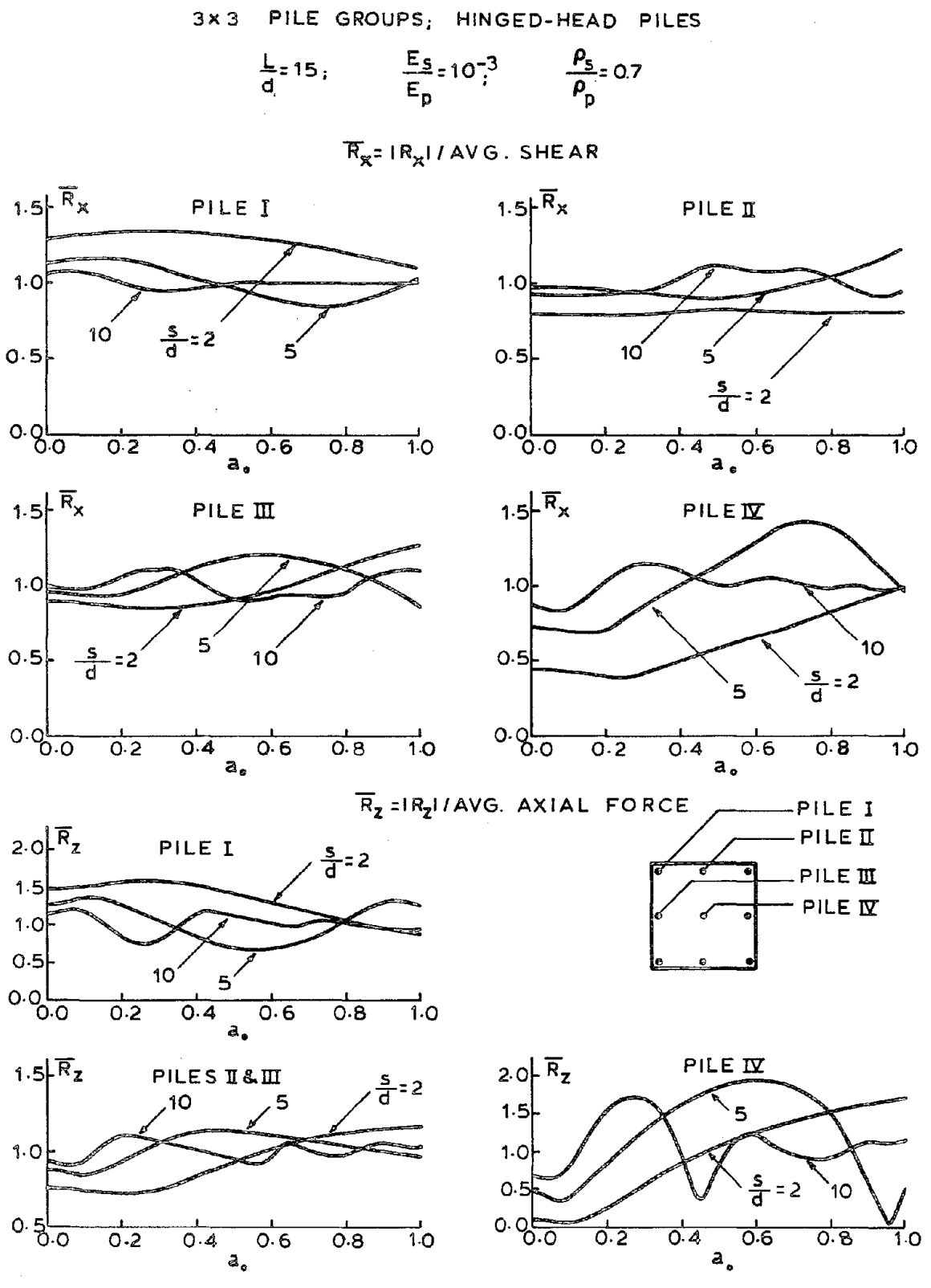

Fig. 3.21 · Distribution of Horizontal and Vertical Forces in 3 x 3 Pile Groups in a Soft Soil Medium (Hinged-Head Piles).

CHAPTER 4

THREE-DIMENSIONAL VS. QUASI-THREE-DIMENSIONAL SOLUTIONS

In the formulation outlined in chapter 2, it was assumed that the forces developed at the pile-soil interface consisted of lateral forces in the x- and y-directions, as well as frictional forces in the z-direction. These forces were then related to their corresponding displacements in the soil mass through a soil flexibility matrix. Similarly, these forces and the corresppnding displacements in the piles were related by certain pile "flexibility matrices." The final step in the formulation was the imposition of the compatibility between the displacements in the soil medium and in the piles.

Clearly, for a three-dimensional pile group analysis one has to develop a formulation which guarantees the full compatibility between the soil and the piles in all three directions (the formulation presented in chapter 2, which was briefly described above, is an example of a three-dimensional solution.) A quasi-three-dimensional solution, on the other hand, refers here to a formulation in which the compatibility condition in at least one direction is relaxed. An example of such a formulation is the one for the analysis of vertical vibration of pile groups in which only the frictional forces at the pile-soil interface and the associated displacements are taken into consideration. Most of the existing pile group solutions are, in fact, of the quasi-three-dimensional type. The underlying assumption for quasi-three-dimensional analyses is that the forces in the direction for which the compatibility condition is relaxed hardly affect the displacements in the main direction.

Clearly, a quasi-three-dimensional formulation requires much less computational effort than a three-dimensional one does; this is due to the fact that the former involves fewer degrees of freedom. Therefore, if justified, a quasi-three-dimensional solution is preferred over a fully three-dimensional one. It is important to point out that quasi-three-dimensional formulations are useful only for the analysis of symmetric pile groups. This is due to the fact that the motions of an unsymmetric pile group in the principal directions are coupled, and a quasi-three-dimensional formulation is not, in general, capable of modeling the coupling effect.

In what follows the results of a number of quasi-three-dimensional solutions are presented and compared with their three-dimensional counterparts, which were presented in chapter 3.

Figure 4.1 shows the horizontal and vertical dynamic stiffnesses for 4 x 4 pile groups in the soft soil medium ($E_s/E_p = 10^{-3}$). The horizontal dynamic stiffness is obtained by considering, in the formulation, only the horizontal pile-soil interface forces in the direction for which the stiffness is evaluated, whereas the vertical dynamic stiffness is obtained by considering only the vertical forces at the pile-soil interface (frictions and pile-tip forces). Comparison between this figure and Fig. 3.5, which was obtained by the three-dimensional formulation, shows that the two solutions are almost identical, even for close spacing.

Figure 4.2 presents the horizontal and vertical dynamic stiffnesses for pile groups with s/d = 5 in the stiff soil medium ($E_s/E_p = 10^{-2}$). Comparison of these results with those in Fig. 3.7 again shows an excellent agreement between the two solutions.

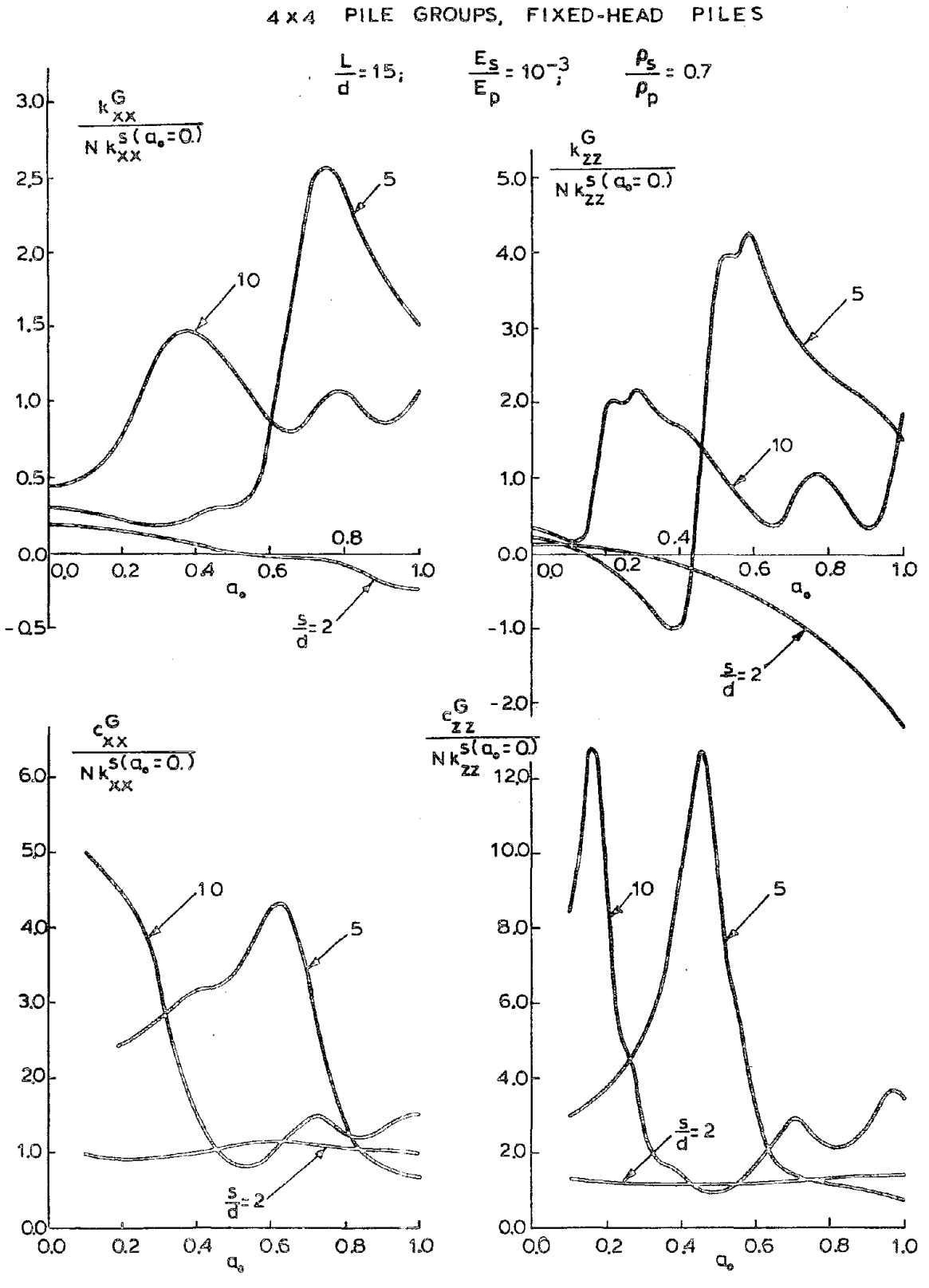

Fig. 4.1 - Horizontal and Vertical Dynamic Stiffnesses of 4 x 4 Pile Groups in a Soft Soil Medium by the Quasi-Three-Dimensional Formulation.

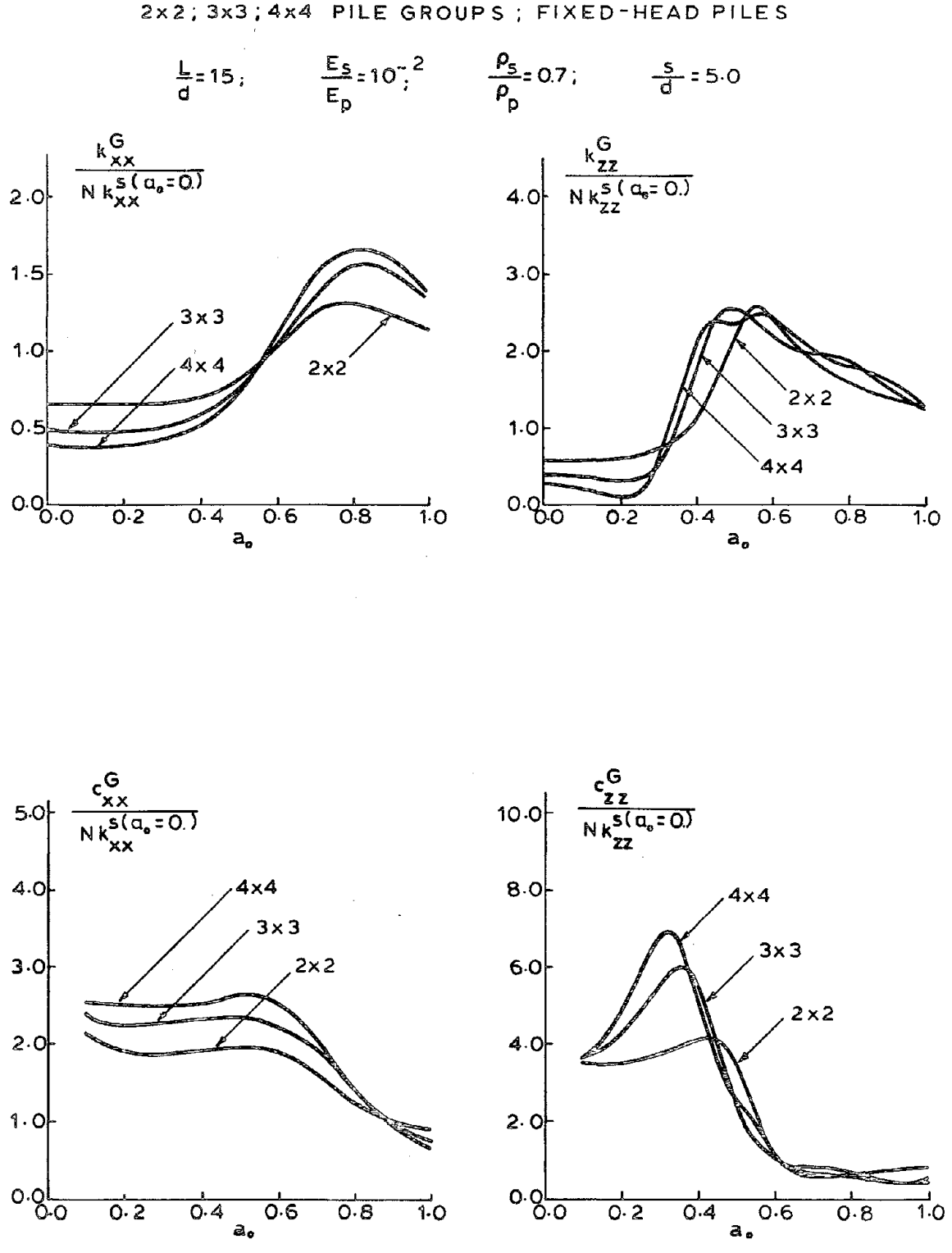

Fig. 4.2 - Horizontal and Vertical Dynamic Stiffnesses of Pile Groups with s/d = 5 in a Stiff Soil Medium by the Quasi-Three-Dimensional Formulation.

For the rocking mode of vibration, both the horizontal and vertical forces at the pile soil interface have nonnegligible effects on the behavior of the group; therefore, for a quasi-three-dimensional analysis, it is assumed that the vertical forces as well as the horizontal forces in the direction of rocking are present. In addition, in order to introduce the basic assumption of quasi-three-dimensional solutions, it is assumed that horizontal forces produce only horizontal displacements and vertical forces cause only vertical displacements. Similarly, for the torsional mode of vibration, only the two components of the horizontal forces at the pile-soil interface, which are assumed to be uncoupled, are included in the analysis. Fig. 4.3 shows the rocking and torsional dynamic stiffnesses for 4 x 4 groups in the soft soil medium, and Fig. 4.4 shows the same quantities for groups with s/d = 5 in the stiff soil medium. Comparison of these results with the corresponding results by the three-dimensional analysis (Figs. 3.10 and 3.12, respectively) suggests that the results of these two solutions agree fairly well, except for a slight discrepancy observed in the torsional stiffnesses.

Finally, Figs. 4.5 and 4.6 present a number of examples for seismic analyses by a quasi-three-dimensional formulation, similar to the one used for the evaluation of rocking stiffnesses. Fig. 4.5 shows the absolute value of the transfer functions for displacement and rotation of the pile cap for the 4 x 4 group in the soft soil medium and Fig. 4.6 shows the same quantities for different pile groups with s/d = 5 in the stiff soil medium. Comparing plots in Figs. 4.5 and 4.6 with those in Figs. 3.16 and 3.18, one can conclude that the results of the two solutions

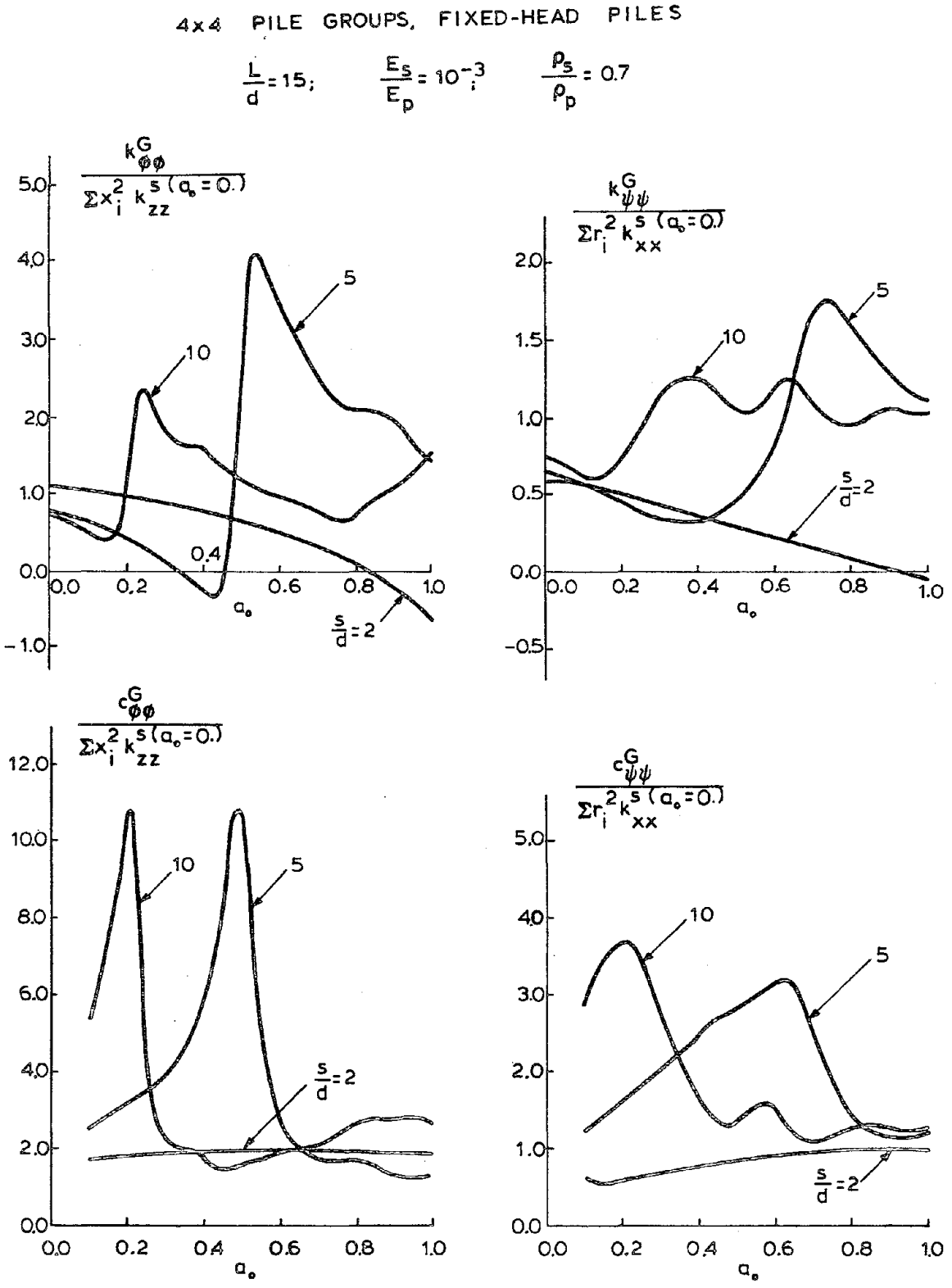

Fig. 4.3 - Rocking and Torsional Dynamic Stiffnesses of 4 x 4 Pile Groups in a Soft Soil Medium by the Quasi-Three-Dimensional Formulation.

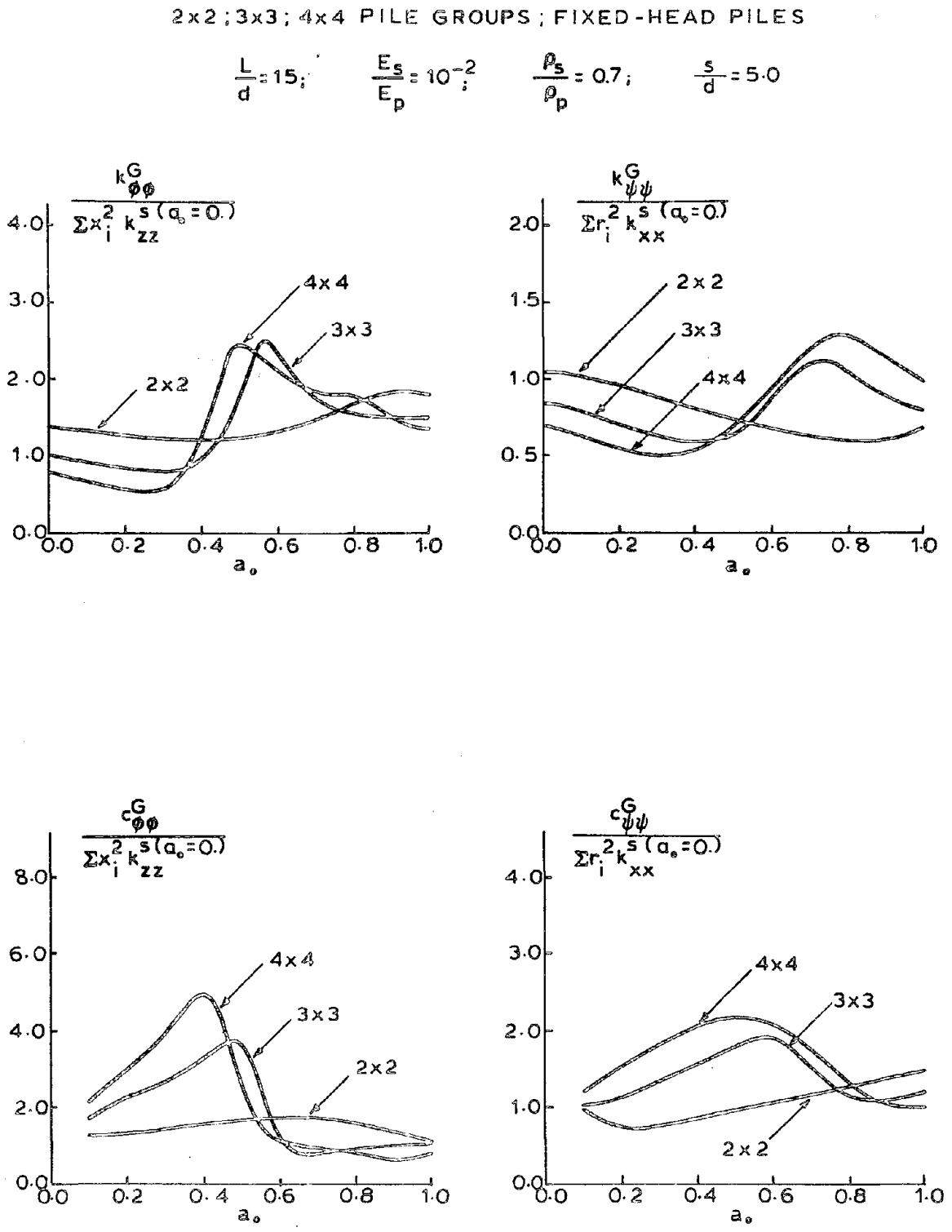

Fig. 4.4 - Rocking and Torsional Dynamic Stiffnesses of Pile Groups with s/d = 5 in a Stiff Soil Medium by the Quasi-Three-Dimensional Formulation.

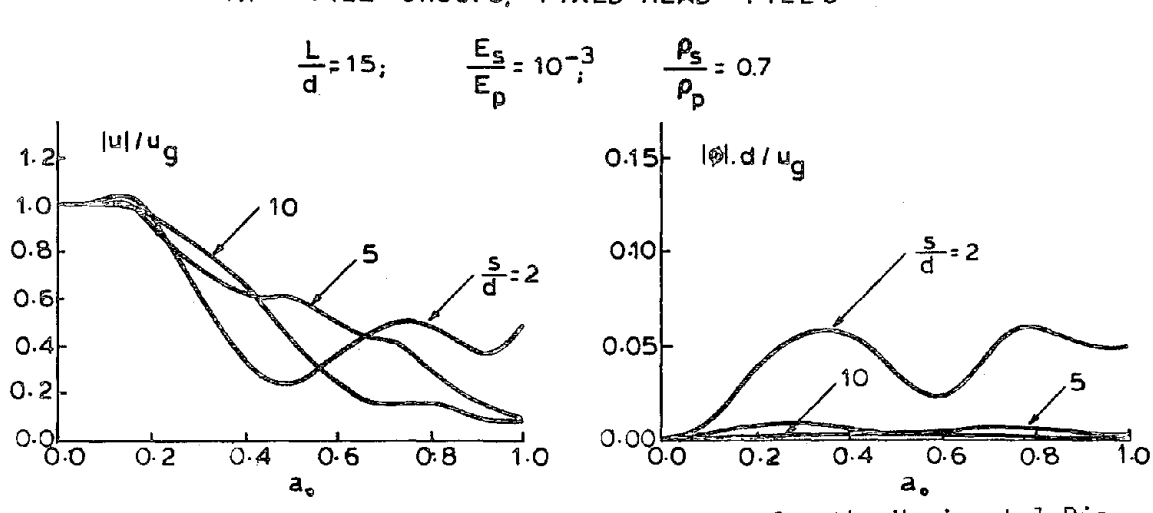

Fig. 4.5 - Absolute Value of Transfer Functions for the Horizontal Displacement and Rotation of the Pile Cap for 4 x 4 Pile Groups in a Soft Soil Medium by the Quasi-Three-Demensional Formulation.

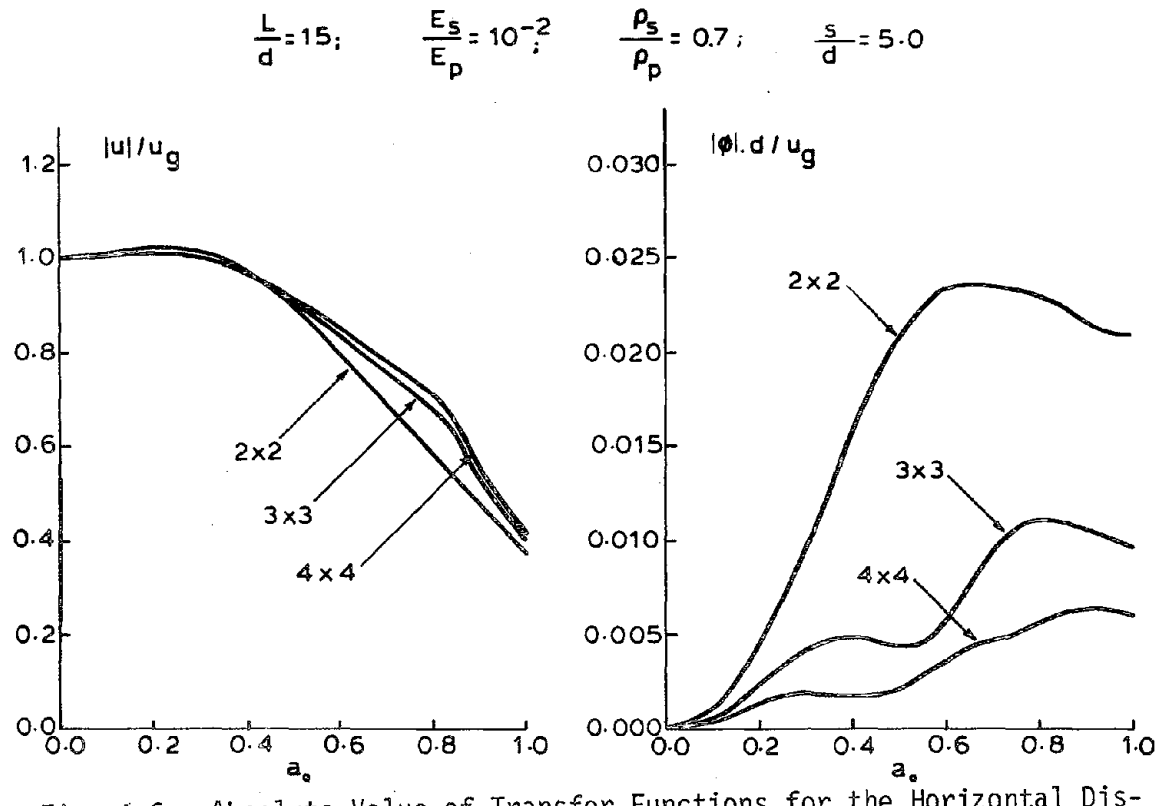

Fig. 4.6 - Absolute Value of Transfer Functions for the Horizontal Displacement and Rotation of the Pile Cap for Pile Groups with s/d = 5 in a Stiff Soil Medium by the Quasi-Three-Dimensional Formulation.

agree fairly well in the frequency range of interest for seismic analyses.

Therefore, in general, quasi-three-dimensional formulations are capable of accurately characterizing the dynamic responses of symmetric pile groups and they can replace the more involved three-dimensional solutions.

CHAPTER 5 - THE SUPERPOSITION METHOD

The three-dimensional formulation presented in chapter 2, as well as the modified version of it, namely the quasi-three-dimensional formulation described in chapter 4, require, in general, solution of a large system of equations. This is due to the fact that on each pile segment there are a number of unknown interaction forces that have to be related to their corresponding displacements, through the soil or pile flexibility matrices. As the number of piles in a group increases, the size of these matrices poses considerable computational difficulties on the analysis. Therefore, it is highly desirable to develop simplified solution schemes which enable one to analyze large pile group systems by reducing them to smaller and simpler systems. The superposition method is an example of such simplified pile group solution schemes.

The superposition method originally proposed by Poulos (1968, 1971) is frequently used to formulate pile group problems. In this approximate scheme, only two piles are considered at a time in the formation of a global flexibility matrix which relates the forces and displacements only at the pile heads. The method clearly relies on the observation that the presence of other piles does not significantly affect the motion of the two piles under consideration.

The entries in the global flexibility matrix are usually obtained from tabulated solutions for two piles that are commonly referred to as interaction factors; these factors are presented in terms of the distance separating the piles and the material properties of the system.

The available tabulated solutions for the interaction factors are for static loads only. In order to extend the applicability of the method

to dynamic loads it is necessary to develop appropriate factors for this purpose.

A dynamic interaction factor for two piles (in which a unit harmonic load is applied on the first pile and the displacements are evaluated for the second one) is defined as follows:

$$\text{Interaction factor} = \frac{\text{Dynamic displacement of pile 2}}{\text{Static displacement of pile 1, considered individually}}$$

in which the word displacement is used to denote either a translation or a rotation. In addition to interaction factors, for the purpose of assembling the global flexibility matrix of the group, one also needs the dynamic load factors for individually loaded piles (single piles), which are available in the literature.

Figures 5.1 and 5.2 present interaction factors for the piles embedded in an elastic halfspace with $E_s/E_p = 10^{-3}$ and for s/d = 2, 5 and 10. (These parameters are the same as those used for the pile groups for which the stiffness characteristics were examined in Figs. 3.3, 3.4 and 3.5). In Fig. 5.1, $I_{u_x F_x}$ refers to the horizontal displacement of pile 2 due to the horizontal force on pile 1. Other interaction factors: $I_{u_z F_z}$, $I_{u_x M_x}$ and $I_{\phi_x M_x}$ define, in a similar manner, the connection between the applied force and the induced displacement.

The plots in Figs. 5.1 and 5.2 give the interaction curves for $\theta=0$ and $\theta=\pi/2$ only. For any other angle, the interaction factors can be obtained from those for $\theta=0$ and $\theta=\pi/2$. Consider the two piles shown in Fig. 5.3a. If F_x and F_y are the two components of the horizontal force on pile 1, then one can write

$\frac{L}{d}=15$; $\frac{E_s}{E_p}=10^{-3}$; $\frac{\rho_s}{\rho_p}=0.7$

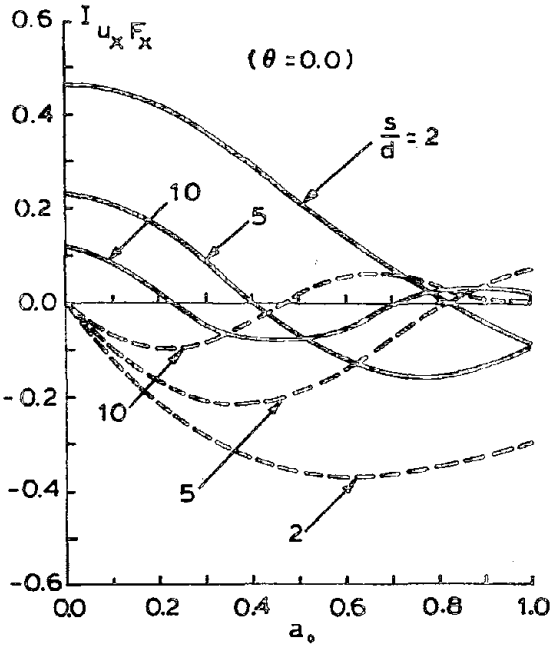

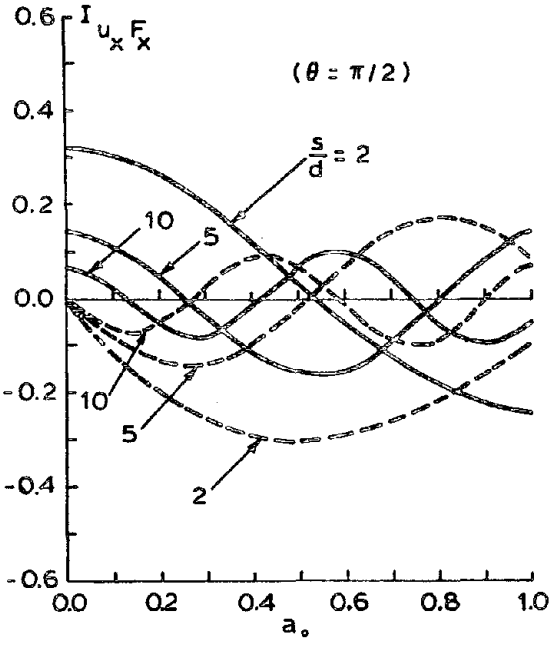

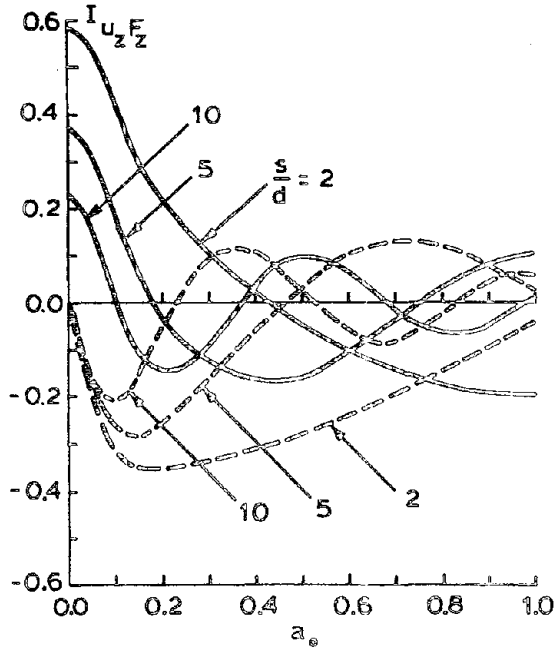

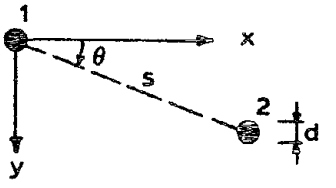

REAL PART

IMAG. PART

$I_{u_x F_x}$ ≡ horizontal displacement of pile 2 due to horizontal force on pile 1

$I_{u_z F_z}$ ≡ vertical displacement of pile 2 due to vertical force on pile 1.

Fig. 5.1 - Interaction Curves for the Horizontal and Vertical Displacement of Pile 2 due to the Horizontal and Vertical Forces on Pile 1.

$\frac{L}{d}=15$; $\frac{E_s}{E_p}=10^{-3}$; $\frac{\rho_s}{\rho_p}=0.7$

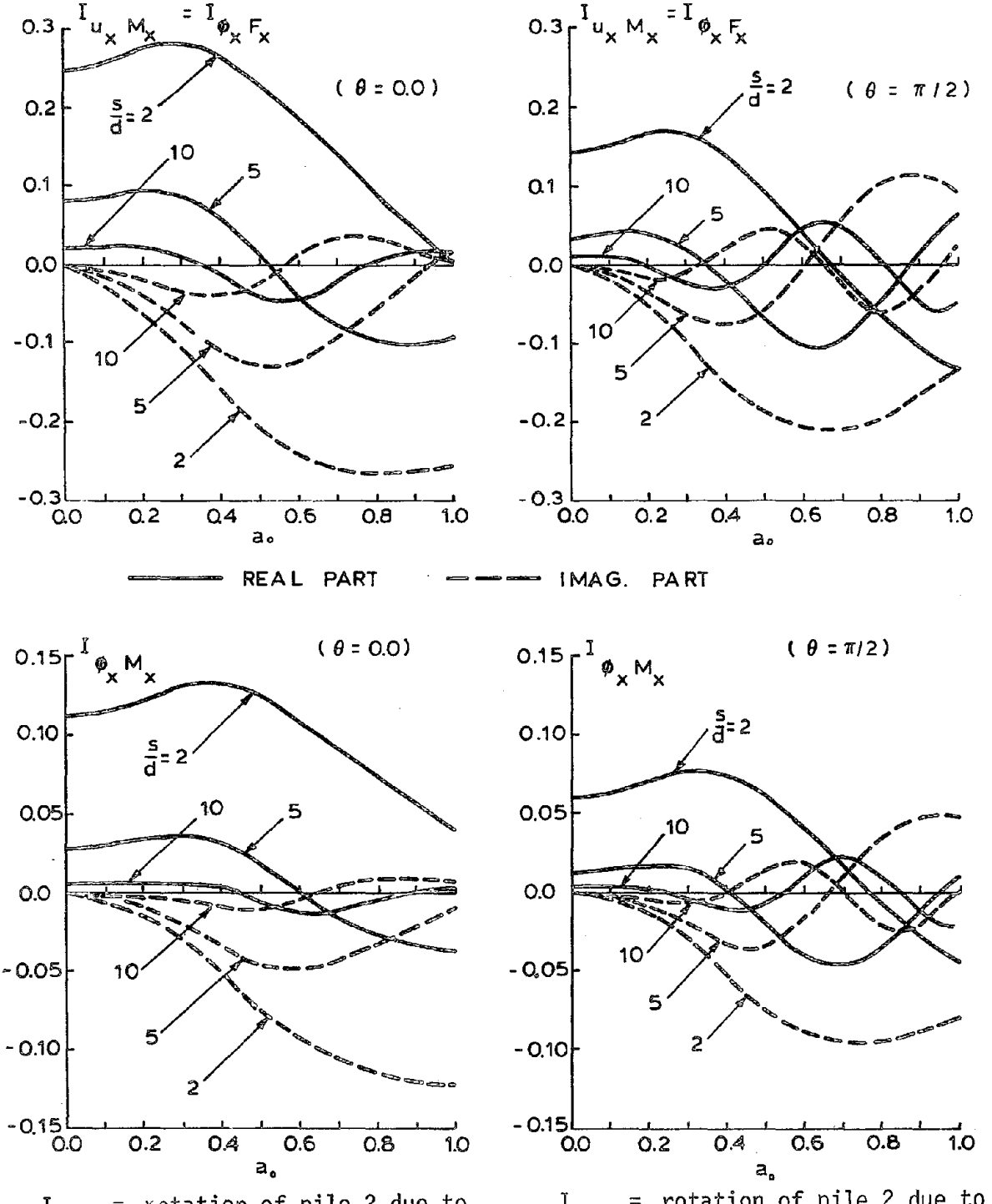

$I_{\phi_x F_x}$ ≡ rotation of pile 2 due to horizontal force on pile 1

$I_{\phi_x M_x}$ ≡ rotation of pile 2 due to moment on pile 1.

Fig. 5.2 - Interaction Curves for the Rotation of Pile 2 due to the Horizontal Force and Moment on Pile 1.

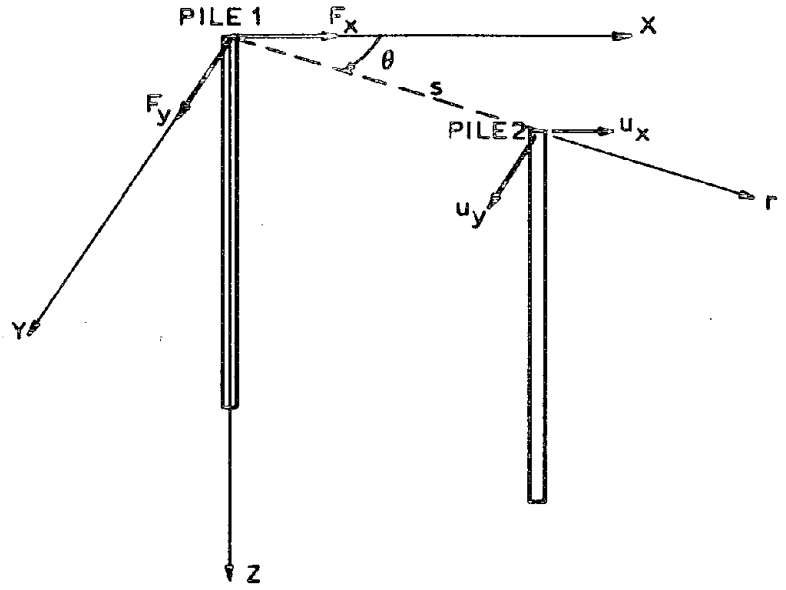

(a) perspective

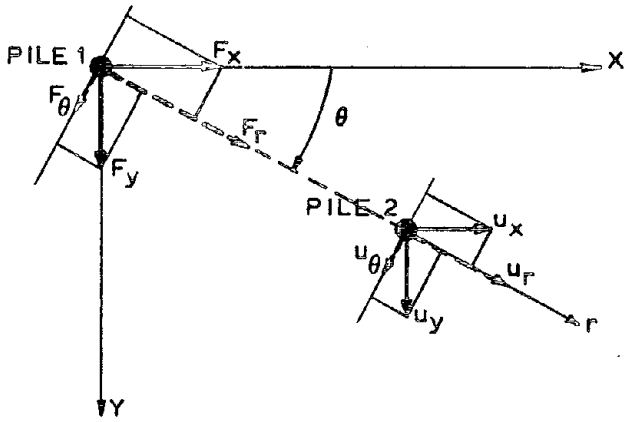

(b) plan view

Fig. 5.3 - Forces and Displacements at the Head of Two Piles.

$$\begin{Bmatrix} F_r \\ F_\theta \end{Bmatrix} = \begin{bmatrix} \cos\theta & \sin\theta \\ -\sin\theta & \cos\theta \end{bmatrix} \begin{Bmatrix} F_x \\ F_y \end{Bmatrix} \tag{5.1}$$

where F_r and F_θ are the components of the horizontal force in the radial and tangential directions. If u_r and u_θ are the radial and tangential components of the displacement of pile 2, then one can use the interaction factors for $\theta=0$ and $\theta=\pi/2$ in order to relate u_r and u_θ to F_r and F_θ. If the interaction factors for $\theta=0$ and $\theta=\pi/2$ are denoted by I_0 and I_{90}, respectively, then one can write

$$\begin{Bmatrix} u_r \\ u_\theta \end{Bmatrix} = \begin{bmatrix} I_0 & 0 \\ 0 & I_{90} \end{bmatrix} \begin{Bmatrix} F_r \\ F_\theta \end{Bmatrix} \tag{5.2}$$

On the other hand, u_x and u_y are related to u_r and u_θ as

$$\begin{Bmatrix} u_x \\ u_y \end{Bmatrix} = \begin{bmatrix} \cos\theta & -\sin\theta \\ \sin\theta & \cos\theta \end{bmatrix} \begin{Bmatrix} u_r \\ u_\theta \end{Bmatrix} \tag{5.3}$$

Finally, combining Eqns. (5.1), (5.2) and (5.3), one gets:

$$\begin{Bmatrix} u_x \\ u_y \end{Bmatrix} = \begin{bmatrix} I_0\cos^2\theta + I_{90}\sin^2\theta & (I_0 - I_{90})\cos\theta\sin\theta \\ (I_0 - I_{90})\cos\theta\sin\theta & I_0\sin^2\theta + I_{90}\cos^2\theta \end{bmatrix} \begin{Bmatrix} F_x \\ F_y \end{Bmatrix} \tag{5.4}$$

Therefore, for an arbitrary angle θ, $I_{u_xF_x}(\theta)$ is given by:

$$I_{u_xF_x}(\theta) = I_{u_xF_x}(0)\cos^2\theta + I_{u_xF_x}(\pi/2)\sin^2\theta \tag{5.5}$$

The relation in (5.4) can be used for other interaction factors involving horizontal forces or moments, as well. For the vertical forces, on the other hand, the interaction factors are independent of θ.

Once the global flexibility matrix of the group is assembled, the foundation (pile cap) stiffnesses are obtained in a manner similar to that outlined in chapter 2 (by imposing kinematic and force boundary conditions at pile heads). Figures 5.4 and 5.5 show the dynamic stiffnesses (horizontal, vertical, rocking and torsional) for the same pile groups of Figs. 3.5 and 3.10 (4 x 4 groups in the soft soil medium, $E_s/E_p = 10^{-3}$) but computed using the superposition method. Comparison of these figures shows that the approximate superposition method yields results that are in good general agreement with those obtained from the full three-dimensional analysis. The accuracy of the method improves as the pile spacing is increased, as expected. Also, Figs 5.6 and 5.7 present the dynamic stiffnesses for the same groups of Figs. 3.7 and 3.12 (groups with s/d = 5 in the stiff soil medium, $E_s/E_p = 10^{-2}$). Again, the results of the superposition analysis agree very well with those of the three-dimensional analysis.

The dynamic interaction curves are also helpful in gaining insight into the behavior of pile groups. Certain important aspects of the problem, such as the large peaks in the variation of dynamic stiffnesses and the considerable dynamic amplification of forces on certain piles can, in fact, be physically interpreted with the help of interaction curves.

Consider, for example, the variation of horizontal stiffness in Fig. 3.3, for s/d = 5. This figure displays a large peak at a frequency $a_o \approx 0.8$. At this frequency the interaction factor, $I_{u_x F_x}(0,0)$ in Fig.5.1

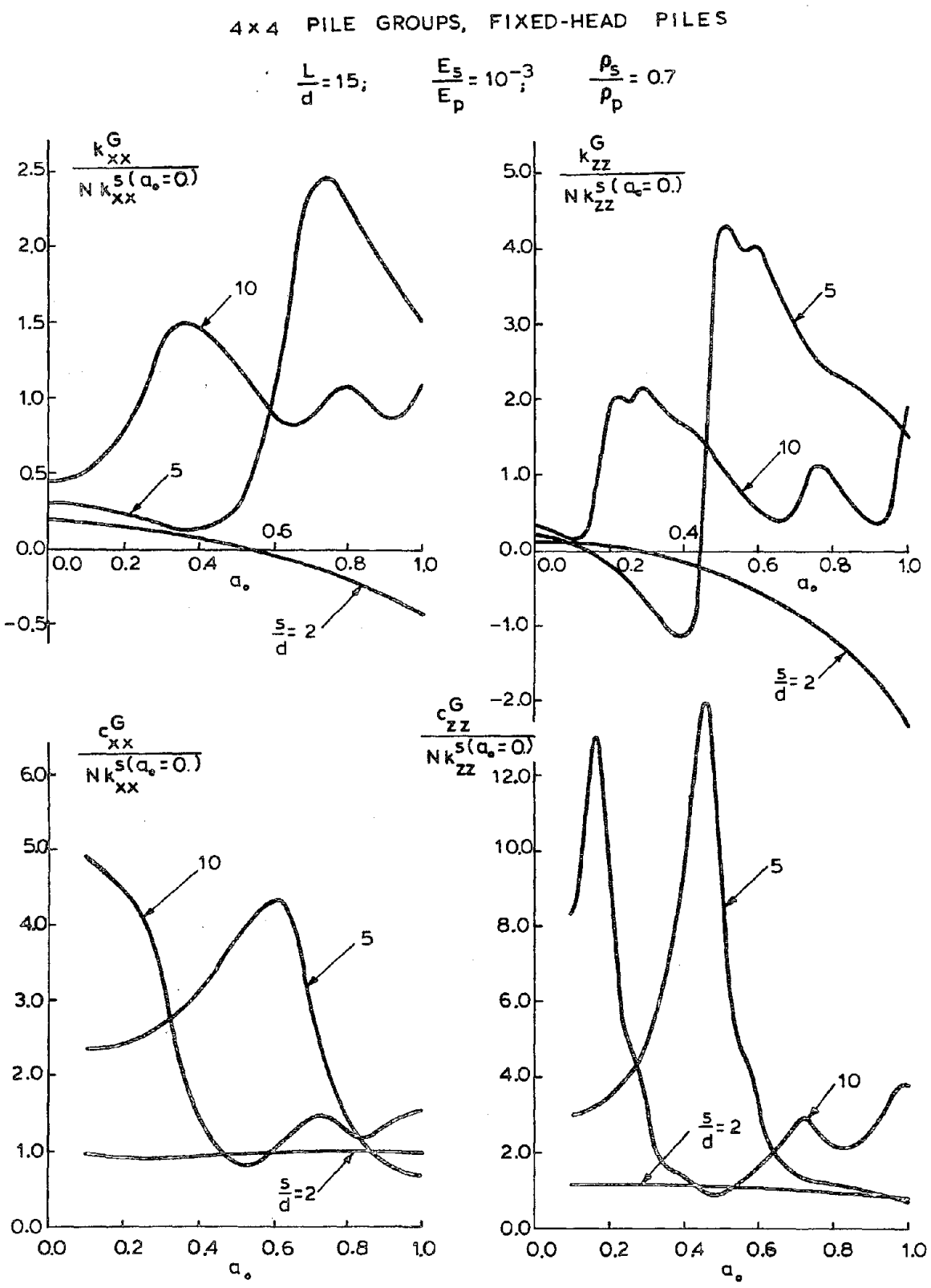

Fig. 5.4 - Horizontal and Vertical Dynamic Stiffnesses of 4 x 4 Pile Groups in a Soft Soil Medium by the Superposition Method.

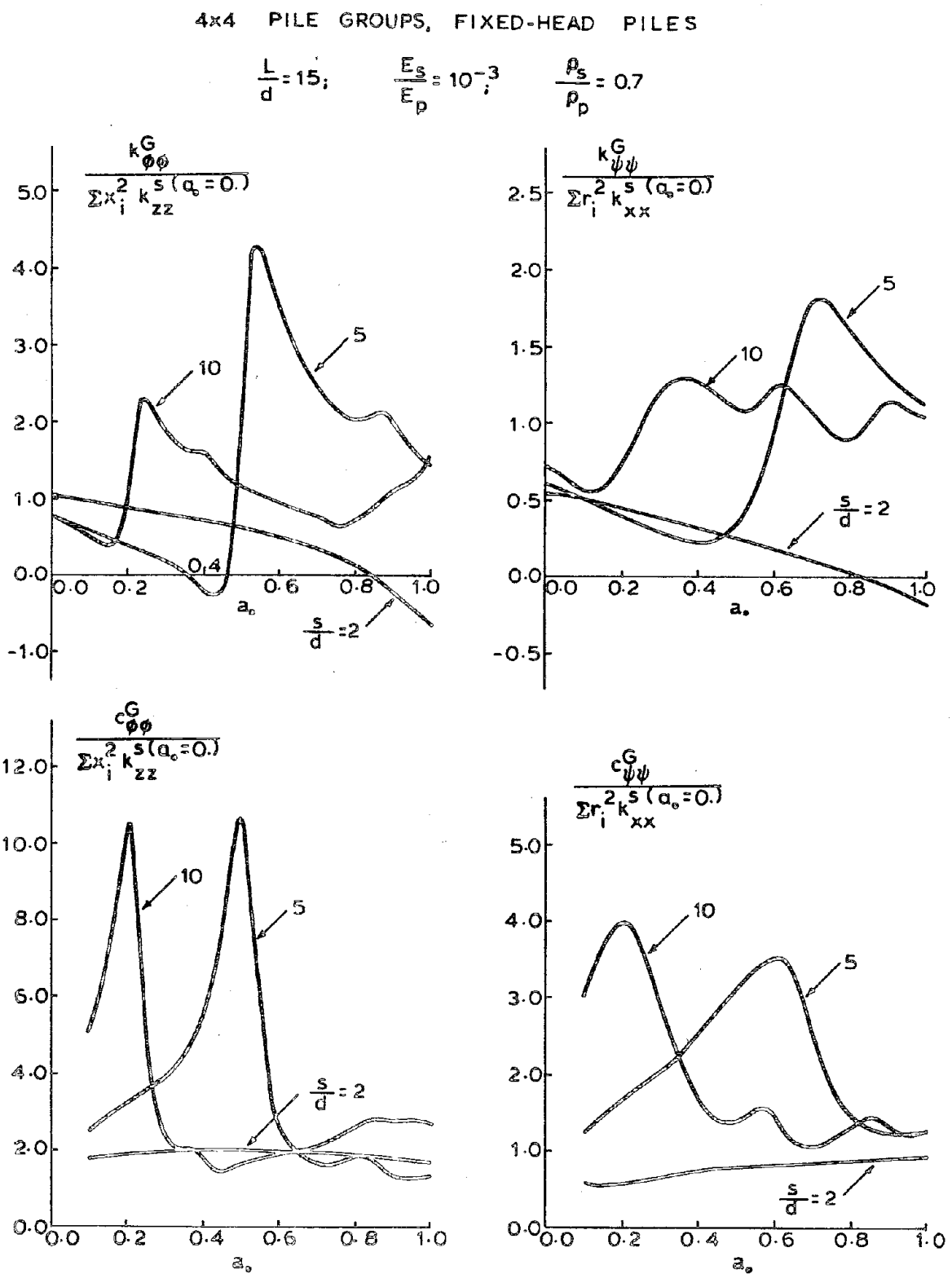

Fig. 5.5 - Rocking and Torsional Dynamic Stiffnesses of 4 x 4 Pile Groups in a Soft Soil Medium by the Superposition Method.

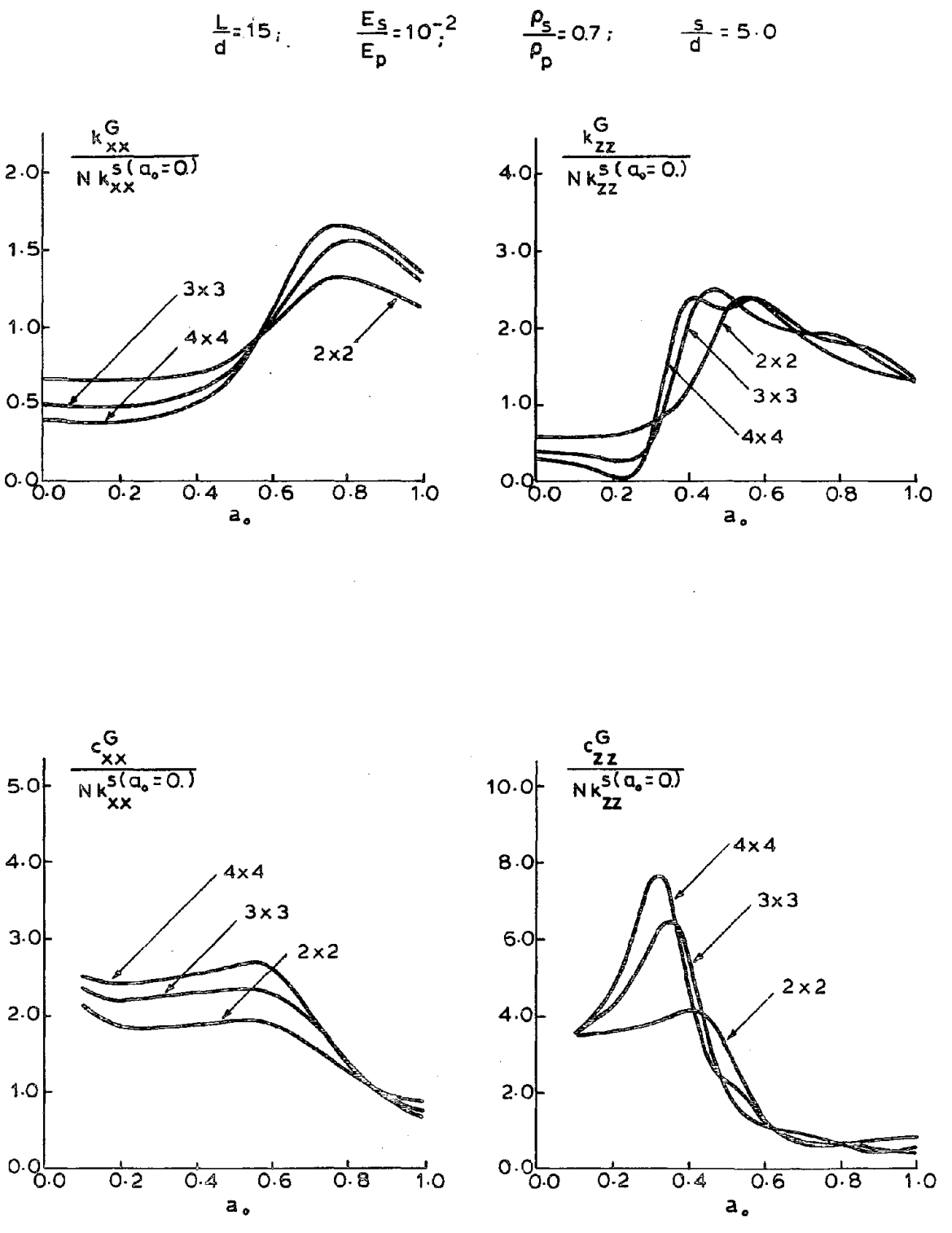

Fig. 5.6 - Horizontal and Vertical Dynamic Stiffnesses of Pile Groups with s/d = 5 in a Stiff Soil Medium by the Superposition Method.

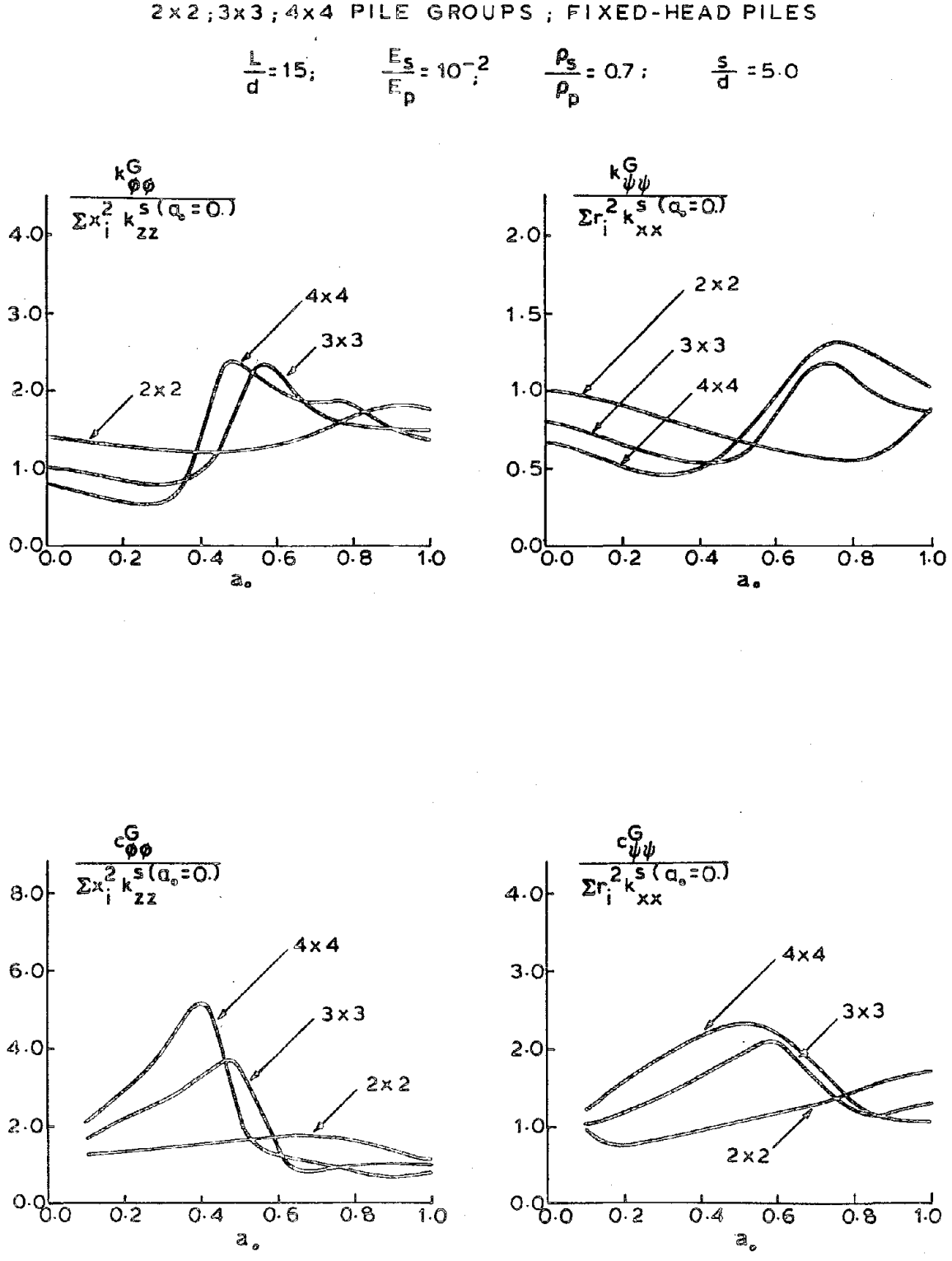

Fig. 5.7 - Rocking and Torsional Dynamic Stiffnesses of Pile Groups with s/d = 5 in a Stiff Soil Medium by the Superposition Method.

is a real, negative number, the physical meaning of which is that the waves set up by the loaded pile excite the second pile in an antiphase motion. Therefore, a larger force (stiffness) must be applied on the piles in the group to enforce the condition of uniform displacement of the pile heads required by the presence of the pile cap.

It is also possible to interpret the similarity between the plots of stiffnesses for different spacings by the similarity between the corresponding interaction curves. In addition, the fact that the interaction effects diminish with an increase in spacing, accounts for the less pronounced variation in stiffnesses for larger spacings. Using these observations, one can then predict that the plot of horizontal stiffness for s/d = 2 in Fig. 3.3 has a peak at $a_0 \approx 2$, which is larger than the one corresponding to s/d = 5.

As far as the force distribution is concerned, Fig. 3.19 shows that the dynamic amplification factor for pile IV and s/d = 5 is a maximum again at $a_0 \approx 0.80$. An argument similar to the one for the stiffness can be brought forward to explain this phenomenon too.

CHAPTER 6 - SUMMARY AND CONCLUSIONS

The purpose of the work presented in the preceding chapters was to investigate the dynamic behavior of pile groups in semi-infinite media and to examine the validity of certain solution schemes.

The formulation was based on the introduction of a soil flexibility matrix as well as dynamic stiffness and flexibility matrices of the piles, in order to relate the discretized uniform forces to the corresponding displacements at the pile-soil interface. A numerical solution for the evaluation of the soil flexibility matrix, along with analytical solutions for the pile stiffness and flexibility matrices were then presented.

The results of pile group analyses presented in chapter 3 suggested the following:

1) The dynamic pile group behavior is highly frequency-dependent. This is due to the characteristics of the waves generated by the piles and the interference of these waves with the different piles of the group.

2) For close spacings the characteristics of group stiffnesses are similar to those of footings; for large spacings, however, the group behavior is dominated by the interactions among the piles.

3) Interaction effects are stronger for softer soil media.

4) Radiation damping generally increases with foundation size.

5) Pile groups subjected to seismic excitations essentially follow the low-frequency components of the ground motion, while filtering to a large extent its intermediate and high-frequency components. The

rotational component, on the other hand, is negligible for typical dimensions of the foundation.

6) The distribution of applied dynamic loads on the pile cap is different from that of static loads. For certain frequency intervals, the piles closest to the center take the largest portion of the load. Also, large dynamic amplification factors for the forces in these piles are expected.

7) Pile groups are less influenced by conditions near the ground surface than single piles are. Therefore, the accuracy of the techniques, which use the result of single-pile nonlinear analyses, or field tests on single piles, along with empirical group reduction factors to derive group stiffnesses is less than expected.

Other subjects addressed in this study were the questions on the accuracy of the quasi-three-dimensional method, and the superposition method for the solution of pile groups. These studies showed that:

1) Quasi-three-dimensional solutions, in which the pile-soil compatibility conditions in a given direction are relaxed and only the effect of pile-soil interface forces in the other directions are taken into account, compare very well with the full three-dimensional solution.

2) The superposition scheme suggested first by Poulos gives reasonable results not only for static loads, but for dynamic loads, as well.

References

1. Apsel, R.J. (1980): "Dynamic Green's Functions for Layered Media and Applications to Boundary Value Problems," Ph.D. Thesis submitted to the Department of Applied Mechanics and Engineering Sciences, University of California, San Diego.

2. Arnold, R.N., Bycroft, G.N. and Warburton, G.B. (1955): "Forced Vibrations of a Body on an Infinite Elastic Solid," Journal of Applied Mechanics, Trans. ASME, Vol. 77, pp. 391-400.

3. Banerjee, P.K. (1978): "Analysis of Axially and Laterally Loaded Pile Groups," in Developments in Soil Mechanics, Edited by C.R. Scott, London, Applied Science Publishers.

4. Blaney, G.W., Kausel, E. and Roesset, J.M. (1976): "Dynamic Stiffness of Piles," Proc. of the 2nd International Conference on Numerical Methods in Geomechanics, Blacksburg, Virginia, pp. 1001-1012.

5. Butterfield, R. and Banerjee, P.K. (1971): "The Elastic Analysis of Compressible Piles and Pile Groups," Geotechnique, Vol. 21, No. 1, pp. 43-60.

6. Kagawa, T. and Kraft, L.M. Jr. (1981): "Dynamic Characteristics of Lateral Load-Deflection Relationships of Flexible Piles," International Journal of Earthquake Engineering and Structural Dynamics," Vol. 9, pp. 53-68.

7. Kausel, E. and Roesset, J.M. (1974): "Soil-Structure Interaction Problems for Nuclear Containment Structures," presented at the Power Division ASCE Specialty Conference held at Boulder, Colorado, August 12-14, pp. 469-498.

8. Kobori, T., Minai, R. and Baba, K. (1977): "Dynamic Behavior of a Laterally Loaded Pile," Proc. of the 9th International Conference on Soil Mechanics and Foundation Engineering, Specialty Session 10; Tokyo, Japan, pp. 175-180.

9. Kobori, T., Minai, R. and Baba, K. (1981): "Dynamic Behavior of a Pile under Earthquake-Type Loading," Proc. of the International Conference on Recent Advances in Geotechnical Earthquake Engineering and Soil Dynamics, University of Missouri-Rolla, Vol. 2, pp. 795-800.

10. Kuhlemeyer, R.L. (1979a): "Vertical Vibration of Piles," Journal of the Geotechnical Engineering Division, ASCE, Vol. 105, No. GT2, pp. 273-287.

11. Kuhlemeyer, R.L. (1979b): "Static and Dynamic Laterally Loaded Floating Piles," Journal of the Geotechnical Engineering Division, ASCE, Vol. 105, No. GT2, pp. 289-304.

12. Matlock, H. (1970): "Correlations for Design of Laterally Loaded Piles in Soft Clay," Proc. of the 2nd Offshore Technology Conference, Houston, Texas, Vol. 1, pp. 577-594.

13. Mindlin, R.D. (1936): "Force at a Point in the Interior of a Semi-Infinite Solid," Physics, 7, pp. 195-202.

14. Nogami, T. and Novak, M. (1976): "Soil-Pile Interaction in Vertical Vibration," International Journal of Earthquake Engineering and Structural Dynamics, Vol. 4, pp. 277-293.

15. Nogami, T. (1979): "Dynamic Group Effect of Multiple Piles under Vertical Vibration," Proc. of the ASCE Engineering Mechanics Division Specialty Conference, Austin, Texas, pp. 750-754.

16. Nogami, T. (1980): "Dynamic Stiffness and Damping of Pile Groups in Inhomogeneous Soil," ASCE Special Technical Publication on Dynamic Response of Pile Foundation, October 1980.

17. Novak, M. (1974): "Dynamic Stiffness and Damping of Piles," Canadian Geotechnical Journal, Vol. 11, No. 4, pp. 574-598.

18. Novak, M. and Nogami, T. (1977): "Soil-Pile Interaction in Horizontal Vibration," International Journal of Earthquake Engineering and Structural Dynamics, Vol. 5, pp. 263-281.

19. Novak, M., Nogami, T. and Aboul-Ella, F. (1978): "Dynamic Soil Reactions for Plain Strain Cases," Technical Note, Journal of the Engineering Mechanics Division, ASCE, Vol. 104, No. EM4, pp. 953-956.

20. Poulos, H.G. (1968): "Analysis of the Settlement of Pile Groups," Geotechnique, Vol. 18, pp. 449-471.

21. Poulos, H.G. (1971): "Behavior of Laterally-Loaded Piles: II - Pile Groups," Journal of the Soil Mechanics and Foundation Division, ASCE, Vol. 97, No. SM5, pp. 733-751.

22. Poulos, H.G. and Mattes, N.S. (1971): "Settlement and Load Distribution Analysis of Pile Groups," Australian Geomechanics Journal , Vol. G1, No. 1, pp. 18-28.

23. Poulos, H.G. and Davis, E.H. (1980): Pile Foundation Analysis and Design, New York, John Wiley and Sons.

24. Reese, L.C., Cox, W.R. and Koop, F.D. (1974): "Analysis of Laterally Loaded Piles in Sand," Proc. of the 6th Offshore Technology Conference, Houston, Texas, Paper OTC 2080.

25. Reese, L.C. and Welch, R.C. (1975): "Lateral Loading of Deep Foundations in Stiff Clay," Journal of the Geotechnical Engineering Division, ASCE, Vol. 101, No. GT7, pp. 633-649.

26. Tajimi, H. (1969): "Dynamic Analysis of a Structure Embedded in an Elastic Stratum," Proc. of the 4th World Conference in Earthquake Engineering, Santiago, Chile, Vol. 3, pp. 53-69.

27. Waas, G. (1980): "Dynamisch Belastete Fundamente auf Genschichtetem Baugrund," VDI-Berichte Nr. 381.

28. Waas, G. and Hartmann, H.G. (1981): "Analysis of Pile Foundations under Dynamic Loads," SMIRT Conference, Paris.

29. Wolf, J.P. and Von Arx, G.A. (1978): "Impedance Function of a Group of Vertical Piles," Proc. of the Specialty Conference on Soil Dynamics and Earthquake Engineering, ASCE, Pasadena, California, Vol. 2, pp. 1024-1041.